

Review

# Electrochemical Detection of Heavy Metal Ions Based on Nanocomposite Materials

Mahendra D. Shirsat<sup>1,2,\*</sup> and Tibor Hianik<sup>1,\*</sup> 

<sup>1</sup> Department of Nuclear Physics and Biophysics, Faculty of Mathematics, Physics and Informatics, Comenius University, 84248 Bratislava, Slovakia

<sup>2</sup> RUSA Centre for Advanced Sensor Technology, Department of Physics, Dr. Babasaheb Ambedkar Marathwada University, Aurangabad 431001, India

\* Correspondence: mdshirsat.phy@bamu.ac.in (M.D.S.); tibor.hianik@fmph.uniba.sk (T.H.)

**Abstract:** Heavy metal ions (HMIs) have acute toxic effects on health and are dangerous for human existence and the ecosystem. Therefore, their sensitive and selective detection is of great importance. In recent years, various nanocomposite materials have been used by researchers for the detection of HMIs by using various modalities of electrochemical techniques. This review summarizes the recent advances in developing electrochemical sensors based on numerous nanocomposite materials for detecting HMIs. Nanocomposite materials, such as metal–organic frameworks (MOFs), organic conducting polymer (OCPs), carbon nanotubes (CNTs), graphene oxide (GO), graphene/reduced graphene oxide (rGO), graphitic carbon nitride, metal oxide, chitosan, MXenes, metal nanoparticle-based nanocomposites, etc., have been explored by various researchers to improve the sensing properties of electrochemical sensors. This review emphasizes nanocomposite materials' synthesis and characterization techniques, modalities for HMI detection using electrochemical techniques, and electrochemical sensors. Moreover, this review highlights the development of portable biosensors for detecting HMIs in real-world scenarios, such as environmental monitoring, food safety, and clinical diagnosis. This review also demonstrates the importance of electrochemical sensors based on nanocomposite materials as a reliable, sensitive, and selective tool for detecting HMIs.

**Keywords:** electrochemical sensor; nanocomposite; heavy metal ions; metal–organic framework; conducting polymer; carbon nanotube; graphene; graphitic carbon nitride



**Citation:** Shirsat, M.D.; Hianik, T. Electrochemical Detection of Heavy Metal Ions Based on Nanocomposite Materials. *J. Compos. Sci.* **2023**, *7*, 473. <https://doi.org/10.3390/jcs7110473>

Academic Editor: Francesco Tornabene

Received: 3 October 2023

Revised: 25 October 2023

Accepted: 9 November 2023

Published: 11 November 2023



**Copyright:** © 2023 by the authors. Licensee MDPI, Basel, Switzerland. This article is an open access article distributed under the terms and conditions of the Creative Commons Attribution (CC BY) license (<https://creativecommons.org/licenses/by/4.0/>).

## 1. Introduction

Due to industrialization, HMIs occurring in various water bodies on the earth's surface is almost unavoidable. Moreover, their composition differs among different localities, depending on the extent of industrialization in that particular locality [1].

Heavy metals have a relatively high atomic weight and density, between 3.5 and 7 g/cm<sup>3</sup> [2]. The most well known heavy metals are iron (Fe), zinc (Zn), arsenic (As), copper (Cu), nickel (Ni), cadmium (Cd), mercury (Hg), lead (Pb), tin (Sn), etc. These metals are available naturally and cannot be degraded or destroyed. Though some HMIs are needed for the human body's functioning, such as iron (Fe(II)), zinc (Zn(II)), manganese (Mn(II)), and cobalt (Co(II)), they can be toxic in large amounts [3]. Whereas HMIs like lead (Pb(II)), mercury (Hg(II)), arsenic (As(II)), and cadmium (Cd(II)) are toxic in nature and contaminants even in small amounts [4]. Some heavy metals such as copper, selenium, and zinc are required as trace elements to keep the human body's metabolism running smoothly. However, at higher concentrations, they can lead to poisoning. The primary sources of daily-purpose water (drinking water) are surface and groundwater. According to the United States Environmental Protection Agency (USEPA), urban regions depend on surface water sources, and rural regions depend on groundwater sources. The surface water includes streams, lakes, ponds, rivers, and oceans. Drilling wells obtain groundwater from under

the ground's surface and between the rocks. Treated water is mainly from surface water, and various physical filters are used to purify it from dust and other particles. Also, various chemicals—chlorine and fluorine compounds—are added to kill microorganisms [5]. More heavy metals can be found in groundwater compared to surface water. However, the possibility of finding heavy metals in the groundwater increases when ore mines or rich minerals are deposited in the vicinity [6]. The permissible maximum contamination level (MCL) recommended by the USEPA for heavy metals is mentioned in Table 1.

**Table 1.** The MCL of some heavy metals in drinking water [7,8].

| Heavy Metal |    | MCL ( $\mu\text{g/L}$ ) |
|-------------|----|-------------------------|
| Antimony    | Sb | 6                       |
| Arsenic     | As | 10                      |
| Cadmium     | Cd | 5                       |
| Chromium    | Cr | 100                     |
| Copper      | Cu | 1.3                     |
| Lead        | Pb | 15                      |
| Mercury     | Hg | 2                       |
| Nickel      | Ni | 100                     |
| Selenium    | Se | 50                      |

Because some heavy metals are very hazardous and can be ingested via drinking water, the USEPA and the European Environment Agency (EEA) recommended the MCL of these heavy metals in the smallest amounts.

The leading causes of water pollution are anthropogenic activities where contaminants are dumped into water bodies (rivers, lakes, oceans), resulting in the degradation of the aquatic ecosystem. There are three types of water pollution. First, surface water pollution is the contamination of rivers and lakes, mainly caused by petroleum spills, industrial chemical waste, waste with a high content of heavy metals, and acid rain. Second, marine pollution is caused by surface water pollution, which kills marine life, disturbing the aquatic ecosystem. Third, groundwater pollution is caused by water movement under the ground, sewage dumping, on-site sanitization plants, hydraulic fracturing, landfills, and chemical fertilizers and pesticides in agriculture [9]. Modern urbanization, industrialization, overpopulation, deforestation, and other factors contribute to environmental deterioration. The degradation of the quality of natural resources and their quantity is known as environmental pollution. Heavy metal pollution in the water can lead to serious environmental and health issues. Heavy metals such as lead, mercury, cadmium, arsenic, and chromium are toxic to humans and aquatic life and can accumulate in the food chain over time. HMIs enter water bodies via various sources, such as industrial discharge, agricultural runoff, and domestic sewage. These pollutants can persist in the water environment for a long time and are difficult to remove. The effects of heavy metal pollution in the water can range from acute toxicity to chronic toxicity, carcinogenicity, and mutagenicity. Exposure to HMIs can lead to various health problems, such as neurological disorders, kidney damage, liver damage, and cancer.

Various treatment methods, such as coagulation–flocculation, adsorption, ion exchange, and membrane filtration, have been developed to combat heavy metal pollution. Additionally, regulations and policies have been established by government authorities to limit the discharge of heavy metals into water bodies. HMIs are toxic substances; therefore, it is imperative to establish relevant techniques for detecting and monitoring them. One practical approach is using sensors to detect and measure the concentration of specific HMIs in a sample. The sensors provide a fast, accurate, and cost-effective way to monitor the presence of HMIs. Furthermore, sensors can be designed to work in various environments, making them ideal for use in laboratory and field settings. Overall, developing and using sensors for HMI detection are crucial for protecting public health and the environment from the harmful effects of these toxic substances.

Nanocomposite materials have emerged as a revolutionary class of materials with immense importance in various technological applications. By incorporating nanoscale components into a host matrix, their unique properties offer unparalleled advantages such as enhanced mechanical strength, improved electrical conductivity, superior thermal stability, and tailored functionalities. These attributes have paved the way for revolutionary advancements in electronics, energy storage, sensors, medicine, etc. Nanocomposite materials have become indispensable in sensors due to their exceptional sensitivity, selectivity, and responsiveness. By incorporating nanoscale components into a host matrix, these materials exhibit unique properties that can be tailored to specific sensing applications. Nanocomposite sensors offer enhanced surface-to-volume ratios, enabling more efficient interaction with analytes and increasing sensitivity, even at low concentrations. Their tunable properties also allow for customizing the sensor's response to stimuli, making them ideal for detecting a wide range of targets, including chemicals, biomolecules, and environmental pollutants. Moreover, their compatibility with various fabrication techniques allows for the development of flexible, wearable, and miniaturized sensor devices.

Nanocomposite-based sensors have gained significant attention in recent years because of their synergistic effect on detecting HMIs with improved sensing properties [10–12]. Researchers worldwide are actively investigating developing and optimizing nanocomposite materials for sensors for HMI detection. Researchers are exploring various nanocomposite materials, including GO, MOFs, CNTs, OCPs, MXenes-based nanocomposites, and metal oxide-based nanocomposites, to detect a range of HMIs [13–18]. These studies highlight the potential of nanocomposite-based sensors for detecting HMIs and demonstrate the importance of continued research and development in this field. Our research group has also explored nanocomposite materials based on MOFs, OCPs, and CNTs to detect HMIs [19–29].

Bodkhe et al. [19] investigated the detection of Pb(II) ions using a nanocomposite material consisting of gold nanoparticles (AuNPs) and single-walled CNTs (SWCNTs) embedded within MOF-199. This nanocomposite exhibited high selectivity and sensitivity in detecting Pb(II) ions. Sayyad et al. [20] presented a novel sensor platform for detecting Cu(II) and Pb(II) ions. They have developed a composite material consisting of L-Cysteine anchored PEDOT: PSS (poly(3,4-ethylenedioxythiophene) field-effect transistor doped with poly(styrene sulfonate)) and rGO. This composite material was utilized to fabricate a field-effect transistor (FET)-based sensor for the detection of Cu(II) and Pb(II) ions, two HMIs of environmental concern. Sayyad et al. [21] investigated PEDOT: a PSS and rGO composite material used as the active sensing layer in an organic FET (OFET) device. The device has specificity toward Hg(II) ions, known to be hazardous heavy metal pollutants. Bodkhe et al. [22] successfully incorporated AuNPs into the copper benzene tricarboxylate (CuBTC) MOF to enhance the detection sensitivity and selectivity for Pb(II) ions. Sayyad et al. [23] developed a sensitive detection method for Cu(II) utilizing a composite material composed of rGO and Gly-Gly (glycylglycine). Mahadik et al. [24] presented a novel approach to the detection of Hg(II) using a composite of polyaniline (PANI)/GO. The composite material was modified using ethylenediaminetetraacetic acid (EDTA) to enhance the detection efficiency, which is known for its strong metal ion chelation properties. Al-Gahouari et al. [25] presented a new approach to improve the selectivity of an electrochemical sensor for detecting Pb(II). The sensor was developed using a hybrid material consisting of rGO and MWCNTs. The study highlights the potential of hybrid nanomaterials and the importance of surface modifications in tailoring the selectivity and sensitivity of electrochemical sensors for HMI detection. Patil et al. [26] investigated a novel approach to develop a highly sensitive electrode for detecting Co(II). They utilized a composite material consisting of PANI and SWCNTs.

Additionally, they modified the composite electrode with dimethylglyoxime (DMG), a ligand known for its strong affinity toward Co(II) ions. To further enhance the sensitivity and performance of the electrode, swift heavy oxygen ions were used for irradiation. This process introduces controlled defects and enhances the material's properties for electro-

chemical sensing applications. Deshmukh et al. [27] presented a novel nanocomposite-modified electrode for the electrochemical detection of Cu(II), Pb (II), and Hg(II) ions. The nanocomposite was prepared by incorporating EDTA, PANI, and SWCNTs. The combination of PANI and SWCNTs further enhanced the electrochemical performance of the modified electrode. Deshmukh et al. [28] adopted a new approach for the determination of Ni(II) using a nanocomposite material consisting of PANI and SWCNTs. The nanocomposite was modified using ethylenediamine (EDA), which is known for its metal ion chelation properties. Deore et al. [29] presented an innovative electrochemical sensor based on a chromium–benzenedicarboxylate MOF for the supersensitive and selective detection of toxic metal ions, including Cd (II), Pb(II), and Hg(II). They thoroughly investigated the interactive mechanism between the MOF and the target metal ions to understand the high sensitivity and selectivity of the sensor. By analyzing the interactions, they were able to demonstrate the excellent performance of the sensor in detecting these toxic metal ions at trace levels.

Many review papers on the electrochemical detection of HMIs are available in the literature. Kajal et al. [30] have provided a comprehensive overview of the potential applications of MOFs for electrochemical sensors for environmental analysis. The authors discussed the unique properties of MOFs, including their high porosity, surface area, and tunable properties, which make them attractive candidates for sensor applications. The paper reviews the recent advancement in electrochemical sensors based on MOFs to detect various environmental pollutants, including heavy metals, organic pollutants, and gases. The authors also highlight the challenges and limitations of MOF-based sensors, including stability, reproducibility, and selectivity issues. Overall, the paper provides a valuable reference for researchers and practitioners interested in applying MOFs in electrochemical sensor development for environmental analysis. While the paper briefly mentions the challenges and limitations of MOF-based sensors, such as stability, reproducibility, and selectivity issues, it does not provide a detailed discussion on how these challenges can be addressed or mitigated, which may limit the practicality and applicability of MOF-based sensors.

Munonde et al. [31] discuss the application of nanocomposites in electrochemical sensors to detect HMIs in environmental water samples. The authors emphasize the importance of detecting trace metals in water as they can cause harmful effects on human health and the environment. The paper describes nanocomposites' development using CNTs, graphene, and metal nanoparticles. The authors also discuss the fabrication and characterization of these nanocomposites. The nanocomposites were tested for their effectiveness in detecting trace metals such as lead, cadmium, and mercury in water samples. The results showed that the nanocomposites had high sensitivity and selectivity toward these metals. The paper also highlights the potential applications of these nanocomposites in environmental monitoring and water treatment. The authors suggest that using these nanocomposites as sensors can lead to the development of more efficient and cost-effective methods for detecting trace metals in water. Overall, the research paper provides valuable insights into using nanocomposites as electrochemical sensors for detecting trace metals in environmental water samples and demonstrates their potential for future water monitoring and treatment applications. While the authors provide promising results for detecting trace metals in water samples using nanocomposites, the research was conducted under laboratory conditions. Further research is needed to evaluate the effectiveness of nanocomposites in real-world scenarios.

Buledi et al. [32] have provided a comprehensive overview of the recent developments in using nanocomposite-based sensors to detect HMIs from aqueous media. The paper discusses the properties and synthesis of various nanomaterials such as CNTs, graphene, and metal oxide nanoparticles and their application in developing sensors for heavy metal detection. The authors review the recent advances in the design and fabrication of nanomaterial-based sensors and their applications for detecting heavy metals in aqueous solutions. They discuss the various sensing mechanisms employed in these sensors, such as

electrochemical, optical, and piezoelectric sensing mechanisms. The paper also highlights the advantages and limitations of each sensing mechanism and the challenges in developing efficient and selective sensors for detecting HMIs.

Furthermore, the authors provide a detailed analysis of the HMIs detected using nanomaterial-based sensors, including lead, cadmium, mercury, and arsenic. They discuss the sources of these heavy metals in the environment and the potential health risks associated with their exposure. In conclusion, the paper emphasizes the importance of developing efficient and selective sensors for detecting heavy metals in aqueous media. The use of nanomaterial-based sensors is shown to be a promising approach due to their high sensitivity, selectivity, and rapid response time. The paper highlights the need for further research to address the challenges faced in developing nanomaterial-based sensors and their application in detecting heavy metals in real-world scenarios. Although the paper provides a detailed analysis of various types of nanomaterials and their application in detecting heavy metals, it does not cover all the available nanomaterials or sensing mechanisms for heavy metal detection.

Other researchers also have attempted to write a review of the electrochemical detection of HMIs based on various nanomaterials [33–43]. However, a comprehensive approach to a review of nanocomposite materials for the detection of HMIs, highlighting their beneficial aspects and limitations in terms of their lower detection limit (at par with the level suggested by the USEPA), sensitivity, selectivity, and stability and the use of real-time detection, has been missing in one way or another.

To put our findings into perspective with the state of the art, it should be remembered that several prior review publications have examined the many operational principles of HMI sensors. In contrast, others have focused on the impact of one particular class of materials used to detect HMIs. However, the present review will provide a comprehensive overview of a wide range of nanocomposite materials, their synthesis techniques, and detection techniques for HMIs, and a performance evaluation of electrochemical sensors. Moreover, we have found some research gaps on nanocomposite materials for detecting HMIs, identified some challenging issues in using single nanostructured materials (CNTs, graphene, OCPs, and MOF), and suggested beneficial aspects of using nanocomposites of these materials for electrochemical sensors. This review summarizes the recent advancements in a wide range of nanocomposites for electrochemical sensor applications. It is expected to enhance the comprehension of the factors that affect electrochemical sensor performance and aid readers and researchers in selecting the appropriate nanocomposites for their intended electrochemical sensing investigations. In addition, this review emphasizes the analysis of the sensors based on various nanocomposite materials, specifically according to the aspects of sensitivity, selectivity, the limit of detection (LOD), stability, repeatability, reproducibility, and linearity, in which the studied results help in selecting a particular nanocomposite for specific HMI detection. Finally, we have provided challenges and futuristic aspects in developing portable devices using nanocomposites for the electrochemical detection of HMIs.

## 2. HMI Sensor Modalities: Recent Trends

Various techniques have been developed and utilized to detect HMIs in aqueous solutions, including but not limited to spectroscopic, chromatographic, and electrochemical methods. Some of the spectroscopic detection techniques commonly employed for the detection of HMIs in aqueous media are atomic absorption spectroscopy (AAS), atomic emission spectrometry (AES), atomic fluorescence spectrometry (AFS), X-ray absorption spectrometry (XAS), inductively coupled plasma–mass spectrometry (ICP-MS), and electron spin resonance (ESR) spectroscopy, etc. [28,44,45]. Chromatographic methods are also widely employed for the detection of HMIs in aqueous solutions, with high-performance liquid chromatography (HPLC), ion chromatography (IC), and gas chromatography (GC) being some of the most commonly used techniques. [46]. While these advanced methods provide accurate and sensitive detection of HMIs in laboratory settings, their practical

application can be challenging due to their complex operating procedures, high costs, the requirement for skilled personnel, sophisticated equipment, and lengthy response times. In contrast to spectroscopy and chromatography techniques, some detection methods offer rapid results, such as electrochemistry-based sensors [47], surface plasmon resonance (SPR) sensors [48], chemo-sensors [49], biosensors [50], and electronic sensors [51]. On the other hand, specific sensors, such as biosensors, may necessitate continuous monitoring by an individual to ensure the complete and accurate detection of HMIs. Of all the available sensors for detecting HMIs, recent developments in electrochemical detection techniques and FET-based sensors have shown promising results for sensing HMIs in aqueous environments, primarily due to their exceptional benefits such as ease of handling, real-time detection, rapid response, low cost, and portability [52,53].

The typical experimental arrangement for the electrochemical detection of HMIs involves an electrolytic cell that contains an ionic conductor (an electrolyte) and an electronic conductor (an electrode). In this instance, the electrolyte is an aqueous solution containing HMIs. The potential of the cell is determined at the interface between the electrode and the solution containing the electrolyte. Several half-reactions occur within the electrolytic cell, with one of the relevant half-reactions typically occurring at the working electrode (WE). The reference electrode (RE) is the other electrode with respect to which the potential of the cell is measured. In a typical electrochemical experiment, an external power supply is utilized to generate an excitation signal and determine the response function in the chemical solution while ensuring that various system variables are maintained constant. This can be represented as follows:

**Excitation signal → Electrode → Response function**

The current is usually transferred between the WE and the counter electrode (CE) in a three-electrode cell setup, where the CE is referred to as the third electrode. Figure 1 illustrates a standard three-electrode cell configuration employed for the electrochemical sensing of HMIs in aqueous solutions.

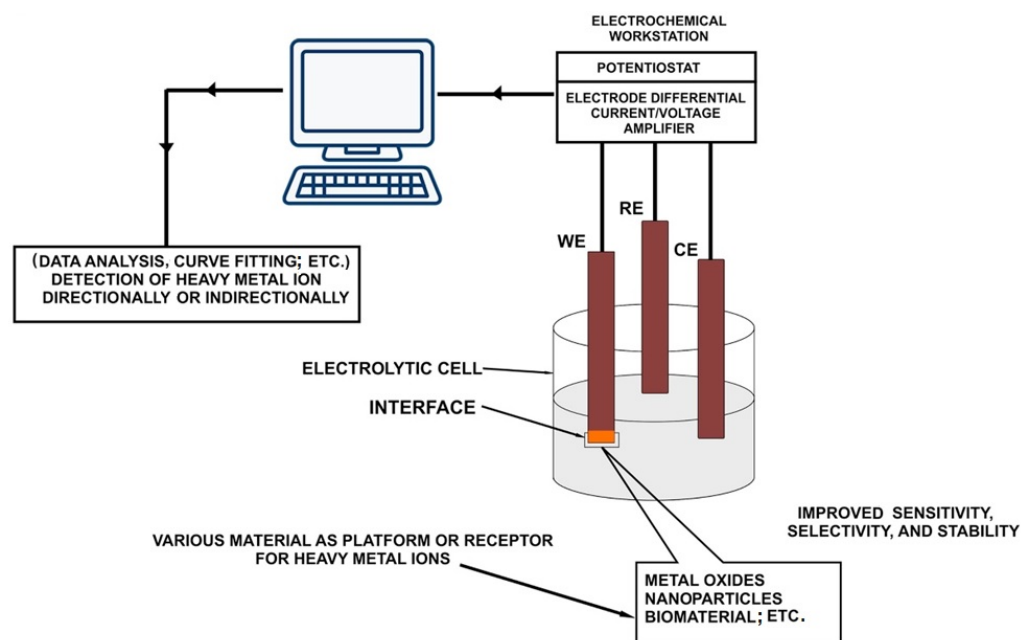


**Figure 1.** The general setup for electrochemical detection of HMIs. Reproduced from [54] with permission from Elsevier.

The present configuration involves the assembly of three distinct electrodes within an electrolytic cell. The WE is subject to controlled modifications utilizing diverse interface materials, thereby acting as a specialized substrate for the manipulation of HMIs. In the framework of this electrochemical configuration, the orchestrated flow of electric

current is primarily confined to the interplay between the WE and the CE. The CE is deliberately positioned in a discrete compartment, spatially segregated from the WE via the implementation of glass separators. The material composition of the CE is judiciously selected to ensure its inertness toward the activities transpiring at the WE, thus maintaining the integrity of the experimental setting. Simultaneously, the potential difference is conventionally established between the WE and the RE, with the facilitation of a high-input impedance apparatus strategically employed to anticipate the extraction of current from the RE. The electrochemical workstation, either as a portable field device or a laboratory instrumentation, establishes a cohesive electrical nexus with the electrode ensemble. This workstation encompasses an integral power source, which serves as the fount for the generation of excitation signals directed toward the electrode configuration. Additionally, the workstation integrates measurement units designed to capture and quantify the responsive signals generated by the system. This electrochemical orchestrator maintains seamless connectivity with a computational infrastructure duly equipped with requisite software platforms tailored to decode, interpret, and subject the experimentally obtained data for comprehensive analysis. In scenarios characterized by solutions exhibiting diminished electrical resistance, a simplified bilayer architecture is invoked. The interplay between the WE and RE encapsulates the essence of a two-electrode cell arrangement, an astute stratagem employed to gauge the nuances underlying electrode potential manifestations [54]. Various electrochemical techniques are available for detecting HMIs in an aqueous solution, categorized by the different electrical signals produced in the solution due to the presence of these ions [55]. Electrochemical techniques for detecting HMIs in an aqueous solution can generate different electrical signals, including current, voltage, electrochemical impedance, charge, and electroluminescence changes. Based on the specific electrical signal generated, electrochemical techniques are classified into several categories: amperometry, voltammetry, potentiometry, electrochemical impedance spectroscopy (EIS), coulometry, and electrochemiluminescence. These techniques have different working principles, advantages, and limitations and can be used in various applications to detect and analyze HMIs in aqueous solutions [56]. An electrochemical measurement can either control the current and measure the resulting potential or control the potential and measure the resulting current. Thus, the measurement techniques are divided into potentiostatic or galvanostatic methods. Most electrochemical techniques for detecting HMIs in an aqueous solution involve controlling one of these parameters to measure the change in the other parameter [54]. Some electrochemical techniques rely on controlling either the current or potential to measure changes in the other parameter, while others, such as potentiometric and impedance measurement techniques, do not require a control signal. Potentiometric methods are used to determine the type of HMIs present by measuring the potential across the electrodes. In contrast, impedance measurement techniques identify changes in double-layer capacitance, solution resistance, and charge transfer resistance caused by HMIs. The detection of HMIs is frequently accomplished using electrochemiluminescence, which measures the light emission generated during the electrochemical reaction. The intensity of this light emission is directly proportional to the concentration of the target analyte [57]. Various electrochemical techniques are employed to detect HMIs in an electrolytic solution based on different measurement signals to determine the analyte concentration and type. These techniques require using various electroanalytical instruments such as high-input impedance potentiometers, galvanostats, and impedance measuring devices. Figure 2 provides a detailed classification of these electrochemical techniques. Illustrated in Figure 2 are electrochemical methods of detection.

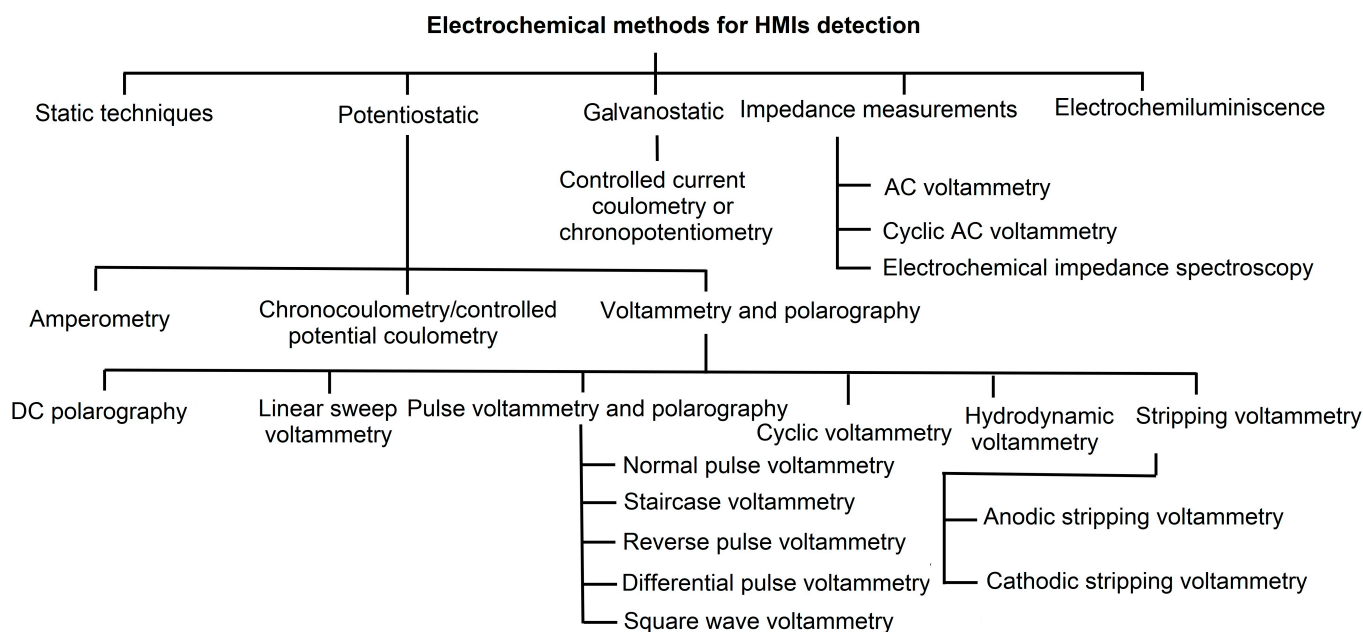


**Figure 2.** Classification tree for various electrochemical methods for HMIs detection. Reproduced from [54] with permission from Elsevier.

HMIs are classified into five main categories such as static techniques, potentiostatic techniques, galvanostatic techniques, impedance measurement, and electrochemiluminescence. In the domain of potentiostatic electrochemical methodologies employed for the detection of HMIs, several techniques are prevalent. Firstly, voltammetry, a technique involving the measurement of current in response to varying applied potentials, offers detailed insights. Variants of this technique such as cyclic voltammetry (CV), differential pulse voltammetry (DPV), and square wave voltammetry (SWV) serve to elucidate electrochemical behaviors, encompassing critical parameters like the oxidation and reduction potentials of HMIs. Secondly, amperometry, which involves monitoring the current at a constant applied potential, is pivotal. This method capitalizes on the proportional current generated upon the reduction or oxidation of HMIs at the electrode surface, boasting high sensitivity and suitability for real-time HMI monitoring applications. In the domain of galvanostatic techniques, chronopotentiometry is a widely employed method. Here, potential measurements are taken at a fixed current over a time, allowing for the correlation of temporal potential changes with varying HMI concentrations. Similarly, EIS analyzes the impedance of an electrochemical cell at a certain frequency range. Using meticulous analysis of impedance spectra, profound insights into the electrode surface characteristics and the underlying electrochemical reactions transpiring at the electrode–electrolyte interface are derived. EIS therefore stands as a pivotal tool, particularly beneficial for comprehending the behavior of HMI sensors within intricate and multifaceted sample matrices.

Apart from the above-mentioned modalities, FET-based devices have garnered wide attention due to their superior characteristics [58]. A FET sensor typically includes three terminals: the source, drain, and gate. The source and drain terminals are connected via sensing channel material, while the back or top gate terminal is used to achieve transistor-like properties. FET sensors work via two main sensing mechanisms: charge modulation and dielectric modulation. In charge-modulated FET sensors, the surface interactions between the sensing channel material and the target analyte cause changes in the channel properties via a direct charge transfer or charge induction effect. Dielectric-modulated FET sensing platforms rely on changes in the gate dielectric constant that result from the binding of the target analyte and sensing probe to perform transduction. As a result, variations in the threshold voltage of the FET sensor occur and can be detected via analysis of the transfer curves. For HMI detection using FET sensors, various sensing channel materials

(e.g., graphene [59], MoS<sub>2</sub> [60], MOF, and MXenes [61]) have been reported, and multiple chemical or biological probes (such as thioglycolic acid (TGA), L-glutathione reduced (GSH), dithiothreitol (DTT), and single-stranded DNA (ssDNA)) have been utilized. The FET sensors utilize the changes in the electrical properties of the sensing channel material caused by the interactions with HMIs. These changes in electrical characteristics are then detected and recorded as response signals, which can be further analyzed for HMIs. By establishing a correlation between the electrical signals generated by the sensing channel material and the concentration of the target analytes, FET sensing platforms can be utilized for the quantitative detection of a wide range of HMIs.

The recent trends in HMI sensor modalities demonstrate remarkable progress toward developing highly sensitive, selective, and reliable sensing platforms. These progressions have uncovered various techniques, including optical, electrochemical, and hybrid approaches, each offering unique advantages for HMI detection. Researchers have achieved remarkable improvements in sensor performance, enabling rapid and accurate detection of HMIs in diverse environmental, industrial, and biological samples due to nanotechnology and material science advancements. The continuous evolution of sensor modalities will address the challenges associated with heavy metal pollution and pave the way for safer and more sustainable environments.

### 3. Portable Electrochemical Sensors

Significant strides have been made in portable electrochemical sensors, with a particular emphasis on detecting HMIs. Leveraging the potential of electrochemical sensing, these cutting-edge developments offer a swift, highly sensitive, and remarkably selective approach to identifying and quantifying these hazardous pollutants.

These portable electrochemical sensors are designed to be small, lightweight, and easy to use. Recent developments in this field have focused on improving the performance of electrochemical sensors. For example, researchers have developed novel electrode materials, like graphene and CNTs, that can enhance the sensitivity of the sensors. They have also used different types of functional groups to modify the electrode surface, improving the selectivity of the sensors.

Portable, handheld sensing devices for the electrochemical detection of HMIs have gained significant attention in recent years due to their ease of use, cost-effectiveness, and portability. These devices are typically designed to be compact, battery-powered, and integrated with a smartphone or other mobile devices, enabling real-time monitoring of HMIs in the field. Several commercial portable and handheld electrochemical sensors for HMIs are available. These devices typically use ion-selective electrodes (ISE) or screen-printed electrodes (SPE) to measure the concentration of HMIs in a sample. Despite the availability of commercial devices, there is still a need for more sensitive, accurate, and reliable portable sensing devices for the electrochemical detection of HMIs. Ongoing research efforts are focused on developing new sensing platforms that can overcome the limitations of current devices, such as poor selectivity, sensitivity, and stability. Recent developments in this field have focused on improving the portability and user-friendliness of these sensors. Researchers have developed smartphone apps that can control the sensors and analyze the data collected [62–68]. Researchers have also developed miniaturized sensors that can be easily carried in a pocket or attached to a keychain [68–71].

Jiang et al. [62] have reported a novel smartphone-based electrochemical cell sensor for evaluating the toxicity of the HMIs Cd(II), Hg(II), and Pb(II). The objective of the research is to create a sensor for assessing the toxicity of these HMIs in rice using a smartphone-based electrochemical cell. The authors used a 3D printing technique to fabricate a low-cost, disposable electrochemical cell sensor. The sensor was then coupled with a smartphone to measure the electrochemical signals of HMIs. The results exhibited that the sensor was highly sensitive and could detect HMIs at low concentrations. The authors also compared the performance of the developed sensor with that of a traditional electrochemical sensor and found that their sensor was more sensitive and had a lower LOD. Overall, the study

suggests that the smartphone-based electrochemical cell sensor can be a promising tool for evaluating the toxicity of HMIs in rice samples.

Recent developments in this field have made significant improvements in the detection of HMIs. However, the existing portable devices for detecting HMIs ions have several shortcomings that can limit their accuracy, reliability, and usability. Some of these shortcomings are:

- Limited sensitivity: Existing portable devices may not be sensitive enough to detect low concentrations of HMIs accurately.
- Poor selectivity: Portable devices can suffer from poor selectivity, leading to false-positive or false-negative results, particularly in complex samples.
- Limited stability: Some portable devices may have a limited operational lifespan due to the degradation of electrodes or instability of the sensing materials, leading to reduced accuracy and reliability.
- Limited sample handling: Some portable devices may require complex sample preparation steps or may not be suitable for use in the field.

Researchers must develop new sensing platforms offering higher sensitivity, selectivity, and stability to address these shortcomings. These platforms include:

- Advanced electrode materials: For example, nanomaterials can improve the sensitivity and selectivity of portable sensing devices.
- Advanced sensing techniques: Researchers are exploring relevant sensing techniques, such as EIS, to enhance the selectivity and sensitivity of portable sensing devices.
- Microfluidic systems: Integrating microfluidic systems into portable devices can enable better control of sample handling and reduce the need for complex sample preparation.
- Machine learning algorithms: Integrating machine learning algorithms can improve the accuracy and reliability of portable sensing devices by enabling real-time data analysis and pattern recognition.

Integrating microfluidic systems into portable devices offers numerous advantages that can significantly improve sample handling and reduce the need for complex sample preparation in various applications. Microfluidics is a technology that deals with manipulating small volumes of fluids within microscale channels, allowing precise control over fluid flow, mixing, and reaction processes. When integrated into portable devices, microfluidic systems offer the following benefits:

- (i) Reduced sample volume: Microfluidic devices require much smaller sample volumes than traditional laboratory setups. This is particularly useful when dealing with rare or expensive samples, as it minimizes waste and allows more tests to be conducted with limited resources.
- (ii) Faster analysis: The inherent characteristics of microfluidic systems enable rapid fluid manipulation, leading to faster reaction times and shorter analysis durations. This is beneficial for point-of-care diagnostics and field-based testing, where quick results are crucial.
- (iii) Enhanced precision and accuracy: Microfluidic systems offer precise control over fluid flow, mixing, and reaction conditions. This level of control leads to higher accuracy in measurements and reduces variability in the results.
- (iv) Portability and accessibility: The compact nature of microfluidic devices makes them highly portable, enabling their use in remote or resource-limited areas where access to sophisticated laboratory infrastructure may be limited.
- (v) Integration with other technologies: Microfluidic systems can be easily integrated with other detection and analysis technologies, such as optical sensors, biosensors, and imaging systems, further enhancing the functionality and versatility of portable devices.

Overall, addressing the shortcomings of existing portable devices for detecting HMIs will require integrating advanced materials, techniques, and algorithms to enhance the sensitivity, selectivity, stability, and usability of these devices.

The development and advancement in portable electrochemical sensors have transformed the field of analytical chemistry by enabling real-time, on-site analysis in various applications. These compact and user-friendly devices offer several advantages, including portability, simplicity, and rapid response times. With the tremendous efforts of researchers ensuring continuous advancements in sensor design, miniaturization, and connectivity, portable electrochemical sensors will play an increasingly vital role in addressing critical challenges and improving our quality of life by providing reliable, accessible, and point-of-need analytical solutions.

#### 4. Nanocomposites for the Detection of HMIs

##### 4.1. MOF-Based Nanocomposites

MOFs are hybrid crystalline porous materials consisting of metal ions and organic 'linker' molecules with an extraordinarily large internal surface area. MOFs have gained attention as a material for detecting HMIs due to their unique structural and chemical properties.

MOFs have several unique characteristics, such as an interconnected pore structure, a uniform pore size, a tunable intra-framework chemical functionality, and an ultrahigh-specific surface area. Moreover, MOFs have the highest reported Brunauer–Emmett–Teller (BET) surface area, which has exceeded  $7000 \text{ m}^2/\text{g}$ , much higher than other porous materials [72]. This aspect of a MOF is advantageous for sensing applications. MOFs have been extensively used for electrochemical applications for the past decade [73]. Modified electrodes with MOFs with active species are ideal for electrochemical sensors for electro-analytical purposes. The highly specific surface areas of MOFs can be utilized to support catalytically active sites with a higher density than other materials.

Moreover, the interconnected porosity of MOFs allows the facile diffusion of the targeted analyte to access these active sites [74]. Moreover, the entire pore structure of MOFs can accommodate various chemical functionalities via diverse synthetic approaches while preserving a substantial degree of porosity [75]. This unique attribute endows MOFs with unparalleled flexibility as electroanalytical platforms, surpassing conventional materials' tunability. Various MOFs have also been used for electrochemical sensors and other applications [76–80].

Several MOFs have been studied and utilized for detecting HMIs due to their high surface area, tunable pore size, and unique chemical properties. Some commonly used MOFs for HMI detection include the following: MIL-101 is a chromium-based MOF known for its high porosity and large surface area. It has been employed for the detection and adsorption of various heavy metal ions, including Cr(III), Cd(II), and Hg(II). The structure of MIL-101-Cr is shown in Figure 3. The assemblage comprises Cr(III) octahedral clusters that intricately link via 1,4-benzenedicarboxylates (terephthalate), culminating in an intricate and immensely porous three-dimensional framework. In the graphical representation, chromium atoms are denoted in green, oxygen atoms in red, and carbon atoms in gray. The exchangeable anions, namely  $\text{NO}_3^-$ ,  $\text{F}^-$ ,  $\text{Cl}^-$ ,  $\text{I}^-$ , and  $\text{CF}_3\text{SO}_3^-$ , are illustrated in blue.

UiO-66 is a zirconium-based MOF with high thermal and chemical stability. It has been employed to detect and remove various HMIs from water, including Pb(II), Cd(II), and Hg(II). The molecular structure of the UiO-66 type MOF compounds is shown in Figure 4. The structural characteristics of UiO-66-type MOFs are elucidated as follows: (top) the MOF is fashioned due to the autonomous amalgamation of metal clusters (depicted in light green) and BCD ligands. This intricate process reveals a striking arrangement wherein each metal cluster intricately coordinates with 12 adjacent clusters (depicted in light blue), resulting in an extraordinarily resilient framework; (bottom) the crystal packing arrangement is observed from two unique perspectives, unveiling the porous attributes inherent to this particular cohort of MOFs.

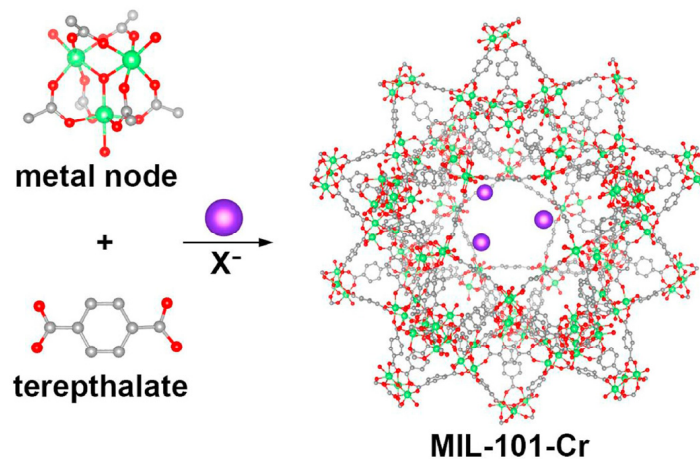


Figure 3. Molecular structure of MIL-101-Cr. Reproduced from [81] with permission from Elsevier.

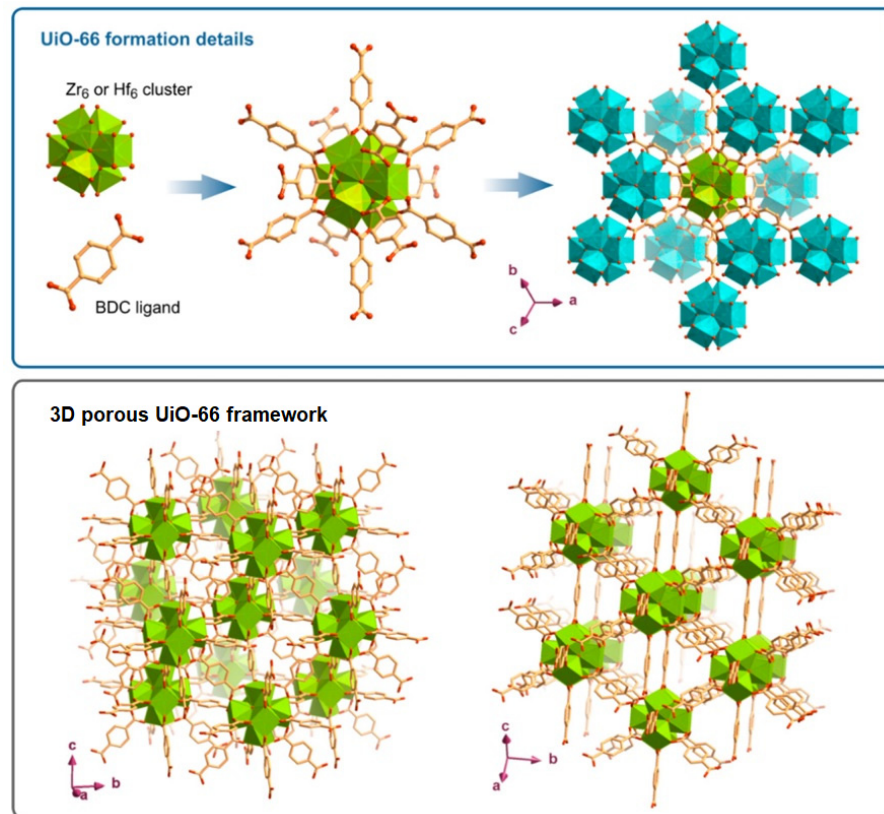
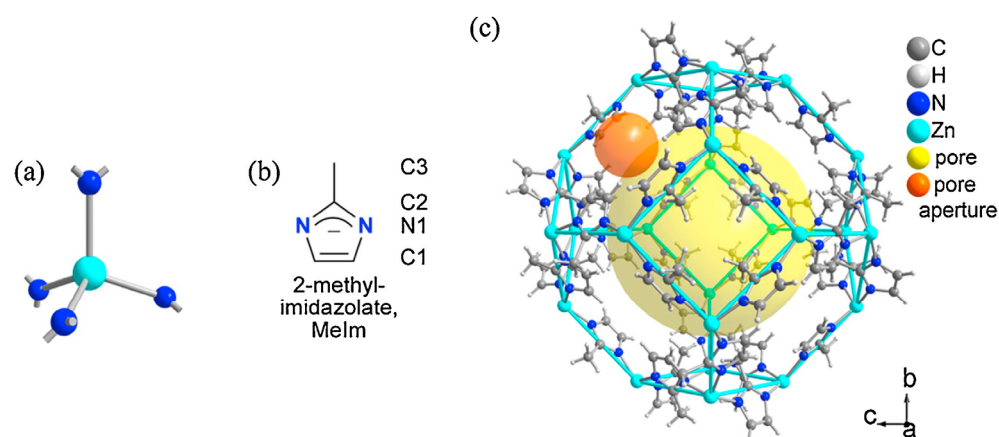


Figure 4. Structural details of the UiO-66-type MOF compounds [82].

Zeolitic imidazolate framework-8 (ZIF-8) is a zinc-based MOF that has been explored for detecting HMIs like Pb(II) and Cd(II) due to its high stability and selective adsorption properties. Figure 5 depicts the constituents and structure of a prototypical three-dimensional MOF of ZIF-8. The elemental components of ZIF-8 consist of tetrahedral nitrogen-coordinated Zn(II) ions (as illustrated in Figure 5a) and 2-methylimidazolate organic ligands (depicted in Figure 5b). These components are intricately arranged and interconnected to form a cage-like unit cell of ZIF-8, as exemplified in Figure 5c. Within each unit cell, a micropore with a diameter measuring approximately 1.16 nm is present, denoted by the yellow sphere in Figure 5c.



**Figure 5.** Structure of ZIF-8. (a,b) The building blocks, and (c) the unit structure of ZIF-8. Reproduced from [83] with permission from Elsevier.

These MOFs have unique structures and properties that make them suitable for HMI detection and removal applications. Researchers continue to explore and develop new MOFs with enhanced selectivity and sensitivity for detecting specific HMIs in different environmental samples.

Some advantages of using MOFs for HMIs detection include the following:

- **Selectivity:** MOFs can be designed with specific ligands to selectively capture certain HMIs, enabling the detection of individual or multiple metal ions in complex samples.
- **Sensitivity:** MOFs have a high surface area and porosity, allowing for efficient adsorption of HMIs and resulting in highly sensitive detection with low detection limits.
- **Tunable properties:** MOFs have tunable properties, including pore size, surface area, and functionality, which can be tailored to enhance their performance for specific HMIs.
- **Fast response time:** MOF-based sensors have a fast response time due to the efficient electron transfer properties of MOFs, allowing for the real-time detection of HMIs.
- **Stability:** MOFs are stable in various chemical and physical conditions, making them suitable for harsh environments.

Overall, MOFs have the potential to be highly effective and efficient materials for HMI detection with applications in environmental monitoring, food safety, and industrial processes. Despite their promising advantages, MOFs also have some limitations, including:

- **Cost:** The production of MOFs can be costly, particularly for large-scale applications. This can limit their use in some industries.
- **Stability:** While MOFs are generally stable, some can degrade over time or in certain conditions, affecting their performance and lifespan as sensors.
- **Reproducibility:** MOFs can be difficult to synthesize with high reproducibility, making it challenging to ensure consistent performance between different batches of sensors.
- **Detection range:** MOF-based sensors may have limited detection ranges for specific HMIs, making them less suitable for detecting trace levels of those ions.
- **Poor electronics conductance:** MOFs have poor electronics conductance, which limits their use for sensor applications.

These limitations highlight the need for continued research and development to optimize MOF-based nanocomposites for HMI detection and to overcome these challenges. Therefore, to address these limitations, researchers have explored other active materials like carbon nanostructures, metal oxide, metal nanoparticles, graphene, etc. Among the different materials, rGO has gained substantial attention from researchers and has been widely used as a nanocomposite with MOFs for detecting HMIs [84–94]. Researchers have explored the use of pristine MOFs [80] and other materials to obtain nanocomposites of MOFs to detect HMIs, for electrochemical applications, and for other applications [80,92,93,95–98].

Fang et al. [84] have reported the development of an electrochemical sensor for detecting ciprofloxacin in water samples using nanocomposites of a Zr(IV)-based MOF and rGO. They have synthesized the Zr(IV)-based MOF and rGO separately and then combined them to create nanocomposites. They found that the addition of rGO to the MOF improved the electrochemical properties of the nanocomposites, making them more sensitive to ciprofloxacin. Then, they tested the nanocomposites for the electrochemical detection of ciprofloxacin in water. They found that the sensor had a linear range of detection between 0.02 and 1  $\mu\text{M}$  and a LOD of 6.67 nM, much lower than the MCL set by the USEPA for ciprofloxacin in drinking water. This research demonstrates the potential of using these nanocomposites as a highly sensitive and selective electrochemical sensor for detecting ciprofloxacin in water samples.

Cui et al. [90] have reported the development of an electrochemical sensor for the detection of Ni(II) using a zeolitic imidazolate framework-8@dimethylglyoxime/ $\beta$ -cyclodextrin/rGO (ZIF-8@DMG/ $\beta$ -CD/rGO). In this work, they combined dimethylglyoxime (DMG) with ZIF-8 based on 2-Methylimidazole (2-MI) and obtained the enrichment unit of ZIF-8@DMG. It was then loaded on conductive rGO modified with  $\beta$ -cyclodextrin ( $\beta$ -CD). The finally synthesized composite ZIF-8@DMG/ $\beta$ -CD/rGO was used to develop a sensor for detecting Ni(II). The coordination bonding and hydrogen bonding were explored to link DMG to ZIF-8. Moreover, the DMG acted as ligand molecules of Ni(II) (Figure 6). The sensor shows good sensitivity and selectivity toward Ni(II) ions, with a wide linear range of 0.01–1.0  $\mu\text{M}$  and a low LOD of 0.005  $\mu\text{M}$ . The sensor also shows excellent stability and reproducibility, making it a promising tool for detecting Ni(II) ions in environmental and industrial settings.

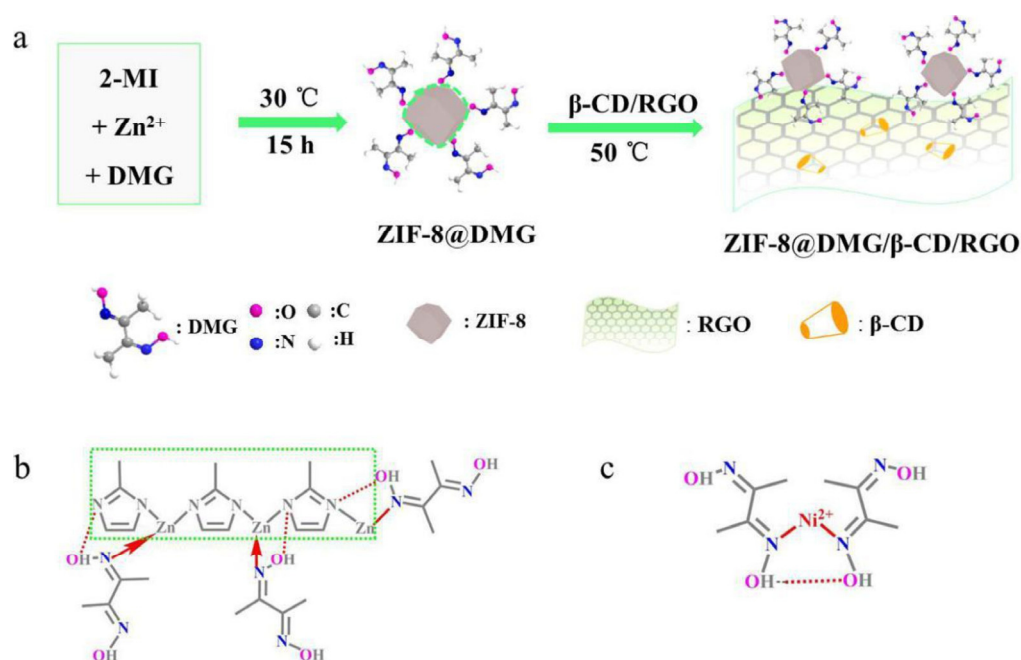


**Figure 6.** Schematic illustrations for (a) fabrication of ZIF-8@DMG/ $\beta$ -CD/rGO; (b) possible interaction mechanism between ZIF-8 and DMG (red arrows represent coordination bonds; red dotted lines represent hydrogen bonds); (c) possible interaction mechanism between DMG and Ni(II) (red arrows represent coordination bonds; red solid lines represent hydrogen bonds). Reproduced from [90] with permission from Elsevier.

Wang et al. [99] have presented the development of a sensitive and selective electrochemical sensor for detecting Pb and Cu ions. The sensor was based on a MOF/polypyrrole (MOF/PPy) nanocomposite functionalized electrode. Employing a chemical polymerization process, PPy nanowires were synthesized, and subsequently, an in situ electrochemical technique was employed to deposit the MOF (NH<sub>2</sub>-MIL-53(Al)) onto the PPy nanosub-

strates. MIL-53 (Matériaux de l'Institut Lavoisier, MIL) belongs to the very prospective classes of MOFs with unique physical properties.

The DPV technique has been employed to assess the electrochemical performance of the sensor. A distinct peak was observed for various concentrations of Pb(II) and Cu(II) during the DPV analysis. Nonlinear enhancement in peak currents was observed in the concentration range of 1 to 400  $\mu\text{g/L}$  (Figure 7), whereas a linear increase in peak currents was observed in the low concentration range of 1 to 20  $\mu\text{g/L}$ . High sensitivity and selectivity toward Pb and Cu ions were observed in the sensor, with LODs of 0.315  $\mu\text{g/L}$  and 0.244  $\mu\text{g/L}$ , respectively. The sensor was also highly stable and reproducible, even after multiple testing cycles.

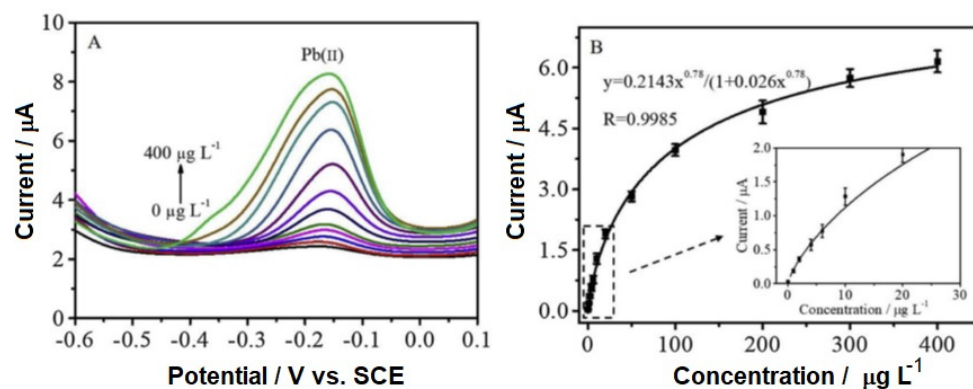


**Figure 7.** DPV response (A) and calibration curve (B) toward Pb(II) in the concentration range of 1–400  $\mu\text{g/L}$ . Reproduced from [99] with permission from Elsevier.

The researchers further tested the sensor's performance in natural water samples collected from tap water. The sensor accurately and precisely detected Pb and Cu ions in these samples. Overall, the study demonstrates the potential of MOF/PPy nanocomposite functionalized electrodes as highly sensitive and selective electrochemical sensors for detecting HMIs in water.

Ru et al. [100] have presented a new method for detecting arsenic in water using a combination of UiO-67 MOF, GO, and platinum nanoparticles (PtNPs). UiO-67 has been synthesized based on Biphenyl-4,4'-dicarboxylic acid (BPDC) as a ligand in the presence of  $\text{ZrCl}_4$ . The UiO-67 MOF has a porous structure that can adsorb and concentrate arsenic, while GO and PtNPs improve the electrochemical properties of the sensor. The sensor was highly sensitive and selective for detecting arsenic in water, with a lower LOD than the safety standard set by the World Health Organization (WHO), as shown in Figure 8. The work concludes that this new sensing platform could be helpful for environmental monitoring and toxicological evaluation. Moreover, their investigation includes the development of a quick, simple, eco-friendly, and sensitive detection method for arsenic in water. Finally, the investigation includes that it has only been tested on a limited range of environmental samples, and further testing is needed to determine its applicability in different contexts.

Zhao et al. [101] have described a new method for detecting HMIs in water samples. The sensing platform comprises cobalt-/nitrogen-doped carbon (NC) composite polyhedrons linked with MWCNTs. Moreover, the sensing platform was also fabricated by growing nanoporous ZIF-67 on MWCNTs, followed by carbonization. Due to its large specific surface area and excellent electrical conductivity, the resulting platform offers numerous active sites for metal ion attachment. Figure 9 shows the schematic diagram of the construction process of the Co@NC/MWCNT-modified electrode and the simultaneous detection of Cd(II) and Pb(II). The platform was tested for detecting these ions in water and showed a relatively wide linear range and low LOD.

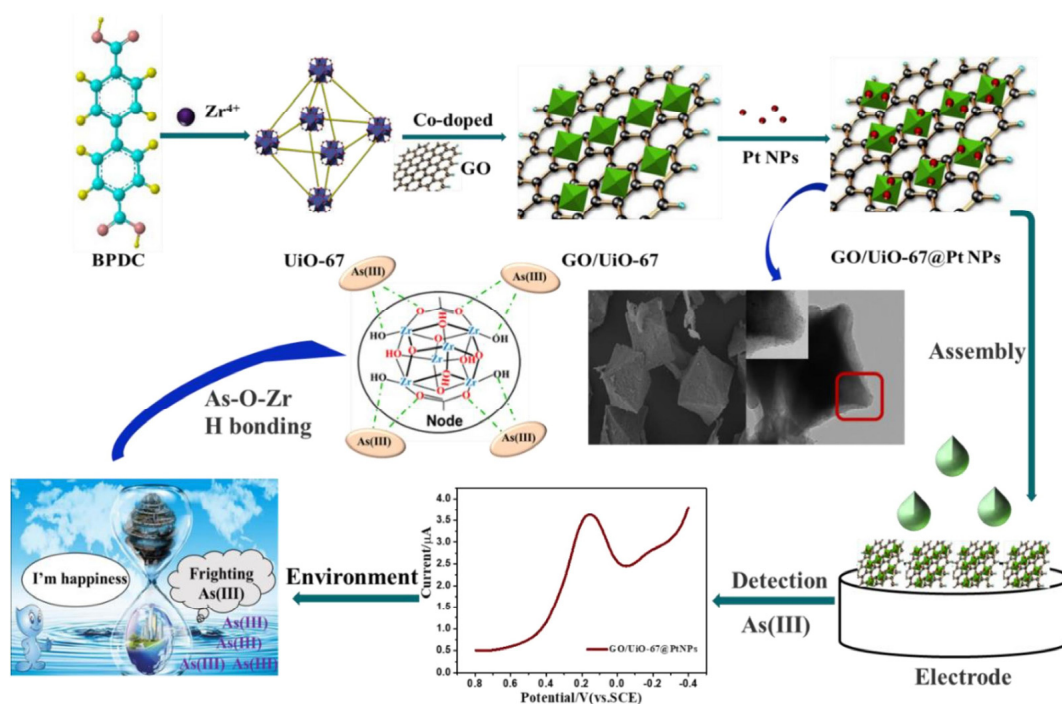


Figure 8. Schematic illustration of the fabrication process of GO/Uio-67@PtNPs for the electrochemical detection of As(III) in water samples. Reproduced from [100] with permission from Elsevier.

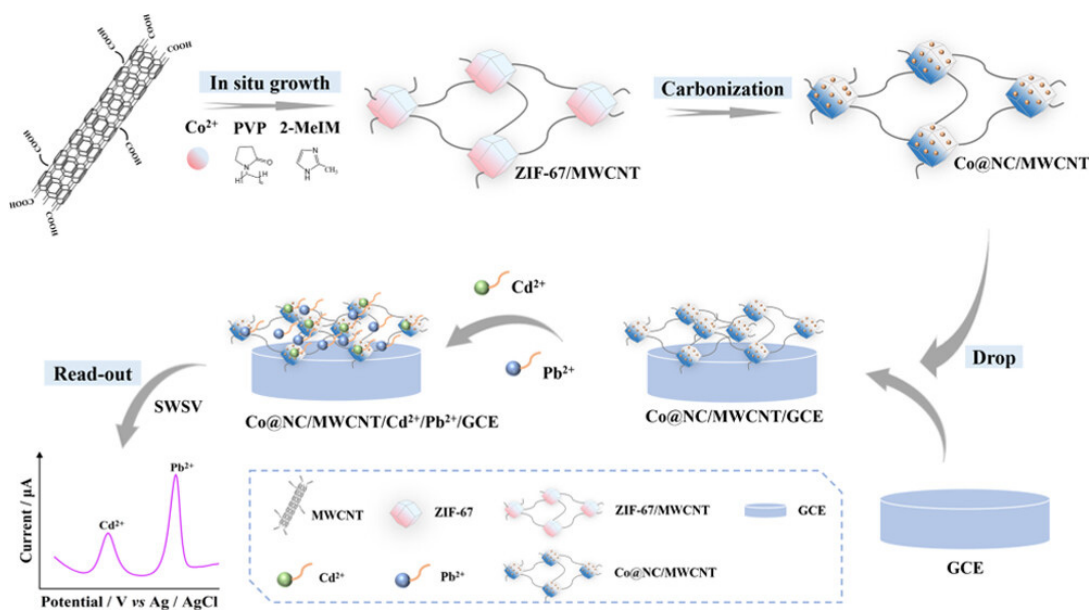


Figure 9. Schematic diagram of the construction process of the Co@NC/MWCNT-modified electrode and the simultaneous detection of Cd(II) and Pb(II). Reproduced from [101] with permission of the American Chemical Society.

Additionally, the platform also demonstrated good anti-interference performance in actual water samples. Moreover, this work concludes that the platform can be used in trace HMI monitoring in natural water environments. However, the investigation has been focused on only two types of HMIs and there is a need for further testing in a wider range of water samples.

Yang et al. [95] have also prepared a new nanocomposite material by attaching mercaptan-functionalized MOFs to three-dimensional kenaf stem-derived carbon (3D-KSC) for the removal and electrochemical detection of Hg(II). The researchers used the coordi-

nation between the Zr(IV) and 2,5-dimercaptoterephthalic acid to prepare the Zr-DMBD MOFs, which were then attached to the 3D-KSC. They also conducted electrochemical measurements and tested the material's ability to remove Hg(II) from natural wastewater. The nanocomposite material showed high sensitivity ( $324.58 \mu\text{A} \cdot \mu\text{M}^{-1} \cdot \text{cm}^{-2}$ ), a linear detection range of  $0.25 \mu\text{M}$ – $3.5 \mu\text{M}$ , and a low LOD of  $0.05 \mu\text{M}$ . It also effectively removed Hg(II) from the natural wastewater.

Moreover, the researchers concluded that the Zr-DMBD MOFs/3D-KSC nanocomposite material was effective for both the removal and detection of Hg(II). This composite has exhibited high sensitivity, selectivity, stability, and reproducibility. This shows great potential as a practical solution for real-world applications. The investigation resulted in the development of a new nanocomposite material that can effectively remove and detect Hg(II) from wastewater. The material has several positive aspects, including high sensitivity, selectivity, stability, and reproducibility. The investigation did not explore the potential for scaling up the production of the nanocomposite material or the cost-effectiveness of using it for practical applications. Additionally, the investigation did not explore the potential for the material to remove or detect other HMIs.

In conclusion, MOF-based nanocomposites have emerged as highly promising materials for detecting HMIs. These nanocomposites offer a unique combination of properties that make them ideal candidates for sensitive and selective detection of HMIs. Incorporating MOFs into nanocomposites provides a high surface area, tunable pore sizes, and exceptional adsorption capabilities, allowing for efficient capture and enrichment of HMIs from complex sample matrices.

#### 4.2. OCP-Based Nanocomposites

OCPs are one of the ideal materials for electrochemical sensors due to their distinctive chemical and electrical properties. Some reasons why OCPs are suitable for electrochemical sensors include the following:

- Electrical conductivity: OCPs are highly conductive, which enables the detection of HMIs due to changes in the electrical properties of the polymer upon interaction with the metal ions.
- Electroactive nature: OCPs are electroactive and can undergo reversible redox reactions at their surface. This property makes them well suited for electrochemical sensors, which rely on redox reactions to detect and quantify analytes.
- Sensitivity: OCPs have high sensitivity to HMIs, allowing for detection at low concentrations.
- Selectivity: The selectivity of OCPs for HMIs can be tailored by modifying the polymer structure or incorporating specific ligands or functional groups, enabling the detection of specific metal ions in complex samples.
- Overall, the unique properties of OCPs make them well suited for electrochemical sensors to detect HMIs, with applications in environmental monitoring, food safety, and industrial processes.

OCPs are highly sensitive to HMIs due to several key factors:

- (i)  $\pi$ -conjugated structure: OCPs possess a  $\pi$ -conjugated backbone consisting of alternating single and double bonds. This extended  $\pi$ -electron system allows for easy delocalization of electrons, making OCPs electronically conductive. Delocalized  $\pi$ -electrons enhance the interaction between the polymer and HMIs, resulting in increased sensitivity.
- (ii) Functional groups: OCPs often contain functional groups with a high affinity for HMIs. These functional groups can act as active metal ion coordination or chelation sites. The presence of these groups increases the chances of specific metal ion binding and enhances the sensitivity of OCPs to HMIs.
- (iii) Surface area: Many OCPs have a porous structure with a high surface area. This increased surface area provides more active sites for HMIs to interact with the polymer, amplifying the sensitivity.

- (iv) Redox activity: OCPs can undergo redox (reduction–oxidation) reactions, leading to changes in their conductivity when exposed to HMIs. The presence of metal ions can affect the redox properties of the OCPs, leading to measurable changes in conductivity or electrochemical signals, which can be used for sensing.

Due to these factors, OCPs have shown great promise in developing highly sensitive and selective sensors for HMIs.

Despite their advantages, conducting polymers also have some limitations for use in electrochemical sensors for the detection of HMIs, including:

- Reproducibility: OCPs can be difficult to synthesize with high reproducibility, making it challenging to ensure consistent performance between different batches of sensors.
- Long-term stability: Some OCPs can undergo degradation over time, affecting their performance and lifespan as sensors.
- Interference: Other ions or molecules in the sample matrix can compete for adsorption sites on the conducting polymer, leading to false positives or reduced sensitivity for detecting the target HMIs.
- Detection range: OCP-based sensors may have limited detection ranges for specific HMIs, making them less suitable for detecting trace levels of those ions.
- Environmental impact: OCPs may have environmental impacts due to their non-biodegradable nature, although efforts are being made to develop more sustainable alternatives.

Therefore, to address these limitations, researchers have explored other materials, such as graphene, CNTs, metal nanoparticles, etc., to form nanocomposites with OCPs [102–117]. These composites offer several advantages, such as high sensitivity, selectivity, stability, and reproducibility, making them suitable for detecting HMIs in various applications. OCP-based nanocomposites are designed to adsorb and capture HMIs from aqueous solutions, and the captured ions are then detected using electrochemical techniques. Incorporating materials such as graphene, CNTs, and metal nanoparticles into the polymer matrix can enhance the sensor's performance by improving the electron transfer rate and increasing the active surface area of the sensor.

The choice of the composite material, its synthesis method, and the electrochemical detection method used can significantly influence the sensor's performance. Composite-based sensors have been successfully applied to detect HMIs in various matrices such as water, soil, and food samples. These sensors have potential applications in environmental monitoring, industrial process control, and medical diagnostics.

Fall et al. [118] have reported a rGO@CNT@Fe<sub>2</sub>O<sub>3</sub>/PPy nanocomposite for the electrochemical detection of Pb(II). The authors started by synthesizing a nanocomposite material comprising rGO, CNTs, iron oxide nanoparticles (Fe<sub>2</sub>O<sub>3</sub>), and PPy. This nanocomposite was then used as a sensing material to detect Pb(II) ions in water samples. The study showed that the rGO@CNT@Fe<sub>2</sub>O<sub>3</sub>/PPy nanocomposite had excellent electrochemical properties, such as a high surface area, good conductivity, excellent stability, and strong adsorption ability toward Pb(II) ions. A linear calibration curve was obtained for the sensor utilizing the rGO@CNT@Fe<sub>2</sub>O<sub>3</sub>/PPy nanocomposite, with a range of 0.02 to 0.26 μM ( $R^2 = 0.992$ ), a sensitivity of 162.8 μA·μM<sup>-1</sup>, and a LOD of 0.1 nM. The nanocomposite showed a broad linear range and a low LOD for Pb(II) ions, indicating its high sensitivity for detecting this heavy metal in water. The authors conducted several experiments to assess the rGO@CNT@Fe<sub>2</sub>O<sub>3</sub>/PPy nanocomposite's performance in detecting Pb(II) ions. The findings demonstrated that the nanocomposite was highly sensitive and selective toward Pb(II) ions, even in the presence of other interfering ions. The synthesis process of rGO@CNT@Fe<sub>2</sub>O<sub>3</sub>/PPy onto the GCE and the electrochemical detection of Pb(II) using SWV are depicted in Figure 10.

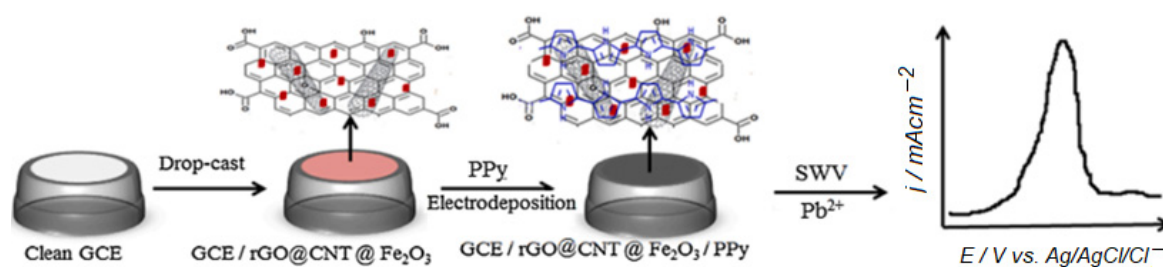


**Figure 10.** A comprehensive schematic illustrating the synthesis of rGO@CNT@Fe<sub>2</sub>O<sub>3</sub>/PPy on the GCE and electrochemical detection of Pb(II). Reproduced from [118] with permission of Elsevier.

Overall, the study demonstrated that the rGO@CNT@Fe<sub>2</sub>O<sub>3</sub>/PPy nanocomposite is a promising material for the electrochemical detection of Pb(II) ions in water samples. Developing such materials is essential for environmental monitoring and protection, as lead contamination in water sources can pose serious health risks to humans and the environment.

A novel electrochemical sensor for detecting Hg(II) has been developed using a Pt/g-C<sub>3</sub>N<sub>4</sub>/PANI nanocomposite, as reported by Mahmoudian et al. [106]. A nanocomposite consisting of platinum, graphitic carbon nitride (g-C<sub>3</sub>N<sub>4</sub>), and PANI was used to fabricate the sensor. A simple and cost-effective method was used to synthesize the Pt/g-C<sub>3</sub>N<sub>4</sub>/PANI nanocomposite and was characterized using various techniques. The electrochemical properties of the Pt/g-C<sub>3</sub>N<sub>4</sub>/PANI nanocomposite were evaluated, and it was found that the nanocomposite exhibited excellent electrocatalytic activity toward the reduction of Hg(II) ions. The fabricated sensor demonstrated a wide linear range of 1–500 nM, with a low LOD of 0.014 nM. The sensor also exhibited good selectivity toward Hg(II) ions, even in the presence of other interfering ions. Overall, the results suggest that the Pt/g-C<sub>3</sub>N<sub>4</sub>/PANI nanocomposite is a promising material for developing high-performance electrochemical sensors to detect Hg(II) ions in environmental and industrial applications. The study highlights the potential of using nanocomposites to develop advanced sensing technologies.

Deshmukh et al. [119] documented an electrochemical method for detecting Pb(II) ions using a nanocomposite platform comprising EDTA-modified PPy/SWNTs. The modified PPy/SWNTs nanocomposite was characterized using various analytical techniques. The authors have investigated the performance of three different electrodes, viz. bare PPy/SSE, PPy/SWNTs/SSE, and EDTA-PPy/SWNTs/SSE, for detecting Pb(II) ions. The highest Pb(II) sensing peak was observed in response to the EDTA-PPy/SWNTs/SSE nanocomposite (Figure 11).

The study demonstrated that this nanocomposite exhibited excellent electrocatalytic activity towards the oxidation of Pb(II) ions and high selectivity and sensitivity. The LOD was found to be as low as 0.07 μM, much lower than the permissible limit set by the WHO. The performance of the sensor based on EDTA-PPy/SWNTs composite exhibited excellent sensitivity for Pb(II) detection over the concentration range from 8 × 10<sup>2</sup> μM to 0.15 μM in 0.5 M H<sub>2</sub>SO<sub>4</sub>. However, the linearity of the sensor was not very appreciating.

In conclusion, OCP-based nanocomposites have emerged as promising and innovative materials for detecting HMIs. These nanocomposites combine the unique properties of conducting polymers with the enhanced functionalities offered by nanomaterials, resulting in highly sensitive, selective, and efficient sensing platforms.

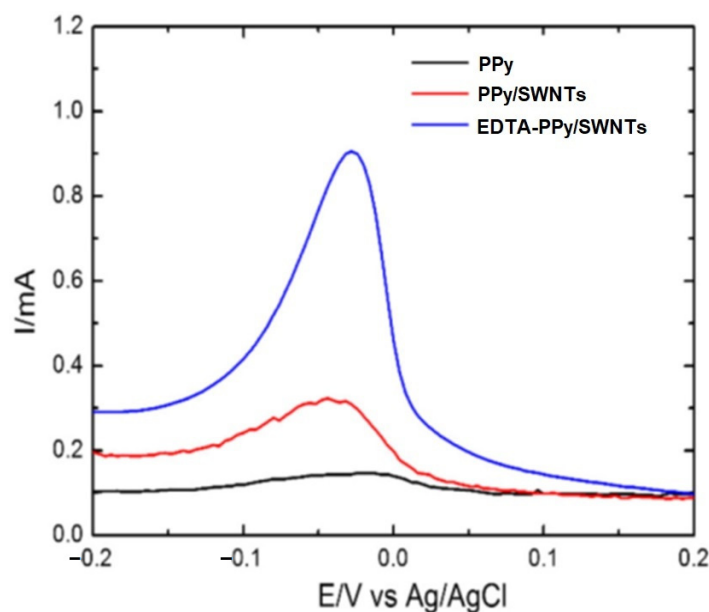


**Figure 11.** DPV-based response of electrodes covered by unmodified PPy, PPy/SWNTs, and EDTA-PPy/SWNTs toward  $8 \times 10^2 \mu\text{M}$  Pb(II) ions dissolved in 0.2 M acetate buffer solution (ABS) pH 4.9, due to the accumulation of metal ions using dip-coating technique followed by stripping with DPV technique. The applied DPV parameters were viz. an increment of 5 mV, the step amplitude of 50 mV, and a pulse period of 0.2 s in 0.5 M  $\text{H}_2\text{SO}_4$  [119].

#### 4.3. CNT-Based Nanocomposites

CNTs are promising materials for detecting HMIs due to their unique structural and chemical properties. Some of the advantages of using CNT-based nanocomposites for HMIs detection include:

- High sensitivity: CNTs have a large surface area and high aspect ratio, allowing efficient HMI adsorption. This results in highly sensitive detection with low detection limits.
- Selectivity: The surface chemistry of CNTs can be modified to selectively capture specific HMIs, enabling the detection of individual or multiple metal ions in complex samples.
- Rapid response time: CNT-based sensors have a fast response time due to CNTs' efficient electron transfer properties. This allows for real-time detection of HMIs.
- Durability: CNTs are highly durable and can withstand harsh chemical and physical conditions, making them suitable for use in various environmental and industrial settings.
- Low cost: CNT-based sensors are relatively inexpensive to produce compared to traditional HMI detection methods, making them a cost-effective alternative.

Overall, CNTs have the potential to be effective and efficient materials for HMI detection with applications in environmental monitoring, food safety, and industrial processes. CNT-based nanocomposites have shown great promise for various applications, including detecting HMIs. However, they do come with certain challenges. While CNTs can exhibit high sensitivity toward HMIs, achieving high sensitivity and selectivity simultaneously can be challenging. Many HMIs have similar chemical properties, making it difficult to distinguish between them solely based on CNT interactions.

Similarly, proper functionalization of CNTs is crucial to enhance their selectivity and sensitivity. Attaching specific molecules or functional groups that selectively interact with target HMIs is complex and requires precise control. Achieving uniform functionalization across nanotubes in a composite can also be challenging. Systematic efforts will be required to address these challenges.

CNTs and their composites have been comprehensively explored for the electrochemical detection of HMIs. In addition, various research groups have also explored other allotropes of carbon along various nanostructured materials for the detection of HMIs.

Various methodologies have been adopted to enhance the synergy of these materials using doping and functionalization processes and developing a hybrid system [19,101,120–128]. In their study, Wu et al. [120] proposed the creation of an economical sensor using  $\text{Fe}_3\text{O}_4$  nanoparticles and fluorinated MWCNTs (F-MWCNTs) for the simultaneous electrochemical detection of multiple heavy metals in both environmental and food samples. The resulting  $\text{Fe}_3\text{O}_4$ /F-MWCNTs composite, synthesized using a hydrothermal method, demonstrated exceptional sensitivity and selectivity. Notably, the developed electrochemical sensor exhibited remarkable performance in detecting Cd(II), Pb(II), Cu(II), and Hg(II) ions using square wave anodic stripping voltammetry (SWASV). It was observed that F-MWCNTs have played a significant role in improving the characteristics of the developed sensor. The recorded sensitivities were as follows: 108.79, 125.91, 160.85, and 312.65  $\mu\text{A}\cdot\mu\text{M}^{-1}\cdot\text{cm}^{-2}$  toward Cd(II), Pb(II), Cu(II), and Hg(II), respectively. These values were significantly higher when compared to the  $\text{Fe}_3\text{O}_4$ /MWCNTs and  $\text{Fe}_3\text{O}_4$ -based sensors. The  $\text{Fe}_3\text{O}_4$ /F-MWCNTs sensor showcased exceptional performance regarding its detection range and sensitivity. Specifically, it exhibited a linear detection range of 0.5–30.0  $\mu\text{M}$  for Cd(II), Pb(II), Cu(II), and 0.5–20.0  $\mu\text{M}$  for Hg(II), with LODs of 0.05, 0.08, 0.02, and 0.05 nM for Cd(II), Pb(II), Cu(II), and Hg(II), respectively. This confirms the impact of F-MWCNTs on composite formation and their utility in improving the sensing characteristics. Furthermore, the sensor's performance was in good agreement with conventional detection methods (ICP-MS or AFS) when tested on soybean and river water samples. Moreover, the sensor demonstrated outstanding selectivity, recovery, reproducibility, and stability. Although  $\text{Fe}_3\text{O}_4$  has wide applications, its use is hindered due to the aggregation issues caused by high surface energy, leading to less catalytic activity. Hence, the composite of  $\text{Fe}_2\text{O}_3$  with F-MWCNTs leads to a synergistic effect in the HMI detection. The fluorination of the MWCNTs raised their conductivity. One possible explanation for the improved heavy metal detection performance of F-MWCNTs is the strong electronegativity of fluorine. This property is believed to impart negative charges on the F-MWCNTs, enhancing the adsorption of HMIs and ultimately resulting in better detection performance.

Bodkhe et al. [19] reported Au-modified SWCNTs incorporated into MOF-199 to detect Pb(II) ions. In this work, the solvothermal route was adopted to synthesize the composite. They observed a significant decrease in the surface area of MOF-199 (1374.98  $\text{m}^2/\text{g}$ ) due to modification by the Au-SWCNTs, i.e., 856.11  $\text{m}^2/\text{g}$ . They used the DPV method to detect the Pb(II) ions. A calibration plot was generated for the electrochemical response of Au/SWCNTs@MOF-199 to Pb(II) ions over a range of 1 pM–0.1 mM ( $R^2 = 0.9958$ ), demonstrating the sensor's high sensitivity.

Additionally, the sensor exhibited a low LOD of 25 pM and a rapid response time of just a few seconds. The proposed system shows the lowest possible LOD compared to earlier reported work. However, scalability toward actual/real samples and the feasibility of the proposed materials for use with flexible substrates is missing in this article. The DPV depicted in Figure 12 demonstrates the selective detection of Pb(II) ions compared to other metal ions. The DPV response indicated the presence of distinctive, well-defined, and separated reduction peaks located at approximately  $-0.45$  V and  $-0.01$  V, solely for Pb(II) ions. The peak shift observed may be attributed to the solution pH, resulting in a rapid stripping response of the electrode.

Additionally, the formation of lead oxide during the accumulation stage with the sensing material (Au/SWCNTs@MOF-199) was concluded. The current peaks for the other metal ions were not as significant as for Pb(II). This confirms that Au/SWCNTs@MOF-199 is selective only for Pb(II) ions.

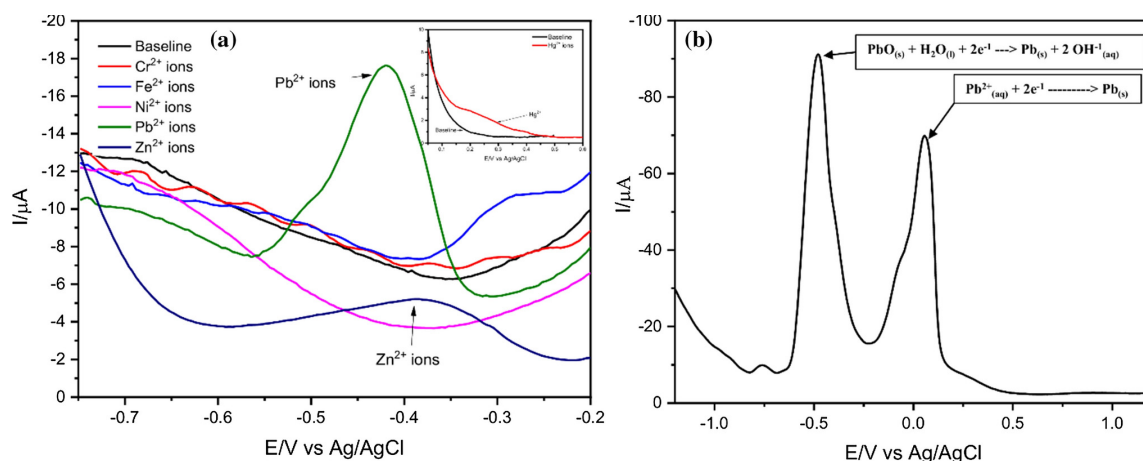


**Figure 12.** (a) Individual sensing response of various metal ions (see inset); (b) interference study of detection of Pb(II) ions. Reproduced from [19] with permission from Springer.

Xu et al. [121] have created a cost-effective, highly sensitive, and active electrochemical sensor by functionalizing  $\text{Fe}_3\text{O}_4/\text{MWCNTs}/\text{laser-scribed graphene}$  composites with a chitosan-modified GCE ( $\text{Fe}_3\text{O}_4/\text{MWCNTs}/\text{LSG}/\text{CS}/\text{GCE}$ ). This sensor was designed to detect Cd(II) and Pb(II) simultaneously using SWASV. Using in situ plating of a bismuth film, they observed favorable electrochemical responses with a broad linear range between 1 and 200  $\mu\text{g}/\text{L}$  and ultralow LODs of 0.1 and 0.07  $\mu\text{g}/\text{L}$  for Cd(II) and Pb(II), respectively. The sensor demonstrated excellent reproducibility, repeatability, stability, and practical applicability, making it highly reliable.

A reliable and sensitive anodic stripping voltammetry (ASV) technique was reported by Le et al. [122], utilizing a series of MWCNTs modified with antimony oxide ( $\text{Sb}_2\text{O}_3/\text{MWCNTs}$ ) paste electrode. This technique was successfully utilized for the electrochemical detection of Cd(II) and Pb(II) ions. Initially, a paste electrode was prepared using a composite of MWCNTs. The MWCNT bulk electrode was subsequently modified using different concentrations (1%, 3%, and 4%) of  $\text{Sb}_2\text{O}_3$ , thereby enhancing the detection capability for Cd(II) and Pb(II) ions. The 3 wt.%  $\text{Sb}_2\text{O}_3/\text{MWCNT}$  electrode displayed outstanding analytical detection capabilities for Cd(II) and Pb(II) using the linear sweep anodic stripping voltammetry (LSASV) technique. The current response exhibited proper linear curves in relation to the concentration of Cd(II) (80–150 ppb) and Pb(II) (5–35 ppb). Interestingly, the analytical sensitivity of the Cd(II) and Pb(II) was 1.93 and 2.69  $\mu\text{A}\cdot\text{L}\cdot\mu\text{g}^{-1}$ , respectively, higher than 1.5 and 1.3 times the individual ion's sensitivity.

Mariyappan et al. [123] conducted a study where they synthesized Sr-doped FeNi-S nanoparticles using a one-step pyrolysis process. These nanoparticles were subsequently integrated with SWCNTs using ultrasonication, forming Sr@FeNi-S/SWCNTs. The electrochemical impedance analysis performed on the Sr@FeNi-S/SWCNT electrode indicated enhanced kinetic charges for transport, outperforming both Sr@FeNi-S and SWCNTs individually. A GCE was modified with Sr@FeNi-S/SWCNTs to enable the selective and sensitive electrochemical determination of trace amounts of Hg(II) using DPV. The results demonstrated a wide linear range of 0.05 to 279  $\mu\text{M}$ , a low LOD of 0.52 nM for Hg(II), and a sensitivity of 1.84  $\mu\text{A}\cdot\mu\text{M}^{-1}\cdot\text{cm}^{-2}$ . This kind of sensing properties are suitable for the real-time sensing of HMIs.

Katowah et al. [124] successfully engineered a distinctive network core-shell structure by incorporating poly(pyrrole-co-o-toluidine) (PPCOT)—NiFe<sub>2</sub>O<sub>4</sub> (NF) NPs along with cross-linked SWCNTs (C-SWCNTs). This well-designed nanocomposite architecture was specifically utilized for the detection of Fe<sup>3+</sup> ions. The superior performance of the sensor can be attributed to the advantageous 3D structure of the C-SWCNTs, which facilitates a significantly enlarged specific surface area, thereby enhancing the electrical conductivity of the ternary PPCOT/NF/C-SWCNT nanocomposite. The fabricated sensor exhibited a

remarkable sensitivity of  $11.02 \mu\text{A} \cdot \mu\text{M}^{-1} \cdot \text{cm}^{-2}$  and a low LOD of  $97.08 \pm 4.85 \text{ pM}$ . Moreover, the sensor demonstrated excellent linearity over a concentration range of 0.1 nM to 0.01 mM, with exceptional reproducibility and response time characteristics. Reproducibility is an important sensor parameter for developing portable sensing devices. Therefore, the synthesized composite can be used in potable sensing devices.

A research team of Yıldız et al. [125] recently published a study on the development of an electrochemical sensor utilizing a pencil graphite electrode (PGE) that had been coated with a combination of MWCNT and nano-sized sodium montmorillonite (NNaM). During the analyte deposition process, bismuth nanoparticles (BiNPs) were added onto the electrode surface to enhance the sensor's performance and improve the electrochemical analysis. The electrochemical quantification of heavy metal cations, namely Zn(II), Cd(II), Pb(II), and Cu(II), was achieved at potentials of approximately  $-1.0$ ,  $-0.70$ ,  $-0.47$ , and  $0.00 \text{ V}$ , respectively. These cations were quantified within linear concentration ranges of  $2.36\text{--}180.0 \mu\text{M}$ ,  $0.32\text{--}240.0 \mu\text{M}$ ,  $0.03\text{--}80.0 \mu\text{M}$ , and  $0.52\text{--}40.0 \mu\text{M}$ , respectively. The results of electrochemical quantification demonstrated that the sensor provides a cost-effective solution with a highly conductive surface area. Moreover, the electrode generates significantly higher SWAS signals, making it a more efficient tool for electrochemical analysis than an unmodified PGE. The repeatability and reproducibility of BiNP/MWCNT-NNaM/PGE electrodes were  $\text{RSD} < 9.5\%$  and  $\text{RSD} < 8.0\%$ , respectively. The interference effects of cations such as Mn(II), Al(III), Ni(II), Sb(III), Co(II), Fe(III), Cr(III), Ca(II), Mg(II), and  $\text{Na}_3\text{PO}_4$ , at concentrations ten-fold lower than the analytes, were found to be tolerable ( $<4.5\%$ ). Remarkably low LODs of  $0.707 \mu\text{M}$ ,  $0.097 \mu\text{M}$ ,  $0.008 \mu\text{M}$ , and  $0.157 \mu\text{M}$  were observed for Zn(II), Cd(II), Pb(II), and Cu(II), respectively. Here, the bismuth nanoparticles (BiNPs) played a significant role in improving the sensing properties of the sensor in terms of sensitivity, LOD, cross-sensitivity, etc.

A recent study by Zhao et al. [101] introduces a novel sensing platform, Co@NC/MWCNT, for the simultaneous monitoring of Cd(II) and Pb(II). This platform is based on ZIF-67-derived cobalt-/nitrogen-doped carbon (NC) composite polyhedrons linked with MWCNTs. The MWCNTs are first grown in situ with nanoporous ZIF-67, followed by carbonization to endow the composite with good electrical conductivity and a large specific surface area. This provides more active sites for subsequent metal ion attachment. The proposed sensing platform showed a relatively more comprehensive linear range of  $0.12\text{--}2.5 \mu\text{M}$ , with lower LODs of  $4.5 \text{ nM}$  (Cd(II)) and  $4.9 \text{ nM}$  (Pb(II)) under optimal parameters.

Yu et al. [126] developed a facile and efficient method for synthesizing a nanocomposite by integrating CNTs with MOFs. The utility of this nanocomposite was demonstrated in constructing an electrochemical sensor specifically designed for detecting Cd(II) in aqueous solutions. To create the sensing surface of the sensor, a droplet of the CNT-MOF nanocomposite was cast onto the electrode and subsequently dried at room temperature. The resulting electrode was then immersed in a Cd(II)-containing acetate buffer solution for electrochemical measurements. Comprehensive electrochemical characterizations confirmed the excellent conductivity and impressive Cd(II)-responsive properties of the CNT-MOF nanocomposite. The electrochemical sensor exhibited satisfactory analytical performance for Cd(II) determination, encompassing a wide linear detection range from  $0.3 \mu\text{M}$  to  $150 \mu\text{M}$  and a low LOD of  $0.2 \mu\text{M}$ , and demonstrated good selectivity. The electrical conductivity of the MOF was comprehensively addressed by synthesizing a composite of the MOF with the CNTs, which confirmed the excellent sensing properties of the developed sensor.

In a recent study conducted by Tan et al. [127], a novel hybrid material named  $\text{NH}_2\text{-UiO-66@ZIF-8}$  (NU66@Z8) was synthesized by integrating an amino-functionalized zirconium-based MOF ( $\text{NH}_2\text{-UiO-66}$ ) with a zinc-based zeolitic imidazolate framework (ZIF-8). This hybrid material, featuring a core-shell architecture, was further combined with carboxylated MWCNTs (CMWCNTs) to fabricate an electrochemical platform for the detection of Pb(II) and Cu(II). The platform was created by depositing the NU66@Z8-CMWCNT composite onto a GCE. Under optimized conditions, the developed sensor

demonstrated exceptional sensing capabilities, including a low LOD of 1 nM for Pb(II) and 10 nM for Cu(II), along with a broad determination range of 0.003–70  $\mu\text{M}$  for Pb(II) and 0.03–50  $\mu\text{M}$  for Cu(II). Moreover, the sensor exhibited high selectivity toward common interfering ions and good repeatability. The real sample recoveries obtained using the proposed sensor ranged from 95.0% to 103% for Pb(II) (with an RSD  $\leq$  5.3%) and from 94.2% to 106% for Cu(II) (with an RSD  $\leq$  5.9%). These results strongly suggest that the NU66@Z8/CMWCNT electrochemical platform is suitable for accurately examining trace heavy metals in the natural environment. It is well known that the functionalization entity attached to the active sites of MOFs will play a vital role in improving their utility for various applications. This study also used an amino-functionalized  $\text{NH}_2\text{-UiO-66}$  with a ZIF-8 MOF for the electrochemical detection of HMIs. The results confirm the importance of the functionalization entity in improving the sensing characteristics.

In conclusion, CNT-based nanocomposites have shown great promise as advanced materials for detecting HMIs. Their unique properties, including high surface area, exceptional mechanical strength, and outstanding electrical and chemical characteristics, make them ideal candidates for sensitive and selective HMI sensing applications. Integrating CNTs into nanocomposites enhances their sensing performance by providing an increased surface area for heavy metal adsorption, improving sensitivity and lower detection limits.

#### 4.4. Graphene-, GO-, and rGO-Based Nanocomposites

Graphene has emerged as a promising material for detecting HMIs due to its unique structural and chemical properties. Some of the advantages of using graphene for HMIs detection include the following:

- High sensitivity: Graphene has an exceptionally high surface-area-to-volume ratio, allowing for efficient HMI adsorption. This results in highly sensitive detection with low detection limits.
- Selectivity: The surface chemistry of graphene can be modified to selectively capture specific HMIs, enabling the detection of individual or multiple metal ions in complex samples.
- Rapid response time: Graphene-based sensors have a fast response time due to graphene's efficient electron transfer properties. This allows for real-time detection of HMIs.
- Stability: Graphene is highly stable and can withstand harsh chemical and physical conditions, making it suitable for use in various environmental and industrial settings.
- Low cost: Graphene-based sensors are relatively inexpensive to produce compared to traditional HMI detection methods, making them a cost-effective alternative.

Graphene's unique properties make it an attractive material for HMI detection with potential applications in environmental monitoring, food safety, and industrial processes. Graphene, GO, and rGO are all promising materials for the electrochemical detection of HMIs due to their unique properties. However, they also come with several challenges when used in nanocomposites for this specific application. While graphene-based materials have a high surface area and excellent electrical conductivity, achieving high sensitivity and selectivity for specific HMIs can be challenging. Modifying graphene surfaces with selective functional groups to enhance ion recognition without sacrificing conductivity is complex.

Similarly, preparing graphene-based nanocomposites often involves intricate fabrication processes, which can be difficult to reproduce consistently. Variability in the preparation methods can lead to inconsistencies in the sensor performance and hinder reliable detection. Addressing these challenges requires more comprehensive and strategic planning to develop reliable, stable, and sensitive graphene-based nanocomposites for the electrochemical detection of HMIs. Graphene/GO and rGO nanocomposites have been explored by various researchers to detect HMIs [129–143].

Cheng et al. [132] have reported the synthesis of rGO and silver nanoparticle (AgNPs) nanocomposites to detect HMIs. The hydrothermal reduction method was used to prepare

the rGO/AgNP composites in this work. The synthesized rGO/AgNP composites were labelled as FxG where x was the volume of the added AgNO<sub>3</sub> solution (2 mL, 4 mL, 6 mL, and 8 mL, respectively), and accordingly, four different combinations, viz. F2G, F4G, F6G, and F8G, were investigated. The scheme of the synthesis of the AgNP and rGO/AgNP composites is shown in Figure 13. In the first step, the GO dispersed in aqueous ammonia (NH<sub>3</sub>H<sub>2</sub>O) was functionalized using triethylenetetramine (TETA). The functionalized GO (FGO) was transformed into a rGO/AgNP composite in the presence of AgNO<sub>3</sub> using the hydrothermal reduction method. The authors reported an extremely low LOD below 0.1 pM. However, the lowest concentration of heavy metals examined was only 1 nM.

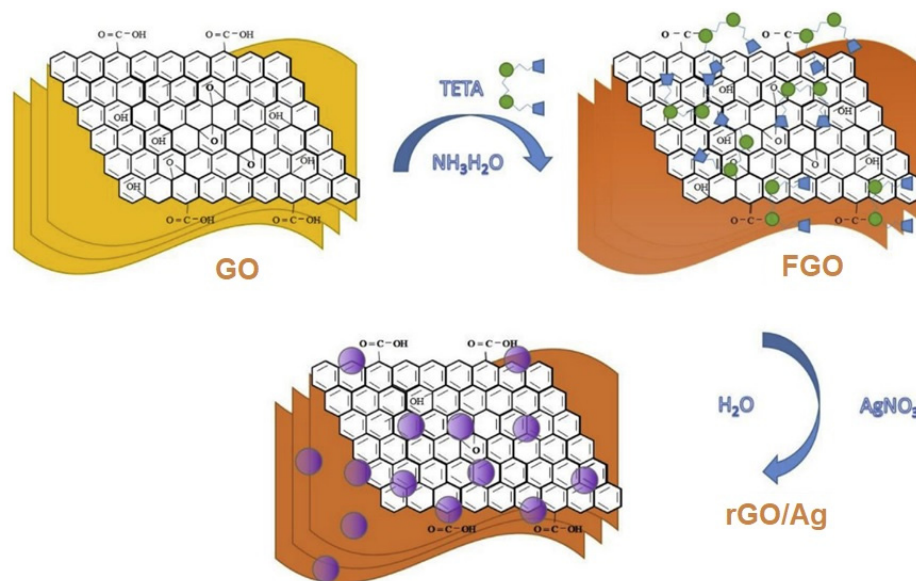


**Figure 13.** The scheme of the formation of AgNP and rGO/AgNP composites. Reproduced from [132] with permission from Elsevier.

In conclusion, graphene-/rGO-based nanocomposites hold great potential for revolutionizing HMI detection technologies. Their remarkable properties, combined with the ability to be tailored to specific applications, make them valuable tools in the sensitive and selective detection of heavy metal contaminants to protect the environment and ensure human well-being. Continued research and development in this field will further explore the full potential of graphene-/rGO-based nanocomposites for addressing pressing environmental and health challenges related to heavy metal pollution.

#### 4.5. Graphitic-Carbon-Nitride-Based Nanocomposites

Graphitic carbon nitride (g-C<sub>3</sub>N<sub>4</sub>) has several advantages for the detection of HMIs:

- High sensitivity: g-C<sub>3</sub>N<sub>4</sub> has a high surface area and strong adsorption ability, allowing it to capture and detect trace amounts of HMIs in the solution.
- Selectivity: g-C<sub>3</sub>N<sub>4</sub> has a high selectivity toward HMIs due to its surface's unique electronic and chemical properties. This means it can distinguish between HMIs and detect only the specific metal ion(s) of interest.
- Low cost: g-C<sub>3</sub>N<sub>4</sub> is a relatively low-cost material, making it an attractive option for practical applications.
- Stability: g-C<sub>3</sub>N<sub>4</sub> is stable under various conditions, including high temperatures and harsh chemical environments, making it suitable for real-world applications.
- Environmental friendliness: Unlike many other HMI detection methods, g-C<sub>3</sub>N<sub>4</sub> does not rely on toxic reagents or generate harmful waste products, making it an environmentally friendly option.

Detecting HMIs often involves using specific reagents to form complex compounds or undergo specific chemical reactions with the target metal ions. Some of these reagents can

be toxic or hazardous, and their use requires proper handling and safety precautions. Some examples are viz. the following: (i) DMG: DMG is commonly used for detecting Ni(II) ions. It forms a distinctive red complex with Ni(II), which can be easily visualized or measured spectrophotometrically; (ii) Dithizone: Dithizone is used for the detection of certain HMIs like Pb(II), Zn(II), and Cd(II). It forms brightly colored complexes with these metal ions, allowing visual detection. These reagents will not be required while using g-C<sub>3</sub>N<sub>4</sub>-based nanocomposites to detect HMIs.

These advantages make g-C<sub>3</sub>N<sub>4</sub> a promising material for detecting HMIs in various settings, from industrial wastewater treatment to environmental monitoring. While g-C<sub>3</sub>N<sub>4</sub> has several advantages for sensor applications, there are also some challenges that researchers have to face:

- Poor conductivity: g-C<sub>3</sub>N<sub>4</sub> is an insulating material with poor electrical conductivity. This limits its usefulness in specific sensor applications that require high conductivity.
- Limited response time: g-C<sub>3</sub>N<sub>4</sub> sensors can have a relatively slow response time compared to other sensing materials, which may limit their use in specific applications that require fast response times.
- Limited stability: While g-C<sub>3</sub>N<sub>4</sub> is generally stable under a wide range of conditions, it can be prone to degradation over time, particularly under certain environmental conditions. This can impact the sensor's performance and longevity.
- Lack of standardization: There is currently a lack of standardized protocols for synthesizing and characterizing g-C<sub>3</sub>N<sub>4</sub>, making comparing results between different studies difficult.
- Sensitivity to environmental conditions: g-C<sub>3</sub>N<sub>4</sub> sensors can be sensitive to changes in environmental conditions, such as temperature and humidity, affecting their performance.

To address these challenges, researchers have explored the advantageous aspects of g-C<sub>3</sub>N<sub>4</sub> using nanocomposites with other materials to detect HMIs [144–152].

Zheng et al. [144] reported disposable electrochemical sensors fabricated on photo paper using screen printing techniques. Bismuth-modified g-C<sub>3</sub>N<sub>4</sub> (Bi/g-C<sub>3</sub>N<sub>4</sub>) was used for the electrochemical detection of Pb(II) and Cd(II). The Bi/g-C<sub>3</sub>N<sub>4</sub> composite was characterized using structural, spectroscopic, morphological, and electrochemical techniques. An electrode based on a Bi/g-C<sub>3</sub>N<sub>4</sub> composite was investigated for detecting Cd(II) in a concentration range from 30 µg/L to 120 µg/L with a LOD of 17.5 µg/L. Similarly, an electrode based on a Bi/g-C<sub>3</sub>N<sub>4</sub> composite was investigated to detect Pb(II) in the 30 to 110 µg/L concentration range. The authors used a novel composite for determining HMIs using an electrochemical modality. The LOD was below the MCL suggested by the USEPA. The sensor exhibited excellent sensitivity with the capability to carry out real sample analysis. However, the sensor's repeatability, reproducibility, and stability aspects were not discussed.

Eswaran et al. [151] developed a simple, cost-effective, and efficient method for fabricating a nano-engineered poly(melamine)/g-C<sub>3</sub>N<sub>4</sub> network (PM/g-C<sub>3</sub>N<sub>4</sub>)-modified screen-printed carbon electrode (SPE) for the simultaneous electrochemical monitoring of toxic HMIs in environmental water. The team used a single-step in situ electrochemical polymerization deposition technique to deposit g-C<sub>3</sub>N<sub>4</sub> and melamine monomer onto a pre-anodized SPE (ASPE) using the CV method. The resulting modified electrode showed high sensitivity and selectivity toward HMI detection. DPV was used to investigate the performance of the PM/g-C<sub>3</sub>N<sub>4</sub>/ASPE sensor in detecting Pb(II) and Cd(II) ions. The PM/g-C<sub>3</sub>N<sub>4</sub>/ASPE sensor exhibited stable, repeatable, anti-interference behavior with the capability of detecting Pb(II) and Cd(II) ions in natural water samples. The DPV response of PM/g-C<sub>3</sub>N<sub>4</sub> for the detection of Cd(II) and Pb(II) is shown in Figure 14a,b, respectively. The sensor exhibited an excellent linear response in a concentration range from 0.1 to 1.0 µM, and the LODs for Pb(II) and Cd(II) were 0.008 µM and 0.02 µM, respectively. The performance of this sensor was also investigated for actual water samples, which is an advantageous aspect of this article. However, the repeatability and reproducibility aspects of the sensors were not discussed.

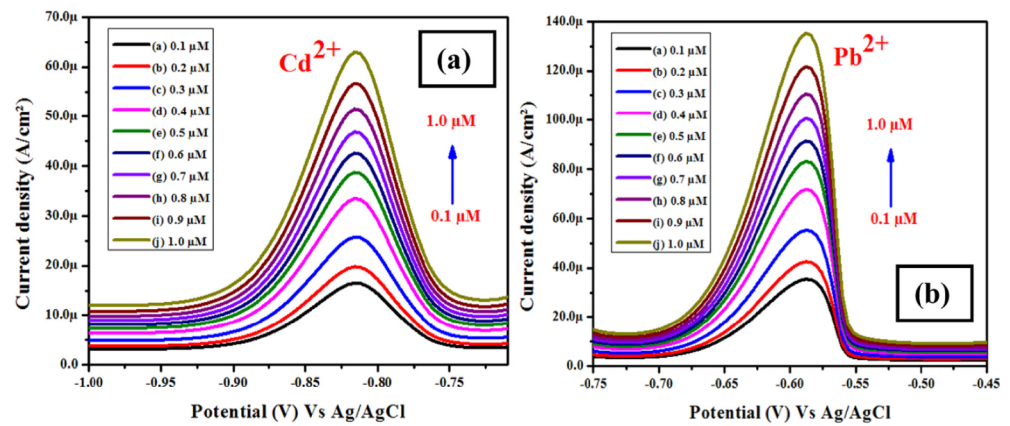


**Figure 14.** The DPV response of the PM/g-C<sub>3</sub>N<sub>4</sub>/ASPE composite-modified electrode of (a) Pb(II) and (b) Cd(II) over a concentration range of 0.1–1.0 μM. Reproduced from [151] with permission from Elsevier.

Hexavalent chromium (Cr(VI)) is a toxic element threatening the human cycle and the environment. Karthika et al. [147] reported a novel electrochemical sensor for detecting this highly toxic element in samples. A g-C<sub>3</sub>N<sub>4</sub>-doped silver molybdate immobilized Nafion (Nf) (g-C<sub>3</sub>N<sub>4</sub>/AgM/Nf)-modified GCE was developed using a straightforward sonochemical approach for the sensor’s construction. The sensor showed excellent selectivity and sensitivity toward the detection of Cr(VI) with a LOD of 1.6 nM and sensitivity of 65.8 μA·μM<sup>-1</sup>·cm<sup>-2</sup>. The sensor also demonstrated good stability and reproducibility with a linear range of 0.1 to 0.7 μM. The proposed sensor can be a reliable and effective tool for detecting Cr(VI) in environmental and industrial samples. The stepwise fabrication of the g-C<sub>3</sub>N<sub>4</sub>/AgM/Nf modified GCE for the Cr(VI) sensor is shown in Figure 15. The sensing response for the g-C<sub>3</sub>N<sub>4</sub>/AgM/Nf modified GCE exhibited a linear response for a range of concentrations of Cr(VI) (10 to 100 μM).

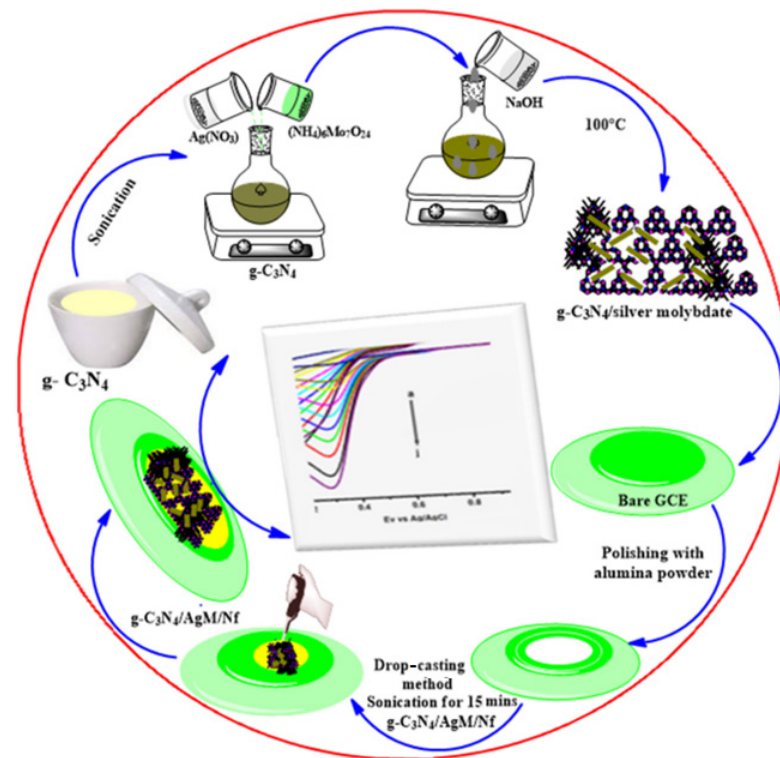


**Figure 15.** The scheme of the stepwise fabrication of g-C<sub>3</sub>N<sub>4</sub>/AgM/Nf-modified GCE for the Cr(VI) sensor. Reproduced from [147] with permission from Elsevier.

In summary, g-C<sub>3</sub>N<sub>4</sub>-based nanocomposites represent a promising frontier in HMI detection technology. Their exceptional properties and tunable selectivity offer a new horizon for developing efficient, sensitive, and selective sensing platforms to safeguard the environment. Continued research and development in this area will undoubtedly open new avenues for addressing the critical challenges of heavy metal pollution.

#### 4.6. Metal-Oxide-Based Nanocomposite

Metal-oxide-based nanocomposites have emerged as a promising solution for detecting HMIs due to their properties to achieve high sensitivity and selectivity of the sensor. These nanocomposites typically comprise a metal oxide nanoparticle and a functional organic or inorganic material. The metal oxide nanoparticles serve as the sensing element, and the functional material enhances the selectivity and sensitivity of the nanocomposite. Several metal oxide nanoparticles, such as zinc oxide, titanium dioxide, and iron oxide, have been incorporated into nanocomposites for HMI detection. Additionally, various functional materials, such as graphene, CNTs, and molecularly imprinted polymers (MIPs), have been used to enhance the selectivity and sensitivity of the nanocomposites. Metal-oxide-based nanocomposites offer several advantages for HMI detection, including high sensitivity, selectivity, and stability.

Moreover, they can be easily integrated into portable devices for the on-site detection of HMIs in environmental samples. While metal-oxide-based nanocomposites offer great potential for detecting HMIs, there are several challenges that researchers will face in their development and use. Some of the key challenges include:

- The successful detection of HMIs within complex samples hinges upon optimizing the sensitivity and selectivity in metal-oxide-based nanocomposites. To achieve this, novel functional materials must be synthesized and enhanced using sensing mechanisms. However, challenges arise due to the potential interference of other ions in the samples, leading to erroneous outcomes. Researchers must devise strategies aimed at mitigating these interferences. Notably, conventional metal oxide nanoparticles often lack the specificity for accurate HMI detection. Their susceptibility to non-selective binding and cross-reactivity with various metal ions further complicates the discrimination between distinct analytes. To address these limitations, the judicious selection of host materials for composite formation becomes pivotal to ensure the desired selectivity in HMI detection.
- Stability and reproducibility: The stability and reproducibility of metal-oxide-based nanocomposites can be affected by environmental factors, such as pH and temperature, impacting their sensing performance. Researchers will need to develop strategies to enhance the stability and reproducibility of these nanocomposites.
- Environmental impact: The potential environmental impact of metal-oxide-based nanocomposites, including their potential release into the environment, is an important consideration that requires careful evaluation.

Therefore, to address these challenges, researchers have explored various nanostructured materials to form nanocomposites with metal oxides for HMI detection and to develop practical applications [116,128,153–169].

A new electrochemical sensing interface utilizing a composite of CeO<sub>2</sub> nanomaterials supported on expanded graphite as the sensitive material was reported by Huang et al. [156]. They synthesized CeO<sub>2</sub> nanomaterials using a hydrothermal method. Three kinds of CeO<sub>2</sub> nanostructures were proposed in the present investigation, and their morphologies are tuned from nanorods (r-CeO<sub>2</sub>) and nanocubes (c-CeO<sub>2</sub>) to nanopolyhedras (p-CeO<sub>2</sub>). Moreover, expanded graphite (EG) has been selected as a support to load these CeO<sub>2</sub> nanomaterials. It has been claimed that an interface using nanorod-shaped CeO<sub>2</sub> nanomaterials supported on expanded graphite exhibits superior electrochemical activity, namely a remarkable signal enhancement for monitoring Cd(II) and Pb<sup>2+</sup> ions. The r-CeO<sub>2</sub> exhibited an excellent electrochemical sensing performance due to the high surface area and the low charge transfer resistance. Simultaneous determination of Cd(II) and Pb(II) ions was

also performed on r-CeO<sub>2</sub>/EG/GCE. The DPV responses for different concentrations of Cd(II) and Pb(II) ions are shown in Figure 16. The sensor based on the r-CeO<sub>2</sub>/EG/GCE composite showed LODs of 0.39 and 0.21 µg/L for Cd(II) and Pb(II) ions, respectively, with good repeatability and reproducibility. However, the stability of the sensor has not been investigated.

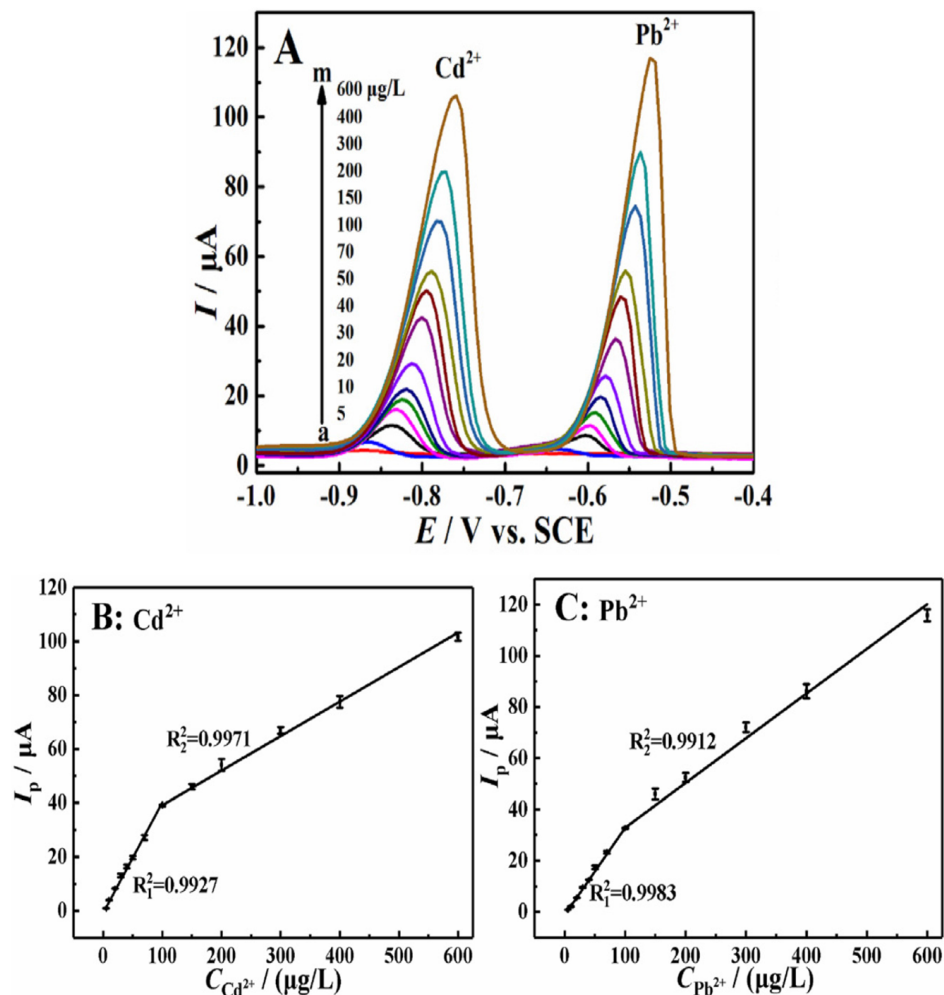


**Figure 16.** (A) DPVs of Cd(II) and Pb(II) with different concentrations; calibration curve for the detection of Cd(II) (B) and Pb(II) (C). The pulse amplitude, pulse width, and scan rate were 50 mV, 40 ms, and 40 mV s<sup>-1</sup>, respectively. Reproduced from [156] with permission from Elsevier.

Singh et al. [166] reported selective and sensitive electrochemical detection of Pb(II) and Cu(II) ions by using cerium-oxide-catalyzed chemical-vapor-deposition-grown carbon nanofibers. Acetylene and cerium oxide were used for growing the Ce-CNFs. As synthesized, Ce-CNFs were multi-parametrically tested for their structural, functional, morphological, and surface area information using X-ray diffraction (XRD), Raman spectroscopy, SEM, and BET. Electrochemical studies of bare GCE and Ce-CNFs/GCE electrodes were undertaken in 0.1 M ABS using CV and DPV methods in optimal experimental conditions. A schematic representation of the steps involved in making a Ce-CNF-based electrochemical sensor for real-time detection of Pb(II) and Cu(II) is shown in Figure 17.

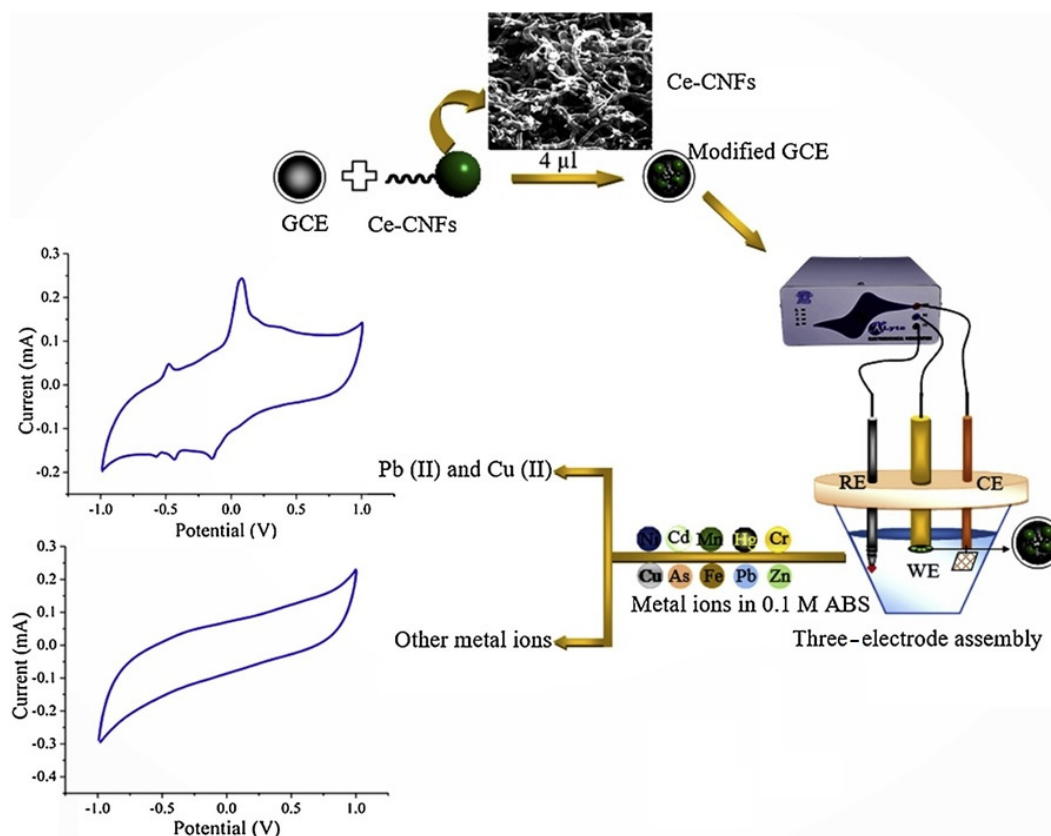


**Figure 17.** The scheme of steps involved in making a Ce-CNF-based electrochemical sensor for real-time Pb(II) and Cu(II) detection. Reproduced from [166] with permission from Elsevier.

The CV response of Ce-CNFs with Cu(II) from a concentration of 0.3 ppb to 10 ppb exhibited significant reproducibility and linearity. It showed excellent linearity from 0.9 ppb to 2.1 ppb of Cu(II). Moreover, DPV analysis was also carried out from  $-0.7$  to  $0.0$  V using optimized parameters. The LOD of Cu(II) was determined at 0.6 ppb.

Wang et al. [167] have reported  $\text{Fe}_3\text{O}_4@\text{PDA}@\text{MnO}_2$  core-shell nanocomposites for the electrochemical detection of Pb(II) ions. In this investigation,  $\text{Fe}_3\text{O}_4@\text{PDA}@\text{MnO}_2$  core-shell magnetic nanocomposites were synthesized for the first time using the solvothermal method. A dense polydopamine (PDA) coating was formed on the surface of the  $\text{Fe}_3\text{O}_4$  to ensure high stability in acidic conditions. The redox activity between the PDA and  $\text{KMnO}_4$  is due to introducing a high-adsorption-capacity  $\text{MnO}_2$  shell into the PDA surface. A  $\text{MnO}_2$  shell with a high adsorption capacity for HMIs was successfully prepared on the  $\text{Fe}_3\text{O}_4$  surface using dopamine and used to detect Pb(II). Further,  $\text{Fe}_3\text{O}_4@\text{PDA}@\text{MnO}_2$  core-shell magnetic NPs were synthesized to improve the sensitivity and selectivity. Figure 18 shows a scheme of the fabrication of the  $\text{Fe}_3\text{O}_4@\text{PDA}@\text{MnO}_2$  core-shell magnetic NPs (A) and the capture, isolation, and detection of the target Pb(II) in the sample solution (B). The DPV technique was used to detect the target analyte. The fabricated sensor linearly detects Pb(II) in the range of  $0.1$ – $150$   $\mu\text{g}/\text{L}$  with an LOD of  $0.03$   $\mu\text{g}/\text{L}$  in optimized electrochemical and chemical conditions in terms of the pH, nanocomposite concentration, supporting electrolytes, and preconcentration time. This method showed excellent repeatability with an RSD value of 2.52% and good stability for up to 4 weeks for  $20$   $\mu\text{g}/\text{L}$  Pb(II). The sensor based on  $\text{Fe}_3\text{O}_4@\text{PDA}@\text{MnO}_2/\text{mGCE}$  can directly monitor trace Pb(II) levels in natural water.

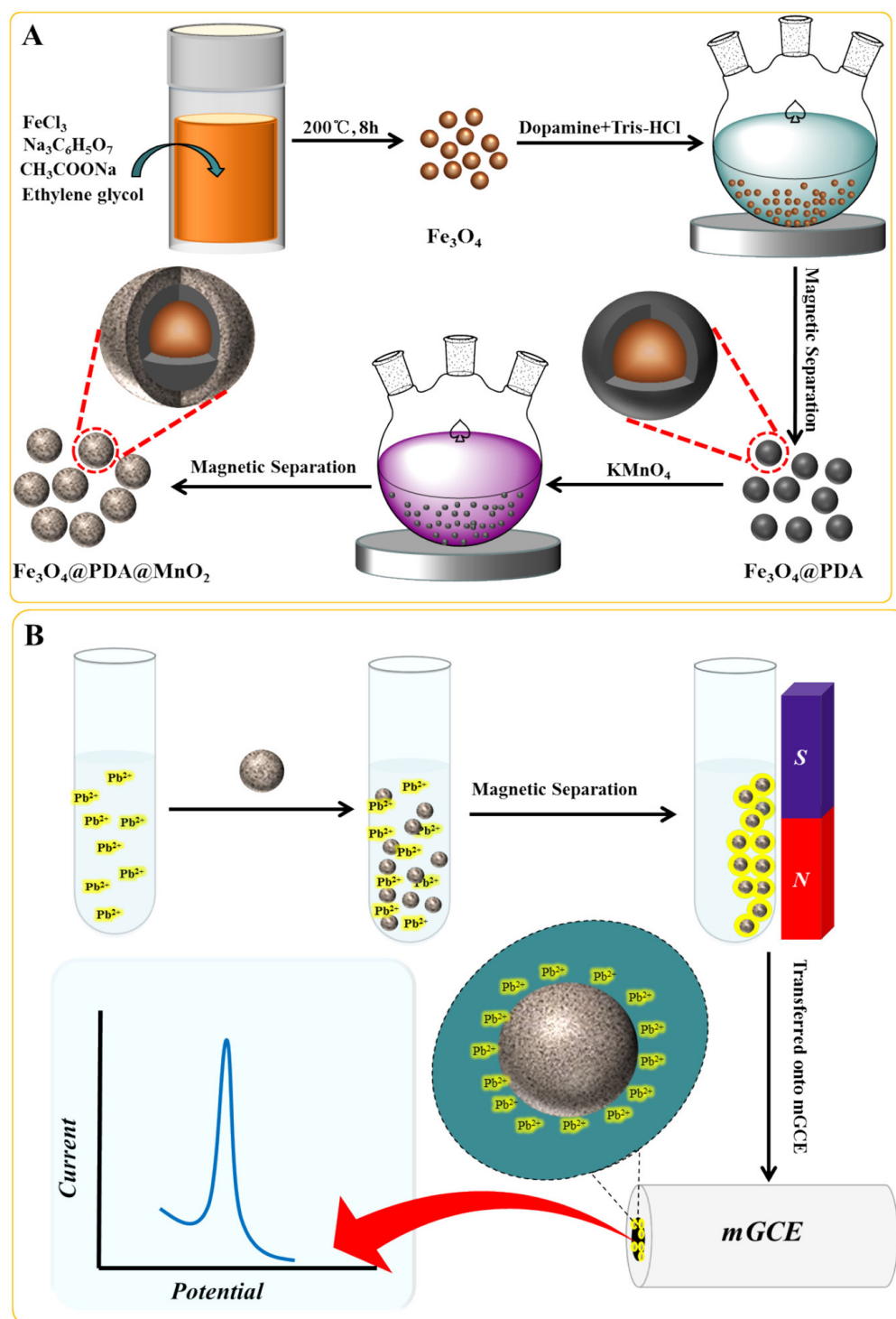


**Figure 18.** The scheme of the fabrication of Fe<sub>3</sub>O<sub>4</sub>@PDA@MnO<sub>2</sub> core-shell magnetic NPs (A) and the capture, isolation, and detection of the target Pb(II) in the sample solution (B). Reproduced from [167] with permission from Elsevier.

In summary, metal-oxide-based nanocomposites represent a promising avenue in HMI detection technology. Metal-oxide-based nanocomposites can be engineered to exhibit specific selectivity toward target HMIs using surface functionalization or doping strategies. This selectivity minimizes the interference from other species, ensuring accurate and reliable detection results.

#### 4.7. Chitosan-Based Nanocomposites

Chitosan-based nanocomposites have shown promise in detecting HMIs in water. These nanocomposites consist of chitosan (CS) and metal oxide nanoparticles, which can interact with HMIs via chelation. This interaction causes changes in the optical or electrical properties of the nanocomposite, which can be detected and measured. CS, as a base material for these nanocomposites, provides several advantages, including biocompatibility, biodegradability, and ease of modification. Overall, CS-based nanocomposites have the potential to be an effective and affordable solution for detecting HMIs in water.

While CS-based nanocomposites offer promising potential for detecting HMIs, researchers may face several challenges in their development and application. Some of these challenges include:

- **Sensitivity:** Achieving a high level of sensitivity to detect trace amounts of HMIs in water, especially in complex or contaminated samples.
- **Stability:** Ensuring the nanocomposites remain stable and do not degrade or lose their effectiveness over time or under different environmental conditions.
- **Interference:** Dealing with potential interference from other substances in the water, such as organic matter, which can affect the detection accuracy.
- **Reproducibility:** Ensuring the detection results are consistent and reproducible over time and across different samples.

Therefore, to address these challenges, researchers are exploring different combinations of materials to form nanocomposites with CS, which has been proved as an excellent platform for detecting HMIs [115,140,142,170–173].

Wang et al. [142] have reported the development of an electrochemical aptasensor for the sensitive detection of Pb(II) using a composite material consisting of CS, rGO, and titanium dioxide (TiO<sub>2</sub>). The aptasensor was fabricated by immobilizing a specific aptamer for Pb(II) onto the composite material and measuring the changes in current upon the binding of Pb(II) to the aptamer. The aptasensor showed high sensitivity and selectivity toward Pb(II) with a LOD of 0.33 ng/L, much lower than the MCL set by the USEPA for Pb(II) in drinking water. The aptasensor was also tested on actual water samples and showed good accuracy and precision. The authors conclude that the developed aptasensor has excellent potential for practical applications in detecting Pb(II) in environmental and biological samples. They have reported a composite containing CS, graphene, and titanium dioxide (CS/rGO/TiO<sub>2</sub>) for detecting Pb(II) ions. The reported CV and EIS results confirmed that the CS/rGO/TiO<sub>2</sub> could improve the electrochemical performance of the electrode and provide a better electrochemical sensing interface. The author reported the development of a novel and sensitive aptasensor for detecting Pb(II) using CS/rGO/TiO<sub>2</sub>. The modified electrode surface was assembled with the complementary strand of the aptamer, which hybridizes with the Pb(II) aptamer to form a DNA double-strand structure. The optimization of experimental parameters, such as the reaction time and the pH of the electrolyte, was performed using DPV.

Moreover, the electrochemical aptasensor was also used to determine the concentration of Pb(II) ions in actual samples with acceptable results. The optimized electrochemical biosensor exhibited a wide range of Pb(II) detection (1 ng/L to 1 µg/L) with a significantly low LOD of 0.33 ng/L, which is well below the MCL suggested by the USEPA and WHO. The DPV responses of the sensor for different concentrations of Pb(II) are shown in Figure 19A, and the calibration curve is shown in Figure 19B. The aptasensor exhibited excellent repeatability, specificity, and stability. Moreover, its performance was evaluated for detecting Pb(II) in food samples, and the results were comparable to those obtained from the ICP-MS method, demonstrating its potential for monitoring Pb(II) levels in food samples.

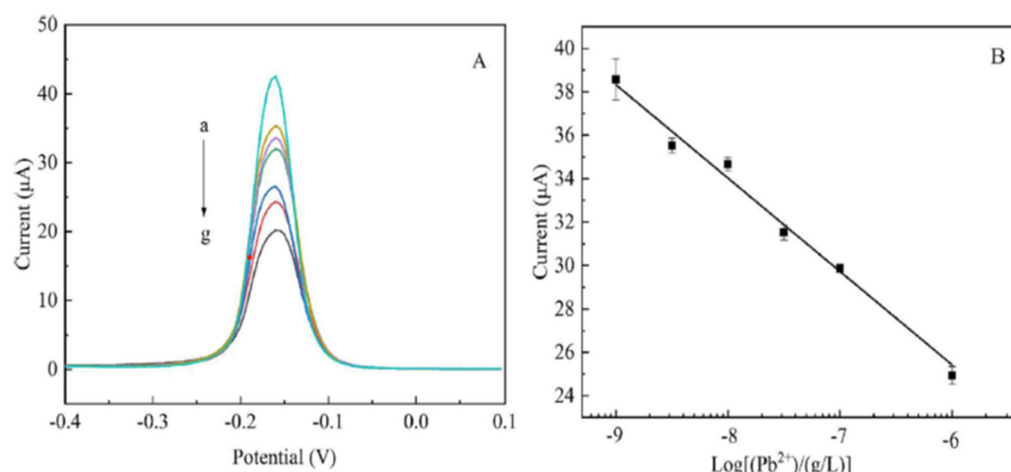


**Figure 19.** (A) DPV responses of different concentrations of Pb(II). The concentration of Pb(II) (g/L): (a) 0; (b)  $10^{-9}$ ; (c)  $10^{-8}$ ; (d)  $5 \times 10^{-7}$ ; (e)  $10^{-7}$ ; (f)  $5 \times 10^{-6}$ ; (g)  $10^{-6}$ , (B) Calibration curve of Pb(II). Reproduced from [142] with permission of Elsevier.

This article reported a novel electrochemical aptasensor for Pb(II) detection based on the specific binding of the apt for the Pb(II) and CS/rGO/TiO<sub>2</sub> composite material. This aptasensor offers the advantages of both rGO's and CS's properties. rGO provides a high surface area and excellent electrocatalysis, which improves the electrochemical sensitivity, while CS offers excellent chemical stability, good biocompatibility, and film-forming abilities.

Guo et al. [140] developed a nanocomposite-modified GCE using rGO/MoS<sub>2</sub>/CS for detecting the Pb(II) in tobacco leaves. The rGO was incorporated to enhance conductivity, while the nano-flowered MoS<sub>2</sub> provided a large specific surface area and active sites for heavy metal reactions. The CS was added to improve heavy metal enrichment and increase the electrocatalytic activity of the electrode. The sensor exhibited excellent performance in terms of reproducibility, stability, and anti-interference ability. The stripping behavior of Pb(II) was studied using SWASV, and the sensor's application conditions were optimized. A schematic diagram of the sensor based on a GCE modified with rGO/MoS<sub>2</sub>/CS and the electrochemical analysis process for Pb(II) is presented in Figure 20. This work used an electrode modified using GO/MoS<sub>2</sub>, rGO/MoS<sub>2</sub>, and rGO/MoS<sub>2</sub>/CS nanocomposites to determine the Pb(II) in an aqueous solution, and the catalytic performance of these electrode-modified materials was evaluated in detail. Among them, the rGO/MoS<sub>2</sub>/CS nanocomposites had the best electrocatalytic performance and sensitivity for Pb(II) detection. The SWASV response of the rGO/MoS<sub>2</sub>/CS/GCE for Pb(II) in the tobacco sample was in a Pb(II) concentration range from 0.005 to 2.0 µM. The LOD of the rGO/MoS<sub>2</sub>/CS/GCE-based sensor was 1.6 nM.

Moreover, the author used a sensor to determine tobacco leaves' Pb(II) content. This work provided a new approach to the determination of Pb(II) in actual tobacco leaf samples, and ICP-MS also verified the results. The LOD was below the MCL suggested by the USEPA and WHO. The operating experimental conditions of the electrode were optimized, such as the pH, deposition potential, and deposition time. The interference study shows that the rGO/MoS<sub>2</sub>/CS nanocomposite is highly selective toward lead ions. Moreover, the sensor based on rGO/MoS<sub>2</sub>/CS/GCE exhibited excellent reproducibility, stability, and anti-interference ability.

In conclusion, CS-based nanocomposites offer a promising solution for HMI detection, combining sensitivity, selectivity, and environmental friendliness. Their application holds significant potential for addressing heavy metal contamination, safeguarding human health, and ensuring the sustainability of our environment.

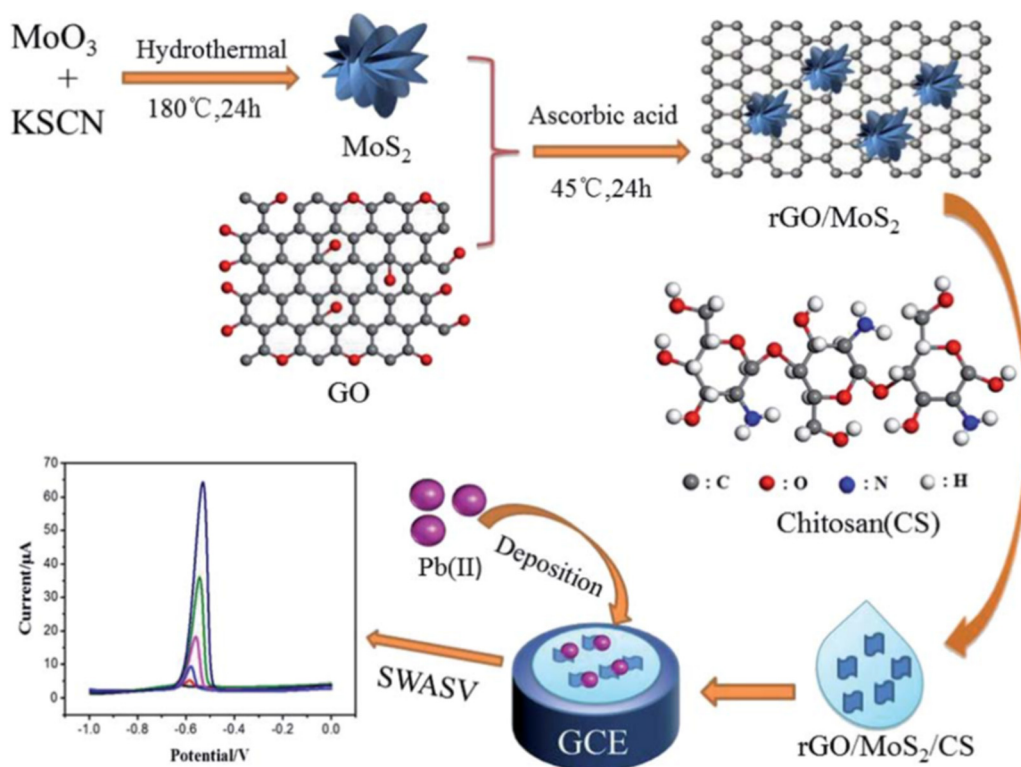


**Figure 20.** Schematic diagram of the constructed sensor based on GCE modified with rGO/MoS<sub>2</sub>/CS and electrochemical analysis process for Pb(II) [140].

#### 4.8. MXene-Based Nanocomposites

MXene-based nanocomposites have emerged as a promising platform for detecting HMIs due to their high surface area, conductivity, and facile surface modification. These nanocomposites typically comprise MXene, a two-dimensional transition metal carbide or nitride, and various other materials, including metal oxides, metal sulfides, and carbon-based materials. The resulting nanocomposites exhibit enhanced sensing properties, such as increased sensitivity, selectivity, and stability, making them attractive candidates for environmental monitoring and biomedical applications. Various detection methods, including electrochemical, optical, and colorimetric, have been employed to detect HMIs using MXene-based nanocomposites. Overall, MXene-based nanocomposites hold great potential for developing effective and efficient sensors for HMI detection. While MXenes have shown great promise for HMI detection, their use still has limitations. The stability of MXene materials is an important factor that can impact their performance and suitability for various applications. MXenes are two-dimensional transition metal carbides, nitrides, or carbonitrides, typically synthesized via selective etching of the A element (such as aluminum or silicon) from MAX phases (such as Ti<sub>3</sub>AlC<sub>2</sub>). The MXenes have a high surface area, which makes them susceptible to oxidation and degradation in specific environments. Exposure to moisture or air can lead to the formation of oxide layers on the surface of MXenes, which can affect their electronic and mechanical properties. In addition, impurities or defects can also impact the stability of MXenes. Researchers have explored various strategies to address these stability issues, such as surface functionalization, doping with other elements, and encapsulation in protective matrices. For example, surface functionalization of MXenes with hydrophobic or hydrophilic groups can improve their stability in different environments. Doping with other elements, such as nitrogen or boron, can also enhance the stability of MXenes and improve their electrochemical performance. Encapsulation of MXenes in protective matrices, such as graphene or polymers, can also prevent their degradation and improve their stability.

Overall, while the stability of MXenes can be challenging to achieve, various researchers have developed and adopted various strategies by synthesizing MXene-based nanocomposites to address these issues and improve their performance for detecting HMIs [174–185].

He et al. reported preparing and applying a bismuth/MXene nanocomposite as an electrochemical sensor for detecting HMIs [174]. This article focuses on developing a new electrochemical sensor for detecting HMIs. The authors synthesized a bismuth/multilayered MXene (Bi/MXene) composite using a simple and efficient method and investigated its performance as an electrochemical sensor for detecting HMIs in water. A nano-form composite of MXenes ( $\text{Ti}_3\text{C}_2\text{T}_x$ ,  $T_x = -\text{O}, -\text{OH}, -\text{F}$ ) was synthesized by depositing bismuth nanoparticles (BiNPs) onto  $\text{Ti}_3\text{C}_2\text{T}_x$  sheets. The results of the study showed that the BiNP/ $\text{Ti}_3\text{C}_2\text{T}_x$  nanocomposite exhibited excellent electrochemical activity and high sensitivity toward HMIs such as Pb(II), Cd(II), and Hg(II). The electrochemical sensor based on the BiNP/ $\text{Ti}_3\text{C}_2\text{T}_x$  nanocomposite also demonstrated good selectivity, stability, and reproducibility. The paper provides a detailed description of the synthesis and characterization of the BiNP/ $\text{Ti}_3\text{C}_2\text{T}_x$  nanocomposite and the fabrication and testing of the electrochemical sensor. The authors also discussed the potential applications of the Bi/MXene composite-based sensor in environmental monitoring and water quality analysis. The performance of the sensor-based BiNPs@ $\text{Ti}_3\text{C}_2\text{T}_x$ /GCE composite was investigated. Figure 21A represents the SWASV curves of Pb(II) at 0, 0.06, 0.08, 0.2, 0.4, and 0.6  $\mu\text{M}$  in the presence of 0.4  $\mu\text{M}$  Cd(II) and the corresponding linear calibration plot against Pb(II) is shown in the inset. Similarly, Figure 21B represents the SWASV curves of Cd(II) at 0, 0.08, 0.1, 0.2, 0.4, and 0.6  $\mu\text{M}$  in the presence of 0.2  $\mu\text{M}$  Pb(II) for the BiNPs@ $\text{Ti}_3\text{C}_2\text{T}_x$ /GCE, and the corresponding linear calibration plot against Cd(II) is shown in the inset. This research paper presents a promising approach for developing highly sensitive and selective electrochemical sensors for detecting HMIs. The sensor based on BiNPs@ $\text{Ti}_3\text{C}_2\text{T}_x$ /GCE has the capability to simultaneously detect Pb(II) and Cd(II) with high sensitivity and good exactness. Utilizing the BiNPs@ $\text{Ti}_3\text{C}_2\text{T}_x$  nanocomposite, the sensor can be an excellent electrode modification material for rapidly and straightforwardly determining the HMIs in the environment.

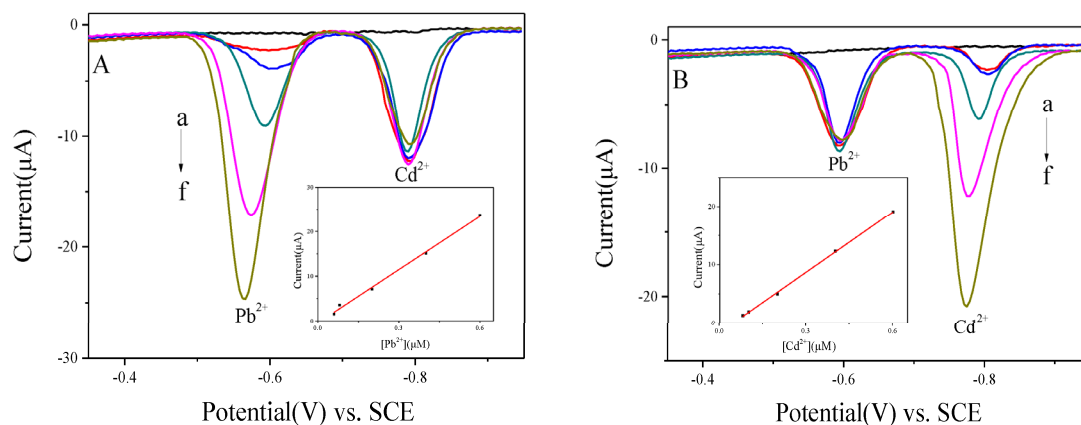


**Figure 21.** (A) SWASV curves of Pb(II) at 0, 0.06, 0.08, 0.2, 0.4, and 0.6  $\mu\text{M}$  in the presence of 0.4  $\mu\text{M}$  Cd(II) for the BiNPs@ $\text{Ti}_3\text{C}_2\text{T}_x$ /GCE and the corresponding linear calibration plots against Pb(II). (B) SWASV curves of Cd(II) at 0, 0.08, 0.1, 0.2, 0.4, and 0.6  $\mu\text{M}$  in the presence of 0.2  $\mu\text{M}$  Pb(II) for the BiNPs@ $\text{Ti}_3\text{C}_2\text{T}_x$ /GCE and the corresponding linear calibration plots against Cd(II) [174].

In summary, MXenes are a highly versatile class of 2D materials that offer numerous benefits when incorporated into composites. The potential for these materials to enhance mechanical, electrical, and thermal properties makes them highly desirable in a wide range of applications, including the detection of HMIs.

#### 4.9. Metal-Nanoparticle- and Other-Material-Based Nanocomposites

Metal-nanoparticle- and other-material-based nanocomposites have been extensively studied as potential materials for detecting HMIs. Metal nanoparticles, such as gold, silver, and copper, have unique optical and electronic properties that make them suitable for sensing applications. They can be easily functionalized with specific ligands that bind selectively to target HMIs. Other materials, such as graphene, CNTs, and MOFs, have also been investigated for their potential in HMI detection. The nanocomposites of nanoparticles and other materials have also been studied for their sensing capabilities. Compared to individual nanoparticles or other materials alone, these composites can provide improved sensitivity and selectivity for HMI detection.

Overall, metal nanoparticles and other materials in nanocomposites show promise in developing efficient and reliable sensing platforms for HMI detection. Researchers studying metal nanoparticles and other material-based nanocomposites for HMI detection may face several challenges during their research. Some of these challenges include:

- Synthesis of metal nanoparticles and other nanocomposites with controlled properties can be challenging. Researchers must carefully control the nanoparticles' size, shape, and surface chemistry to ensure optimal sensing performance.
- Sensitivity and selectivity: Developing high-sensitivity and selectivity sensors for detecting HMIs can be challenging. Researchers must design nanocomposites that selectively bind to target ions while avoiding interference from other species.
- Stability: The stability of metal nanoparticles and other nanocomposites is important for sensing applications. Researchers must ensure the nanocomposites are stable over time and under different environmental conditions to maintain their sensing performance.
- Reproducibility: The reproducibility of sensing results is crucial for practical applications. Researchers need to ensure that the sensing performance of nanocomposites is consistent across different batches and under different conditions.

Therefore, to address these challenges, various possibilities of synthesizing nanocomposite based on metal nanoparticles and other materials have been explored by researchers for the detection of HMIs [186–204].

Naseri et al. [186] reported the development of a robust electrochemical sensor based on a butterfly-shaped silver nanostructure (AgNS/SPCE) for the concurrent quantification of heavy metals in water. The sensor is designed to detect four heavy metals, Pb(II), Cd(II), Hg(II), and Cu(II), commonly found in water. The butterfly-shaped silver nanostructure provides a large surface area for an enhanced sensing performance, while its robustness ensures the stability and reproducibility of the sensor's response. In this work, AgNS was electrodeposited onto the SPCE by applying CV via a sweeping potential between 0 and 1.2 V. The authors also investigated the electrochemical behavior of AgNS/SPCE, described the fabrication process of the sensor, and provided details of its electrochemical characterization. They also demonstrated the sensor's performance in detecting heavy metals in natural water samples and compared its results with those obtained using standard analytical methods. The results show that the sensor exhibits excellent sensitivity, selectivity, and reproducibility for quantifying heavy metals in water. The performance of the sensor based on AgNS/SPCE was investigated for the simultaneous detection of four target metal ions. Figure 22 shows the DPSV responses of the sensor for Cd(II), Pb(II), Cu(II), and Hg(II). Four individual prominent peaks appeared at approximately  $-0.788$  V,  $-0.536$  V,  $-0.209$  V, and  $0.627$  V for Cd(II), Pb(II), Cu(II), and Hg(II), respectively, as can be seen in the DPSV responses.

In conclusion, metal-nanoparticle-based nanocomposites have demonstrated great promise as effective and versatile materials for detecting HMIs. The unique properties of metal nanoparticles and the enhanced functionalities offered by these nanocomposite designs create a highly sensitive, selective, and reliable platform for HMI sensing applications.

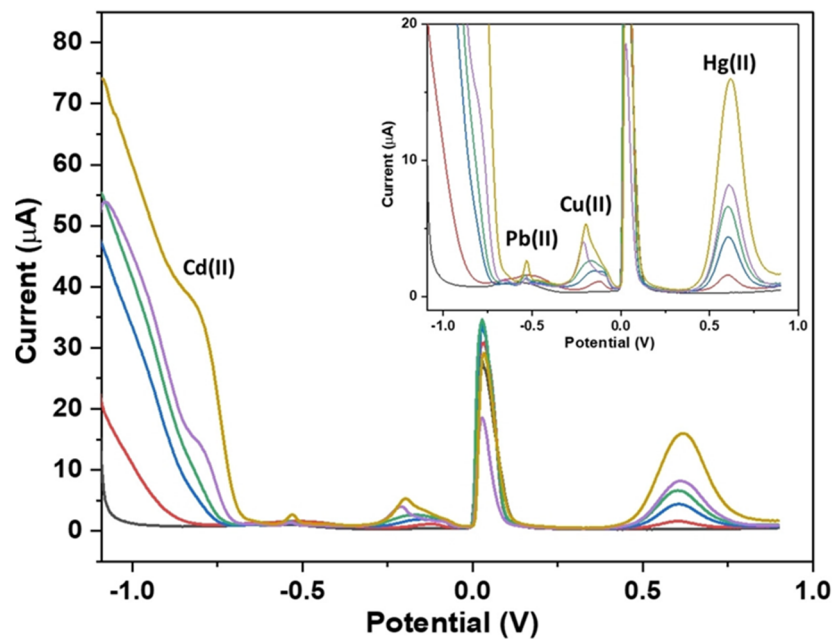


**Figure 22.** DPSV responses of AgNS/SPCE using 0.1 M acetate buffer pH 4.4 containing different concentrations of Cd(II), Pb(II), Cu(II), and Hg(II) [186].

Overall, the study presents a promising approach to developing robust and efficient electrochemical sensors for quantifying heavy metals in water samples, which can have significant implications for environmental monitoring and public health. A summary of the nanocomposites used, the methodology utilized for detection, and the outcomes of the electrochemical sensors regarding sensitivity, the LOD, stability, repeatability, reproducibility, and linearity reported by various researchers is illustrated in Table 2.

**Table 2.** Summary of the properties of the sensors based on nanocomposites for detection of HMIs. (‘Yes’ means the specified characteristics feature of the sensor has been investigated, and ‘No’ means it was not investigated).

| HMIs                                 | Nanocomposite  | Method of Detection | LOD   | Stability (S), Repeatability (Rp), Reproducibility (Re) | Linear Range   | Ref. |
|--------------------------------------|--|---------------------|---|---|--|------|
| Hg(II)<br>Pb(II)<br>Ag<br>Cd(II)     | Sucrose sensor using a platinum ultra-microelectrode | CV                  | Hg(II): $5 \times 10^{-10}$ M<br>Pb(II): $3 \times 10^{-8}$ M<br>Ag: $5 \times 10^{-8}$ M<br>Cd(II): $2.5 \times 10^{-8}$ M | S: No,<br>Rp: No,<br>Re: Yes                            | Hg(II): $(5-12.5) \times 10^{-10}$ M<br>Pb(II): $(5 \times 10^{-8}-2.5 \times 10^{-7})$ M<br>Ag: $(5 \times 10^{-8}-5 \times 10^{-7})$ M<br>Cd(II): $(2.5 \times 10^{-8}-12.5 \times 10^{-8})$ M | [4]  |
| Pb(II)<br>Cd(II)                     | Graphene-MWCNTs                                      | DPASV               | 0.2 µg/L  | S: No,<br>Rp: No,<br>Re: No                             | 0.5–30 µg/L  | [12] |
| Cd(II)<br>Pb(II)<br>Cu(II)<br>Hg(II) | Hydrosulfonyl functional COF (COF-SH)                | SWV                 | Cd: 0.3 µg/L<br>Pb: 0.2 µg/L<br>Cu: 0.2 µg/L<br>Hg: 1.1 µg/L  | S: Yes<br>Rp: Yes<br>Re: No                             | Cd: 0–1000 µg/L<br>Pb: 0–800 µg/L<br>Cu: 0–800 µg/L<br>Hg: 0–1000 µg/L   | [13] |
| Cd(II)<br>Pb(II)                     | Yb-MOF   | DPASV               | Cd: 3.0 ppb<br>Pb: 1.6 ppb  | S: Yes<br>Rp: Yes<br>Re: Yes                            | Cd: 0 to 50 ppb<br>Pb: 0 to 50 ppb   | [15] |
| Cd(II)<br>Pb(II)<br>Cu(II)           | trGNO/Fc-NH <sub>2</sub> -UiO-66                     | DPASV               | Cd: 8.5 nM<br>Pb: 0.6 nM<br>Cu: 0.8 nM  | S: Yes<br>Rp: No<br>Re: Yes                             | Cd: 0.01–2 µM<br>Pb: 0.001–0.1 µM<br>Cu: 0.001–0.1 µM  | [16] |
| Zn(II)<br>Cd(II)<br>Pb(II)           | Fe <sub>2</sub> O <sub>3</sub> /G/Bi                 | DPASV               | Zn: 0.11 µg/L<br>Cd: 0.08 µg/L<br>Pb: 0.07 µg/L   | S: Yes<br>Rp: Yes<br>Re: No                             | Zn: 1–100 µg/L<br>Cd: 1–100 µg/L<br>Pb: 1–100 µg/L   | [17] |
| Pb(II)                               | Au/SWCNTs @MOF-199                                   | DPV                 | 25 pM   | S: No<br>Rp: Yes<br>Re: Yes                             | 1 pM–0.1 mM  | [19] |

Table 2. Cont.

| HMIs                                     | Nanocomposite  | Method of Detection | LOD  | Stability (S), Repeatability (Rp), Reproducibility (Re) | Linear Range   | Ref. |
|--|--|---------------------|--|---|--|------|
| Cu(II)<br>Pb(II)                         | PEDOT:PSS/rGO  | FET                 | Cu: 0.33 µg/L<br>Pb: 2.36 µg/L   | S: No<br>Rp: No<br>Re: No                               | Cu: 1–60 µg/L<br>Pb: 1–60 µg/L   | [20] |
| Cd(II)<br>Pb(II)                         | MOF-derived BCN material   | SWASV               | Cd: 0.41 µg/L<br>Pb: 0.93 µg/L   | S: Yes<br>Rp: Yes<br>Re: Yes                            | Cd: 1–150 µg/L<br>Pb: 2–150 µg/L   | [43] |
| Pb(II)                                   | Transition-metal-ion-assisted PVG  | PVG                 | 0.005 ng/g   | S: No<br>Rp: No<br>Re: No                               | 0.005–100 ng/g   | [44] |
| Pb(II)                                   | Polytetrafluoroethylene (PTFE)   | AAS                 | 0.2 µg/L   | S: No<br>Rp: No<br>Re: No                               | 0.0–8.0 µg/L   | [45] |
| As(III)                                  | 5,10,15,20-tetrakis (4-methoxyphenyl) porphyrinato-cobalt(II) (TMOPP-Co) | FET                 | >10 <sup>-10</sup> M   | S: No<br>Rp: No<br>Re: No                               | 0.1 nM–0.1 mM  | [58] |
| Cd(II)<br>Hg(II)<br>Pb(II)               | rGO/MoS <sub>2</sub>   | DPV                 | Cd: 49.83 µM<br>Hg: 36.94 µM<br>Pb: 733.90 µM<br>(Above are IC <sub>50</sub> values) * | S: No<br>Rp: No<br>Re: No                               | Cd: 5–160 µM<br>Hg: 5–160 µM<br>Pb: 10 to 3000 µM                                | [62] |
| Cd(II), Cu(II),<br>Hg(II), Pb(II)        | rGO/SMOF/PEI modified SPCEs  | DPV                 | Cd: 0.296 µM<br>Cu: 0.055 µM<br>Hg: 0.351 µM<br>Pb: 0.025 µM                           | S: No<br>Rp: No<br>Re: No                               | Cd: 0.50–15.0 µM,<br>Cu: 0.50–13.0 µM,<br>Hg: 1.0–5.0 µM<br>Pb: 0.50–13.0 µM     | [64] |
| Cd(II), Pb(II)<br>and Hg(II)             | Nano Au-modified electrode   | ICP-MS              | Cd: 1.1 µg/L<br>Pb: 1.0 µg/L<br>Hg: 1.2 µg/L   | S: No<br>Rp: No<br>Re: No                               | Cd: 0–200 µg/L<br>Pb: 0–200 µg/L<br>Hg: 0–200 µg/L                               | [65] |
| Pb(II)                                   | Nano Cu WE   | SWV                 | 45 nM  | S: No<br>Rp: No<br>Re: No                               | 0.5–1 µM   | [66] |
| Zn(II), Cu(II),<br>Hg(II), Pb(II)        | DEP chips  | DPV                 | Pb: 2.2 µg/L<br>Hg: 2.5 µg/L<br>Cu: 15.5 µg/L<br>Zn: 10 µg/L                           | S: No<br>Rp: No<br>Re: No                               | Pb: 10–500 ppb<br>Hg: 25–1000 ppb<br>Cu: 25–500 ppb<br>Zn: 10–300 ppb            | [69] |
| Cd(II), Pb(II)                           | Gold/bismuth film  | (SWASV)             | 2.20 µg/L  | S: No<br>Rp: No<br>Re: Yes                              | Cd: 0–300 µg/L<br>Pb: 0–300 µg/L   | [70] |
| Zn, Cr, Cu,<br>Pb, Mn                    | Colorimetric paper strip   | ICP-OES             | Zn: 0.63 mg/L<br>Cr: 0.07 mg/L<br>Cu: 0.17 mg/L<br>Pb: 0.03 mg/L<br>Mn: 0.11 mg/L      | S: Yes<br>Rp: Yes<br>Re: No                             | –  | [71] |
| As(III)                                  | GO/MOF   | DPASV               | 0.06 ppb   | S: No<br>Rp: No<br>Re: Yes                              | 0.2–25 ppb   | [87] |
| Cu(II)                                   | Porphyrinic MOF/rGO nanocomposite  | DPV                 | 1.5 µM   | S: Yes<br>Rp: No<br>Re: No                              | 5–150 µM   | [88] |
| Ni(II)                                   | ZIF-8@DMG/β-CD/RGO   | DPASV               | 0.005 µM   | S: No<br>Rp: No<br>Re: No                               | 0.01–1.0 µM  | [90] |
| Cd(II), Hg(II),<br>Cu(II), and<br>Pb(II) | UiO-66-NH <sub>2</sub> /SPCE   | DPV                 | Cd: 10.90 fM,<br>Pb: 5.98 fM<br>Cu: 2.89 fM<br>Hg: 3.1 fM                              | S: No<br>Rp: No<br>Re: No                               | Cd: 0.01–0.35 pM<br>Pb: 0.01–0.35 pM<br>Cu: 0.01–0.35 pM<br>Hg: 0.01–0.35 pM     | [91] |
| Cd(II), Pb(II),<br>Cu(II), Hg(II)        | Co-TIC4R-I   | SWASV               | Cd: 17 nM<br>Pb: 8 nM<br>Cu: 16 nM<br>Hg: 7 nM   | S: Yes<br>Rp: Yes<br>Re: Yes                            | Cd: 0.10–17.00 µM<br>Pb: 0.05–16.00 µM<br>Cu: 0.05–10.00 µM<br>Hg: 0.80–15.00 µM | [92] |
| Cd(II)<br>Pb(II)                         | CUiO-66/Bi/GCE   | SWASV               | Cd: 1.16 µg/L<br>Pb: 1.14 µg/L   | S: Yes<br>Rp: Yes<br>Re: Yes                            | Cd: 10–50 µg/L<br>Pb: 10–50 µg/L   | [93] |
| Hg(II)                                   | Zr-DMBD MOFs/3D-KSC  | SWASV               | 0.05 µM  | S: Yes<br>Rp: No<br>Re: Yes                             | 0.25–3.5 µM  | [95] |

Table 2. Cont.

| HMIs                              | Nanocomposite                                     | Method of Detection | LOD  | Stability (S),<br>Repeatability (Rp),<br>Reproducibility (Re) | Linear Range   | Ref.  |
|-----------------------------------|---|---------------------|--|---|--|-------|
| Hg(II)                            | Cu-MOF  | DPV                 | 0.063 nM   | S: Yes<br>Rp: Yes<br>Re: Yes                                  | 0.1–50 nM  | [96]  |
| Cd(II), Pb(II),<br>Cu(II), Hg(II) | GaOOH-UiO-MOFs                                    | DPV                 | Cd: 0.016 $\mu$ M<br>Pb: 0.028 $\mu$ M<br>Cu: 0.006 $\mu$ M<br>Hg: 0.019 $\mu$ M | S: Yes<br>Rp: Yes<br>Re: Yes                                  | Cd: 0.35–1.60 $\mu$ M<br>Pb: 0.55–2.50 $\mu$ M<br>Cu: 0.30–1.40 $\mu$ M<br>Hg: 0.10–0.45 $\mu$ M | [97]  |
| Pb (II)<br>Cu (II)                | NH <sub>2</sub> -MIL-53(Al)/PPy                   | DPV                 | Pb: 0.315 $\mu$ g/L<br>Cu: 0.244 $\mu$ g/L                                       | S: Yes<br>Rp: Yes<br>Re: Yes                                  | 1–400 $\mu$ g/L  | [99]  |
| As(III)                           | GO/UiO-67@PtNPs                                   | SWASV               | 0.48 nM  | S: No<br>Rp: Yes<br>Re: Yes                                   | 2.7–33.4 nM  | [100] |
| Cd(II)<br>Pb(II)                  | Co@NC/MWCNT                                       | SWASV               | Cd: 4.5 nM<br>Pb: 4.9 nM   | S: No<br>Rp: No<br>Re: No                                     | 0.12–2.5 $\mu$ M   | [101] |
| Pb(II)<br>Cd(II)                  | Gly/rGO/PANI                                      | SWASV               | Pb: 0.07 nM<br>Cd: 0.072 nM  | S: Yes<br>Rp: Yes<br>Re: Yes                                  | Pb: 0–1.0 $\mu$ M<br>Cd: 0–1.0 $\mu$ M   | [102] |
| Cd(II)<br>Pb(II)                  | Bi-PPy/MWCNT/CPE                                  | SWASV               | Cd: 0.157 $\mu$ g/L<br>Pb: 0.099 $\mu$ g/L                                       | S: Yes<br>Rp: Yes<br>Re: Yes                                  | Cd: 0.16–120 $\mu$ g/L<br>Pb: 0.11–120 $\mu$ g/L   | [103] |
| Cd(II), Pb(II),<br>Cu(II)         | rGO/Ala/PANI                                      | SWASV               | Cd: 0.03 nM<br>Pb: 0.063 nM<br>Cu: 0.045 nM                                      | S: Yes<br>Rp: Yes<br>Re: Yes                                  | 80 pM–100 nM   | [104] |
| Hg(II)                            | Pt/g-C <sub>3</sub> N <sub>4</sub> /PTh NCs       | DPV                 | 0.009 nM   | S: Yes<br>Rp: Yes<br>Re: Yes                                  | 1–500 nM   | [105] |
| Hg(II)                            | Pt/g-C <sub>3</sub> N <sub>4</sub> /PANI NCs      | DPV                 | 0.014 nM   | S: Yes<br>Rp: Yes<br>Re: Yes                                  | 1–500 nM   | [106] |
| Cd(II)                            | 3DGO-Py10   | SWASV               | 3.6 $\mu$ g/L  | S: Yes<br>Rp: Yes<br>Re: Yes                                  | 5–400 $\mu$ g/L  | [107] |
| Mn(II)                            | PMMA-SWCNT NCs/GCE                                | DPV                 | 92.67 $\pm$ 4.63 pM  | S: Yes<br>Rp: Yes<br>Re: Yes                                  | 0.1 nM–0.01 mM   | [108] |
| Cu(II)                            | EDTA-PANI/SWNTs                                   | DPV                 | 1.4 $\mu$ M  | S: No<br>Rp: No<br>Re: No                                     | 0–2 mM   | [112] |
| Hg(II)                            | DETTDC2   | Amperometric        | 12.80 $\pm$ 0.64 pM  | S: Yes<br>Rp: Yes<br>Re: Yes                                  | 0.1 nM–0.01 M  | [116] |
| As(III)                           | Ag@SiO <sub>2</sub> /PANI NFs                     | SWASV               | 0.013 $\mu$ g/L  | S: Yes<br>Rp: Yes<br>Re: No                                   | 0.1–100 $\mu$ g/L  | [117] |
| Pb(II)                            | rGO@CNT@Fe <sub>2</sub> O <sub>3</sub> /GCE       | SWASV               | 0.1 nM   | S: Yes<br>Rp: Yes<br>Re: Yes                                  | 0.02–0.26 $\mu$ M  | [118] |
| Pb(II)                            | DTA-PPY/SWNTs                                     | DPV                 | 0.07 $\mu$ M   | S: No<br>Rp: No<br>Re: No                                     | 0.15–800 $\mu$ M   | [119] |
| Cd(II), Pb(II),<br>Cu(II), Hg(II) | Fe <sub>3</sub> O <sub>4</sub> /F-MWCNTs          | SWASV               | Cd: 0.05 nM<br>Pb: 0.08 nM<br>Cu: 0.02 nM<br>Hg: 0.05 nM                         | S: Yes<br>Rp: Yes<br>Re: No                                   | Cd: 0.5–30.0 $\mu$ M<br>Pb: 0.5–30.0 $\mu$ M<br>Cu: 0.5–30.0 $\mu$ M<br>Hg: 0.5–20.0 $\mu$ M     | [120] |
| Cd(II), Pb(II)                    | Fe <sub>3</sub> O <sub>4</sub> /MWCNTs/LSG/CS/GCE | SWASV               | Cd: 0.1 $\mu$ g/L<br>Pb: 0.07 $\mu$ g/L  | S: Yes<br>Rp: Yes<br>Re: No                                   | 1–200 $\mu$ g/L  | [121] |
| Cd(II), Pb(II)                    | Sb <sub>2</sub> O <sub>3</sub> /MWCNTs            | LSASV               | Cd: 11.23 ppb<br>Pb: 2.68 ppb  | S: No<br>Rp: Yes<br>Re: Yes                                   | Cd: 80–150 ppb<br>Pb: 5–35 ppb   | [122] |
| Hg(II)                            | Sr@FeNi-S/SWCNTs                                  | DPV                 | 0.52 nM  | S: Yes<br>Rp: Yes<br>Re: Yes                                  | 0.05–279 $\mu$ M   | [123] |

Table 2. Cont.

| HMIs   | Nanocomposite  | Method of Detection | LOD   | Stability (S),<br>Repeatability (Rp),<br>Reproducibility (Re) | Linear Range  | Ref.  |
|--|--|---------------------|---|---|---|-------|
| Fe <sup>3+</sup>                             | PPCOT/NF/C-SWCNT   | Amperometric        | 97.08 ± 4.85 pM   | S: No<br>Rp: Yes<br>Re: Yes                                   | 0.1 nM–0.01 mM.   | [124] |
| Zn(II), Cd(II),<br>Pb(II), Cu(II),           | BiNP/MWCNT-<br>NNA/M/PGE   | SWASV               | Zn: 0.707 µM<br>Cd: 0.097 µM<br>Pb: 0.008 µM<br>Cu: 0.157 µM                      | S: No<br>Rp: Yes<br>Re: Yes                                   | Zn: 2.36–40; 40–180 µM<br>Cd: 0.32–2; 2–240 µM,<br>Pb: 0.03–5; 5–80 µM<br>Cu: 0.52–10; 10–40 µM | [125] |
| Cd(II)                                       | CNTs–UiO-66-<br>NH <sub>2</sub> /GCE   | DPV                 | 0.2 µM  | S: No<br>Rp: No<br>Re: No                                     | 0.3–150 µM  | [126] |
| Pb(II) and<br>Cu(II)                         | NH <sub>2</sub> -UiO-66@ZIF-<br>8/MWCNTs   | DPV                 | Pb: 1 nM<br>Cu: 10 nM   | S: Yes,<br>Rp: Yes<br>Re: Yes                                 | Pb: 0–80 mM<br>Cu: 0–50 mM  | [127] |
| Hg(II), Pb(II),<br>Cu(II)                    | ZnFe <sub>2</sub> O <sub>4</sub>   | DPASV               | Hg: 1.61 nM<br>Pb: 7.38 nM<br>Cu: 12.03 nM  | S: Yes,<br>Rp: No<br>Re: Yes                                  | 0.1–1 mM  | [128] |
| Pb(II)                                       | Gold-modified<br>graphene  | Amperometric        | 1.67 pM   | S: Yes,<br>Rp: No<br>Re: Yes                                  | 1 nM–1 mM   | [129] |
| Pb(II), Cd(II)                               | GO-Fe <sub>3</sub> O <sub>4</sub> -PAMAM   | SWASV               | Pb: 130 ng/L<br>Cd: 70 ng /L  | S: Yes,<br>Rp: Yes<br>Re: Yes                                 | Pb: 0.4–120 µg/L<br>Cd: 0.2–140 µg/L  | [130] |
| Cd(II), Pb(II)                               | Porous graphene/<br>carboxymethyl cellu-<br>lose/fondaparinux  | SWASV               | Cd: 0.28 nM<br>Pb: 0.17 nM  | S: Yes,<br>Rp: No<br>Re: Yes                                  | 2–20 nM   | [131] |
| Cu(II), Cd(II),<br>Hg(II)                    | rGO/silver   | DPV                 | Cu: 10–15 M<br>Cd: 10–21 M<br>Hg: 10–29 M   | S: No<br>Rp: No<br>Re: No                                     | –   | [132] |
| Zn(II), Cd(II),<br>Pb(II), Cu(II),<br>Hg(II) | FGP/AuNC   | SWASV               | Zn: 0.08 µg/L<br>Cd: 0.09 µg/L<br>Pb: 0.05 µg/L<br>Cu: 0.19 µg/L<br>Hg: 0.01 µg/L | S: Yes<br>Rp: Yes<br>Re: Yes                                  | Zn: 6–7000 µg/L<br>Cd: 4–6000 µg/L<br>Pb: 6–5000 µg/L<br>Cu: 4–4000 µg/L<br>Hg: 6–5000 µg/L     | [134] |
| Hg(II)                                       | SN-rGO   | SWASV               | 8.93 nM   | S: Yes<br>Rp: No<br>Re: Yes                                   | 0.6–1.8 µM  | [137] |
| Cd(II), Cu(II),<br>Hg(II)                    | NCO/N, S-rGO   | DPASV               | Cd: 123 nM<br>Cu: 14.4 nM<br>Hg: 67 nM  | S: Yes<br>Rp: Yes<br>Re: Yes                                  | –   | [138] |
| Cd(II), Pb(II),<br>Cu(II), Hg(II)            | rGO/ZnO-NPs-<br>EDTA   | SWV                 | Cd: 5.6 µM<br>Pb: 6.8 µM<br>Cu: 2.5 µM<br>Hg: 10 µM                               | S: No<br>Rp: No<br>Re: Yes                                    | Cd: 18.5–500 µM<br>Pb: 22.4–700 µM<br>Cu: 8.3–200 µM<br>Hg: 3.3–300 µM                          | [139] |
| Pb(II)                                       | rGO/MoS <sub>2</sub> /CS   | SWASV               | 0.0016 µM   | S: Yes<br>Rp: No<br>Re: Yes                                   | 0.005–0.05–2.0 µM   | [140] |
| Pb(II)                                       | CS/rGO/TiO <sub>2</sub>  | DPV                 | 0.33 ng /L  | S: Yes<br>Rp: Yes<br>Re: Yes                                  | 1 ng–1000 ng/L  | [142] |
| Pb(II)                                       | rGO/AuNPs/ssDNA  | CV                  | 1.52 nM   | S: Yes<br>Rp: No<br>Re: Yes                                   | 5–50 nM   | [143] |
| Pb(II), Cd(II)                               | Bi/g-C <sub>3</sub> N <sub>4</sub>   | SWASV               | Cd: 21.8 µg /L<br>Pb: 10.4 µg /L  | S: No<br>Rp: No<br>Re: No                                     | Cd: 30–120 µg/L<br>Pb: 30–110 µg/L  | [144] |
| Pb(II)                                       | Au/N-deficient-<br>C <sub>3</sub> N <sub>4</sub>   | SWASV               | 0.029 µM  | S: Yes<br>Rp: No<br>Re: Yes                                   | 0.2–0.8 µM  | [145] |
| Cd(II), Hg(II),<br>Pb(II), Zn(II)            | g-C <sub>3</sub> N <sub>4</sub> /O-MWCNTs  | DPSV                | Hg: 0.04 ng/L<br>Pb: 0.008 ng/L<br>Cd: 0.03 ng/L<br>Zn: 0.06 ng/L                 | S: Yes<br>Rp: No<br>Re: Yes                                   | Hg: 4.8–93.0 ng/L<br>Pb: 6.5–110 ng/L<br>Cd: 4.25–79.0 ng/L<br>Zn: 4.2–202.0 ng/L               | [146] |
| Cr(VI)                                       | Graphene<br>carbon-nitride-doped<br>silver-molybdate-<br>immobilized Nafion<br>(g-C <sub>3</sub> N <sub>4</sub> /AgM/Nf) | CV                  | 0.0016 µM   | S: Yes<br>Rp: Yes<br>Re: Yes                                  | 10–100 µM   | [147] |

**Table 2.** *Cont.*

| HMIs                           | Nanocomposite  | Method of Detection | LOD   | Stability (S), Repeatability (Rp), Reproducibility (Re) | Linear Range  | Ref.  |
|--------------------------------|--|---------------------|---|---|---|-------|
| Cd(II), Pb(II), Hg(II)         | Metal-free g-C <sub>3</sub> N <sub>4</sub> /carbon black (CB) composite                            | DPASV               | Cd: 2.1 nM<br>Pb: 0.26 nM<br>Hg: 0.22 nM        | S: No<br>Rp: No<br>Re: Yes                              | Cd: 0–700 nM<br>Pb: 0–300 nM<br>Hg: 0–500 nM            | [148] |
| Cd(II), Pb(II), Hg(II)         | Metal-free g-C <sub>3</sub> N <sub>4</sub> /carbon black composite                                 | DPASV               | Cd: 2.1 nM<br>Pb: 0.26 nM<br>Hg: 0.22 nM        | S: No<br>Rp: No<br>Re: Yes                              | Cd: 0–700 nM<br>Pb: 0–300 nM<br>Hg: 0–500 nM            | [149] |
| Cd(II), Pb(II)                 | Fe <sub>3</sub> O <sub>4</sub> /Bi <sub>2</sub> O <sub>3</sub> /C <sub>3</sub> N <sub>4</sub> /GCE | SWASV               | Cd: 3 nM<br>Pb: 1 nM                            | S: Yes<br>Rp: Yes<br>Re: Yes                            | 0–3 µM  | [150] |
| Pb(II), Cd(II)                 | M/g-C <sub>3</sub> N <sub>4</sub> /ASPE  | DPV                 | Pb: 0.008 µM<br>Cd: 0.02 µM                     | S: Yes<br>Rp: No<br>Re: Yes                             | 0.1–1.0 µM  | [151] |
| Cd(II), Pb(II)                 | pg-C <sub>3</sub> N <sub>4</sub> /CoMn <sub>2</sub> O <sub>4</sub>                                 | SWASV               | Cd: 0.021 µM<br>Pb: 0.014 µM                    | S: Yes<br>Rp: Yes<br>Re: Yes                            | Cd: 0.5–7.0 µM<br>Pb: 0.2–4.4 µM                        | [152] |
| Cd(II)                         | MnO <sub>2</sub> /rGO  | DPASV               | 1.12 µg/L                                       | S: Yes<br>Rp: No<br>Re: No                              | 4.0–130 µg/L  | [153] |
| Pb(II), Cd(II), Cu(II), Hg(II) | NiO/rGO  | SWASV               | 0.01 µM   | S: No<br>Rp: No<br>Re: Yes                              | -   | [154] |
| Cd(II), Pb(II)                 | r-CeO <sub>2</sub> /EG composite   | DPV                 | Cd: 0.39 µg/L<br>Pb: 0.21 µg/L                  | S: No<br>Rp: No<br>Re: Yes                              | 0–100 µg/L  | [156] |
| Hg(II)                         | Sepiolite/pyrite (Sep/FeS <sub>2</sub> )   | SWASV               | 4.12 nM   | S: No<br>Rp: No<br>Re: Yes                              | 10–120 nM   | [157] |
| Pb(II)                         | α-Fe <sub>2</sub> O <sub>3</sub> /NiO heterostructure  | SWASV               | 0.02 µM   | S: Yes<br>Rp: No<br>Re: Yes                             | 0.05–0.9 µM   | [158] |
| Hg(II)                         | Co <sub>3</sub> O <sub>4</sub> /ZnO  | SWASV               | 0.3 µM  | S: Yes<br>Rp: No<br>Re: No                              | 0–2.1 µM  | [159] |
| Pb(II), Cu(II), Hg(II)         | Zr/ZrO <sub>2</sub>  | DPV                 | Pb: 0.8 nM<br>Cu: 0.5 nM<br>Hg: 0.4 nM          | S: No<br>Rp: No<br>Re: No                               | Pb: 0.8 nM–10 µM<br>Cu: 0.5 nM–2 µM<br>Hg: 0.4 nM–10 µM | [160] |
| Cd(II), Pb(II)                 | SnS-Bi <sub>2</sub> O <sub>3</sub>   | SWASV               | Cd: 1.50 nM<br>Pb: 1.40 nM                      | S: No<br>Rp: No<br>Re: No                               | 0–1 µM  | [161] |
| Hg(II)                         | Ru/CeO <sub>2</sub>  | SWASV               | 0.019 µM  | S: No<br>Rp: No<br>Re: No                               | 0–0.9 µM  | [162] |
| Pb(II), Hg(II)                 | MgO-SiO <sub>2</sub>   | SWASV               | Pb: 0.019 µM<br>Hg: 0.041 µM                    | S: Yes<br>Rp: Yes<br>Re: Yes                            | -   | [163] |
| Pb(II), Cd(II)                 | Fe <sub>3</sub> O <sub>4</sub> @G2-PAD   | SWASV               | Pb: 0.17 µg/L<br>Cd: 0.21 µg/L                  | S: No<br>Rp: No<br>Re: No                               | 0.5–80 µg/L   | [164] |
| Hg(II)                         | CuO/PVA  | DPV                 | 0.42 nM   | S: No<br>Rp: No<br>Re: Yes                              | 10–70 µM  | [165] |
| Pb(II), Cu(II)                 | Cerium oxide   | CV, DPV             | Pb: 0.6 ppb<br>Cu: 0.3 ppb                      | S: No<br>Rp: Yes<br>Re: No                              | Pb: 0.6–12 ppb<br>Cu: 0.3–10 ppb                        | [166] |
| Pb(II)                         | Fe <sub>3</sub> O <sub>4</sub> @PDA@MnO <sub>2</sub>   | DPV                 | 0.03 µg/L                                       | S: Yes<br>Rp: Yes<br>Re: No                             | 0.1–150 µg/L  | [167] |
| Cd(II), Pb(II), Cu(II)         | Zn/Fe nanocomposite  | CV                  | Cd: 0.14 mg/L<br>Pb: 0.07 mg/L<br>Cu: 0.04 mg/L | S: No<br>Rp: No<br>Re: Yes                              | 0–16.5 mg/L   | [168] |
| Cd(II), Pb(II)                 | Fe <sub>2</sub> O <sub>3</sub> /Bi <sub>2</sub> O <sub>3</sub>                                     | SWASV               | Cd: 0.56 nM<br>Pb: 0.36 nM                      | S: Yes<br>Rp: Yes<br>Re: Yes                            | 0.002–4 µM  | [169] |
| Zn(II), Cd(II), Pb(II)         | Bi/chitosan  | SWASV               | Zn: 0.1 ppb<br>Cd: 0.1 ppb<br>Pb: 0.2 ppb       | S: No<br>Rp: Yes<br>Re: Yes                             | Zn: 1–5 ppb<br>Cd: 1–5 ppb<br>Pb: 1–10 ppb              | [170] |

Table 2. Cont.

| HMIs                           | Nanocomposite   | Method of Detection | LOD  | Stability (S),<br>Repeatability (Rp),<br>Reproducibility (Re) | Linear Range   | Ref.  |
|--------------------------------|---|---------------------|--|---|--|-------|
| Cu(II)                         | Chitosan/GO   | DPASV               | 0.15 $\mu$ M   | S: No<br>Rp: Yes<br>Re: Yes                                   | 0.5–100 $\mu$ M  | [171] |
| Cd(II)                         | Chitosan/Au/graphene  | DPV                 | 0.162 nM   | S: Yes<br>Rp: Yes<br>Re: No                                   | 0.1–0.9 $\mu$ M  | [172] |
| Pb(II)                         | PVA/Chitosan/rGO  | SWASV               | 0.05 ppb   | S: No<br>Rp: Yes<br>Re: Yes                                   | 1–50 ppb   | [173] |
| Pb(II), Cd(II)                 | Bi/MXene  | SWASV               | Pb: 10.8 nM,<br>Cd: 12.4 nM  | S: Yes<br>Rp: Yes<br>Re: Yes                                  | Pb: 0.06–0.6 $\mu$ M<br>Cd: 0.08–0.8 $\mu$ M   | [174] |
| Pb(II), Cd(II), Zn(II)         | Bi/MXene  | SWASV               | Pb: 0.2 $\mu$ g/L<br>Cd: 0.4 $\mu$ g/L<br>Zn: 0.5 $\mu$ g/L                      | S: Yes<br>Rp: Yes<br>Re: Yes                                  | 1–20 $\mu$ g/L   | [175] |
| Cd(II), Pb(II)                 | Ti <sub>3</sub> C <sub>2</sub> MXene/carbon heterostructure | SWASV               | Cd: 2.55 nM,<br>Pb: 1.10 nM  | S: Yes<br>Rp: Yes<br>Re: Yes                                  | Cd: 0.1–8 $\mu$ M,<br>Pb: 0.25–2 $\mu$ M   | [179] |
| Zn(II), Cd(II), Pb(II)         | Melamine/rGO/MXene aerogel                                  | DPASV               | Zn: 0.48 $\mu$ g/L<br>Cd: 0.45 $\mu$ g/L<br>Pb: 0.29 $\mu$ g/L                   | S: No<br>Rp: Yes<br>Re: Yes                                   | 3–900 $\mu$ g/L  | [180] |
| Cd(II), Pb(II), Cu(II), Hg(II) | Alk-Ti <sub>3</sub> C <sub>2</sub>                          | SWASV               | Cd: 0.098 $\mu$ M<br>Pb: 0.041 $\mu$ M<br>Cu: 0.032 $\mu$ M<br>Hg: 0.130 $\mu$ M | S: Yes<br>Rp: No<br>Re: Yes                                   | Cd: 0.1–1 $\mu$ M,<br>Pb: 0.1–0.55 $\mu$ M<br>Cu: 0.1–1.4 $\mu$ M<br>Hg: 0–1.9 $\mu$ M               | [182] |
| Cd(II), Pb(II), Cu(II), Hg(II) | AgNs/SPCE   | DPSV                | Cd: 0.4 ppb<br>Pb: 2.5 ppb<br>Cu: 7.3 ppb<br>Hg: 0.7 ppb                         | S: No<br>Rp: No<br>Re: Yes                                    | Cd: 5–300 ppb<br>Pb: 5–300 ppb<br>Cu: 50–500 ppb<br>Hg: 5–100 ppb                                    | [186] |
| Cd(II), Pb(II)                 | FeNi <sub>3</sub> /CuS/BiOC                                 | SWASV               | Cd: 0.4 $\mu$ g/L<br>Pb: 0.1 $\mu$ g/L   | S: Yes<br>Rp: Yes<br>Re: Yes                                  | Cd: 1–150.0 $\mu$ g/L<br>Pb: 0.5–120.0 $\mu$ g/L   | [188] |
| Pb(II)                         | Cu–chitosan nanocomposite                                   | SWSAV               | 0.72 ppb   | S: No<br>Rp: Yes<br>Re: No                                    | 0–60 ppb   | [189] |
| Pb(II), Cd(II)                 | BiNP/CoFe <sub>2</sub> O <sub>4</sub>                       | SWASV               | Pb: 7.3 nM<br>Cd: 8.2 nM   | S: Yes<br>Rp: No<br>Re: Yes                                   | Pb: 0.06–0.6 $\mu$ M<br>Cd: 0.08–0.8 $\mu$ M   | [190] |
| Pb(II), Hg(II)                 | Ni NMO-GR   | SWASV               | Pb: 0.050 $\mu$ M<br>Hg: 0.027 $\mu$ M   | S: Yes<br>Rp: Yes<br>Re: Yes                                  | Pb: 1.4–7.7 $\mu$ M<br>Hg: 0.7–607 $\mu$ M   | [191] |
| Pb(II)                         | Ternary nanocomposites CNW, CNW: Ag, AgNPs                  | EIS                 | 10 nM  | S: No<br>Rp: Yes<br>Re: No                                    | 10 nM–1 mM   | [193] |
| Cd(II), Cu(II), Hg(II), Pb(II) | Mg(II)/Al(II)   | SWASV               | Cd: 250 ng/L<br>Cu: 25 ng/L<br>Hg: 250 ng/L<br>Pb: 16 ng/L                       | S: No<br>Rp: Yes<br>Re: Yes                                   | Cd: 0.5–0.20 $\mu$ g/L<br>Cu: 0.05–0.20 $\mu$ g/L<br>Hg: 0.5–20 $\mu$ g/L<br>Pb: 0.05–0.20 $\mu$ g/L | [194] |
| Cd(II)                         | CA-functionalized ZnO                                       | CV, SWV             | 0.41 $\mu$ M   | S: Yes<br>Rp: No<br>Re: No                                    | 0.1–0.50 $\mu$ M   | [195] |
| Pb(II), Cu(II)                 | BFS   | DPV                 | Pb: 0.084 $\mu$ M<br>Cu: 0.44 $\mu$ M  | S: No<br>Rp: No<br>Re: No                                     | 0–80 $\mu$ M   | [196] |
| Cu(II)                         | Ni/NiO/MoO <sub>3</sub> /chitosan                           | DPV                 | 5.69 nM  | S: Yes<br>Rp: Yes<br>Re: Yes                                  | 0–25 $\mu$ M   | [197] |
| Pb(II)                         | Aptazyme-driven DNA   | DPV                 | 0.034 nM   | S: Yes<br>Rp: Yes<br>Re: Yes                                  | 0–0.5 $\mu$ M  | [198] |
| Cr(VI)                         | Polyoxometalates  | DPV                 | 0.174 $\mu$ M  | S: No<br>Rp: Yes<br>Re: No                                    | 2 $\mu$ M–2.61 mM  | [199] |
| Cu(II)                         | Eggshell membrane   | DPV                 | 0.63 $\mu$ M   | S: Yes<br>Rp: Yes<br>Re: No                                   | 1–300 $\mu$ M  | [200] |

Table 2. Cont.

| HMIs                   | Nanocomposite                            | Method of Detection | LOD                                       | Stability (S),<br>Repeatability (Rp),<br>Reproducibility (Re) | Linear Range                               | Ref.  |
|------------------------|--|---------------------|---|---|--|-------|
| Cu(II)                 | PIE/BP                                   | SWASV               | 0.02 $\mu$ M                              | S: No<br>Rp: No<br>Re: No                                     | 0.25–177 $\mu$ M                           | [201] |
| Cu(II), Hg(II)         | CSs                                      | DPASV               | Cu(II): 4.5 nM<br>Hg(II): 12.5 nM         | S: No<br>Rp: No<br>Re: Yes                                    | Cu(II): 0–5 $\mu$ M<br>Hg(II): 0–5 $\mu$ M | [202] |
| As(III)                | Ag, Au alloy NPs                         | DPV                 | 0.003 $\mu$ g/L                           | S: No<br>Rp: Yes<br>Re: Yes                                   | 0.01–10 $\mu$ g/L                          | [203] |
| Pb(II)                 | Ag, Au alloy NPs                         | CV, DPV             | 0.3 ng/L                                  | S: Yes<br>Rp: No<br>Re: Yes                                   | 0.01–10 $\mu$ g/L                          | [204] |
| Pb(II)                 | PPy/CNFs/CPE                             | SWASV               | 0.05 $\mu$ g/L                            | S: Yes<br>Rp: No<br>Re: Yes                                   | 0.2–130 $\mu$ g/L                          | [205] |
| Pb(II)                 | sGO/PPy-SPE                              | DPASV               | 0.07 ppb                                  | S: Yes<br>Rp: Yes<br>Re: Yes                                  | 1.4–28 ppb                                 | [206] |
| Pb(II)                 | PPy/CNT/NH <sub>2</sub> -ITO             | DPV                 | 2.9 nM                                    | S: Yes<br>Rp: Yes<br>Re: No                                   | 10 nM–0.1 $\mu$ M                          | [207] |
| Cd(II), Pb(II)         | GO@Fe <sub>3</sub> O <sub>4</sub> @2-CBT | SWASV               | Cd: 0.03 $\mu$ g/L<br>Pb: 0.02 $\mu$ g/L  | S: No<br>Rp: No<br>Re: No                                     | 0.08–90 $\mu$ g/L                          | [208] |
| Pb(II), Cu(II), Cd(II) | ITO-AP-PPy-ABS                           | DPV                 | Pb: 11.1 nM<br>Cu: 8.95 nM<br>Cd: 0.99 nM | S: Yes<br>Rp: No<br>Re: Yes                                   | –  | [209] |

\* IC<sub>50</sub> values: the HMI concentration corresponding to half maximum cytotoxicity is defined as the IC<sub>50</sub> value.

It can be concluded from Table 2 that the most advantageous approaches to sensor preparation for the detection of various HMIs involve the utilization of a composite of various nanostructured materials. These approaches employ a composite of various nanomaterials, which offer high surface-area-to-volume ratios and enhanced sensitivity. Functionalizing these nanomaterials with selective ligands or receptors allows for specific binding and detection of HMIs. Additionally, integrating the sensor with nanocomposite materials with microfluidic systems enables rapid and efficient sample handling, enhancing the sensor's performance. Another promising approach is the development of electrochemical sensors that utilize modified electrodes. By functionalizing the electrode surfaces with selective materials, such as polymers or MOFs, the HMIs can be selectively captured and quantified. These approaches provide a powerful platform for preparing sensors that offer high sensitivity, selectivity, and rapid response, making them valuable tools for HMI detection in various environmental and analytical applications.

## 5. Sensing Mechanisms of the Electrochemical Detection of HMIs

The sensing mechanism plays a pivotal role in comprehending the properties and performance of a sensor. It is the fundamental process through which a sensor interacts with its environment and translates the target stimulus into a measurable signal. Understanding the sensing mechanism is crucial for several reasons:

**Performance optimization:** Knowledge of the sensing mechanism allows researchers to optimize and fine-tune the sensor's sensitivity, selectivity, response time, and detection limits. The sensor's overall performance can be enhanced by tailoring the mechanism to the specific application.

**Material design and selection:** Different sensing mechanisms require specific materials to function effectively. For instance, some sensors operate based on changes in electrical conductivity, while others rely on optical or chemical interactions. Understanding the sensing mechanism helps guide the selection and design of appropriate materials to achieve the desired sensor properties.

**Interference mitigation:** Interference from external factors can impact a sensor's accuracy. By understanding the sensing mechanism, researchers can identify potential sources of interference and implement measures to mitigate their effects, thus ensuring reliable and accurate measurements.

**Mechanism validation:** Understanding the sensing mechanism allows researchers to validate the sensor's operation. This involves confirming that the observed responses are linked to the intended target stimulus and not influenced by unintended factors.

**Innovation and development:** In-depth knowledge of the sensing mechanism opens doors to innovation. Researchers can explore novel ways to modify existing mechanisms or create entirely new ones, potentially leading to breakthroughs in sensor technology with improved capabilities.

**Data interpretation:** The sensor's output signal directly results from its sensing mechanism. Understanding this relationship is vital for accurately interpreting the data collected by the sensor and drawing meaningful conclusions.

In conclusion, the sensing mechanism is the cornerstone of a sensor's functionality and performance. It guides material selection, interference management, innovation, troubleshooting, and customization, ultimately leading to improved sensor technology across various applications. In the electrochemical detection of HMIs, integrating nanocomposite materials introduces a sophisticated sensing mechanism that enhances selectivity and sensitivity. Incorporating nanocomposite materials into the electrode surface intensifies the binding interactions between the nanocomposites and target HMIs. This interaction leads to distinct electrochemical changes, such as modified peak currents or shifts in peak potentials, which indicate the presence and concentration of the analyte ions. The unique properties of nanocomposites, such as their high surface area, tunable surface chemistry, and enhanced catalytic activity, further amplify the sensor's performance. Understanding the intricate sensing mechanism based on the nanocomposite materials facilitates the design of advanced electrochemical sensors, enabling precise and reliable detection of HMIs even within complex sample matrices.

Sayaad et al. [210] have elucidated a plausible sensing mechanism underpinning the interaction between Cd(II) and the L-Glutathione-modified poly (3,4-ethylenedioxythiophene): polystyrene sulfonate/carboxylated MWCNTs (LGSH@PEDOT: PSS/MWCNTs-COOH) network (schematically illustrated in Figure 23). They assert that an expanded active surface area significantly bolsters the detection of toxic heavy metals, facilitating nanomolar-level analysis in real samples. It is conceivable that the realm of electroanalytical performance in finalized devices might be revolutionized due to the refinement and functionalization of MWCNTs. Introducing -COOH moieties into the sidewalls of the MWCNTs elicits a transformation in their wettability from hydrophobic to hydrophilic, engendering a profusion of active sites primed for sensing endeavors. The selection of LGSH tripeptide as the molecular probe stems from its specific binding affinity for Cd(II) ions. Anticipations are directed toward the delocalized  $\pi$ -bond network of MWCNTs-COOH and the thiophene ring backbone of PEDOT, portending  $\pi$ - $\pi$  interactions within the PEDOT-PSS/MWCNTs-COOH structure [211]. The numerous coordination sites within the LGSH tripeptides, including carboxyl, thiol, and amide groups, are noteworthy and conducive to capturing waterborne pollutants like perilous heavy metals. While the -NH<sub>2</sub> moiety within LGSH is primed for binding to diverse inorganic HMIs, the initial layer's -NH<sub>2</sub> interacts with MWCNTs' -COOH groups, forging -CONH- moieties via chemical reactions.

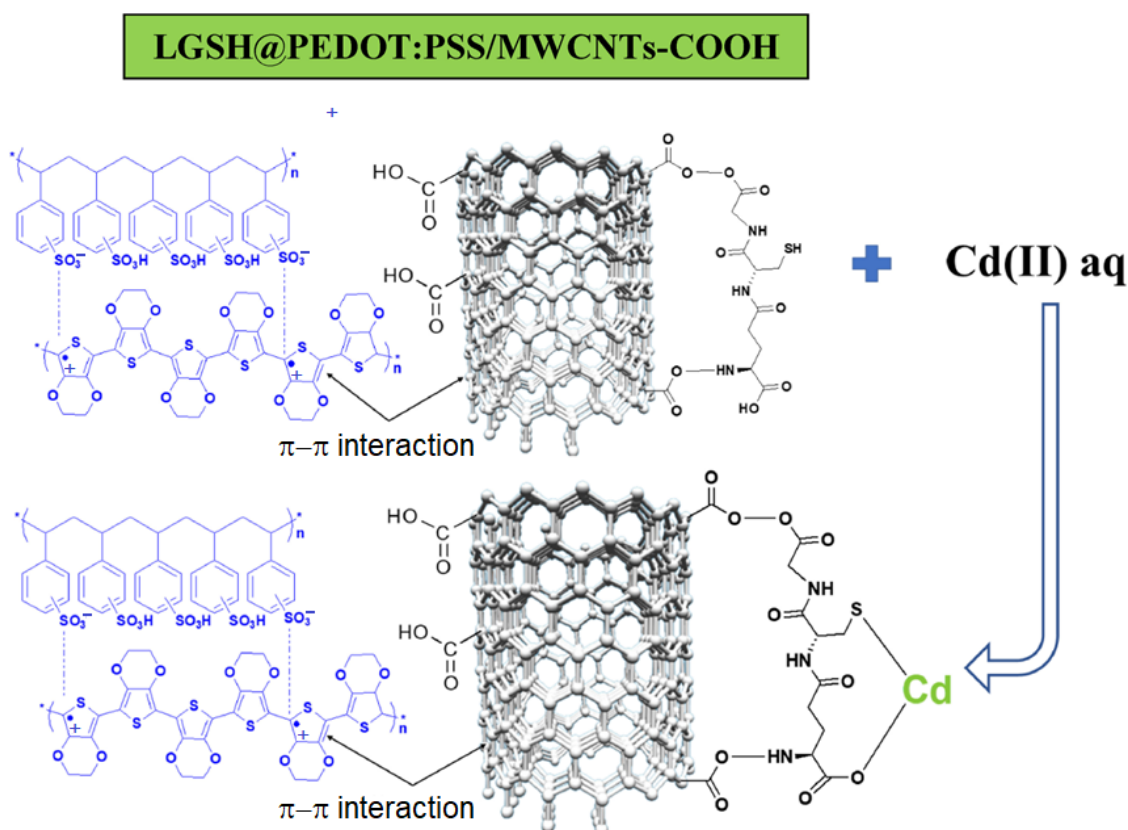


**Figure 23.** Probable Cd(II) sensing mechanism with LGSH@PEDOT: PSS/MWCNTs-COOH network. Reproduced from [210] with permission of Elsevier.

Consequently, the incorporation of carboxylated MWCNTs has substantially influenced the sensing of metal ions, facilitating an enhanced binding propensity of LGSH to Cd(II) across discrete coordination locales. This intricate interaction precipitates the formation of diminutive Cd-LGSH complexes, thereby engendering discernible electrochemical current signals. The intricate, complex formation process emerges as a pivotal mechanism within the analytical inquiries advanced by Pasha et al. The concerted affinity exhibited by Cd(II) ions toward the -SH and -COOH moieties of the LGSH tripeptide, in conjunction with the sidewall-functionalized -COOH moiety, has synergistically orchestrated the establishment of a Cd(II)-LGSH complex, thereby conferring selective detectability exclusively toward Cd(II) ions. The grafting of thiol and carboxyl groups onto Cd(II) ions emerges as a universal strategy for the tailored modification of the PEDOT: PSS/MWCNTs-COOH network using the biologically active LGSH tripeptide. The augmentation of LGSH's functional attributes has elicited marked enhancements in selectivity and a lower LOD for the biosensor platform.

The scheme of the electrochemical detection of HMIs using various nanocomposite materials is shown in Figure 24. Diverse nanocomposite materials, including MOFs, OCPs, CNTs, graphitic carbon nitride, metal oxide, chitosan, MXenes, and metal-nanoparticle-based nanocomposites, could be explored for the electrochemical detection of HMIs. The scheme depicted in Figure 24 involves modifying working electrodes with these materials, enabling oxidation and reduction reactions of specific metal ions upon the application of electrochemical potential. This process generated measurable electrochemical sensing signals, proportionate to the concentration of the HMIs, facilitating precise quantification.

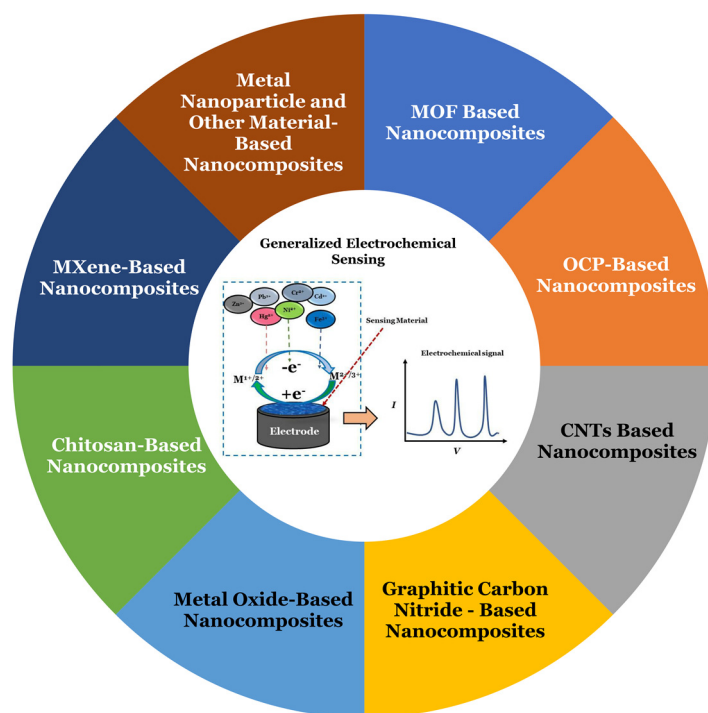


**Figure 24.** Scheme for the electrochemical detection of HMIs using various nanocomposite materials.

## 6. Selectivity of Detection and the Use of Specific Receptors in Conjunction with Carbon Nanomaterials

Detecting HMIs in various environments is paramount due to their toxicity and potential harm to human health and the environment. Achieving selectivity in detecting specific HMIs is crucial to ensure accurate and reliable results. Specific receptors in conjunction with nanocarbon materials can significantly enhance the selectivity of detection for HMIs. This can be achieved by employing the following options.

**Functionalization with chelating agents:** Carbon nanomaterials like graphene and carbon nanotubes can be functionalized using specific chelating agents. Chelating agents are molecules capable of forming coordination bonds with HMIs. By immobilizing chelating agents on the surface of carbon nanomaterials, selective binding of specific HMIs can be achieved. Common chelating agents include organic ligands and polymers with functional groups such as amino, carboxyl, or thiol groups.

**Antibody-based recognition:** Monoclonal antibodies or antibody-mimicking molecules (aptamers) can be immobilized on the surface of carbon nanomaterials. These antibodies or aptamers are specifically designed to bind to certain HMIs. When the target HMI is present in the sample, it binds selectively to the immobilized antibodies or aptamers, leading to a measurable change in the electrical properties of the carbon nanomaterial.

**MIPs** are synthetic polymers with specific binding sites for target molecules. In the context of HMI detection, MIPs can be tailored to bind to particular metal ions selectively. When MIPs are incorporated into or coated onto nanocarbon materials, they can selectively capture the target HMIs, allowing for specific detection.

By employing these strategies, combining specific receptors and nanocarbon materials can lead to highly selective and sensitive detection methods for HMIs, ensuring the accuracy and reliability of environmental monitoring and human safety.

## 7. Summary and Future Prospects

### 7.1. Summary

This review article explored the application of various nanocomposite materials in the electrochemical detection of HMIs. The nanocomposite materials discussed in this review include MOF, OCPs, CNTs, graphene/rGO, graphitic carbon nitride, metal oxide, chitosan,

MXenes, and metal-nanoparticle-based nanocomposites. The advantages and limitations of each material and its nanocomposites for detecting HMIs have been comprehensively discussed, highlighting their sensitivity, selectivity, and stability. For example, MOFs have a high surface area, increasing the electrochemical sensor's sensitivity. The highly porous structure of the MOFs provides many binding sites for HMIs.

Moreover, MOFs can be designed with specific functional groups to selectively bind to certain HMIs, allowing their selective detection of complex samples. However, MOFs can be unstable in aqueous solutions, affecting the electrochemical sensor's reliability and reproducibility. The synthesis of MOFs can be challenging, and their electrochemical properties can depend highly on the synthesis conditions. Despite their high surface area and porosity, MOFs may not always provide the required sensitivity for trace-level detection of HMIs.

OCPs have high sensitivity toward HMIs, making them suitable for trace-level detection. OCPs can be designed with specific functional groups to selectively bind to certain HMIs, allowing their selective detection in complex samples. OCPs are flexible and easily fabricated into different shapes and sizes, making them suitable for various applications. However, OCPs can be unstable in aqueous solutions, affecting an electrochemical sensor's reliability and reproducibility. Other compounds in the sample matrix may interfere with the electrochemical detection of HMIs, affecting the accuracy of the results. Stability can be one of the significant challenges while using OCPs to detect HMIs.

Similarly, CNTs have a high surface-area-to-volume ratio, which results in a high sensitivity for detecting HMIs. CNT-based electrodes can be modified using specific chemical groups to detect HMIs in the presence of other ions selectively. Electrochemical detection using CNT-based electrodes can provide real-time analysis and be conducted rapidly, making it an attractive option for environmental monitoring and industrial applications. The electrochemical detection of HMIs using CNT-based electrodes can achieve a low detection limit due to the high sensitivity and selectivity of the method. CNT-based electrodes are highly stable and can be reused for multiple detections, making them cost-effective. However, preparing CNT-based electrodes is time-consuming and requires expertise in synthesizing and functionalizing CNTs. The presence of other ions can interfere with the detection of HMIs, reducing the accuracy and specificity of the method. The reproducibility of CNT-based electrodes can be affected by variations in the synthesis and functionalization of CNTs, leading to inconsistencies in the results. The disposal of CNTs can pose environmental risks, as they are not readily biodegradable.

This review comprehensively covers the different methods used for synthesizing and functionalizing these nanocomposite materials to address the abovementioned challenges and improve their electrochemical properties for HMI detection. Several options have been explored to form nanocomposites to address these challenges so that highly sensitive, selective, stable, repeatable, and reproducible sensors can be developed to detect HMIs.

## 7.2. Future Prospects

The electrochemical detection of HMIs based on nanocomposite materials is an emerging field with great potential for future applications.

The electrochemical detection of HMIs based on nanocomposite materials holds immense promise and potential. Nanocomposite materials can offer a remarkable platform for enhanced sensitivity, selectivity, and stability in the detection of HMIs. A novel sensing platform can be developed by combining the unique properties of nanomaterials, such as high surface area, tailored surface chemistry, and excellent conductivity, with the specific recognition capabilities of functional materials. Electrochemical sensors based on nanocomposites could revolutionize HMI detection, enabling rapid, on-site analysis with high accuracy and sensitivity. Moreover, tremendous development of novel nanocomposite architectures and fabrication techniques is expected due to continuous advancements in nanotechnology and material science. This will lead to the realization of miniaturized, portable, and cost-

effective devices for real-time monitoring of HMIs in various environmental, industrial, and biological matrices.

The challenging issues of the materials can be intelligently tackled. The properties of the nanocomposites can be further fine-tuned, and sensors with enhanced stability, sensitivity, and selectivity can be developed for HMI detection. Moreover, the following technological aspects can also be achieved.

**Miniaturization:** Nanocomposite-based sensors can be miniaturized, making them suitable for point-of-care testing and on-site monitoring and allowing for portable and on-site monitoring of HMIs. Developing nanocomposite-based sensors with small form factors and low power consumption can lead to their widespread use in various fields.

**Multi-metal detection:** Nanocomposite materials can be engineered to detect multiple HMIs simultaneously. Developing nanocomposite-based sensors with multi-metal detection capabilities can lead to more efficient and cost-effective monitoring of heavy metal contamination.

**Industrial applications:** The electrochemical detection of HMIs based on nanocomposite materials can be used in various industrial applications, such as quality control and process monitoring. Developing nanocomposite-based sensors for industrial applications can improve product quality and increase efficiency.

The electrochemical detection of HMIs based on nanocomposite materials represents a highly promising and rapidly evolving area with significant repercussions for environmental monitoring and public health. The development of novel sensing platforms with superior performance can be ensured due to the unique properties of nanocomposites, including their enhanced sensitivity, selectivity, and stability. The design and fabrication of high-performance electrochemical sensors capable of real-time, on-site analysis can also be ensured by exploring the synergistic combination of nanomaterials and functional materials.

Further directions can also be focused on applying nucleic acid aptamers as receptors immobilized at nanocomposite materials for the selective detection of HMIs [203,212]. Overall, the future of the electrochemical detection of HMIs based on nanocomposite materials looks promising, and further research and development in this field can lead to innovative and practical applications.

**Author Contributions:** Conceptualization, M.D.S. and T.H.; writing—original draft, M.D.S.; writing—review and editing, M.D.S.; funding acquisition, T.H. All authors have read and agreed to the published version of the manuscript.

**Funding:** This work was funded under the European Union's Horizon 2020 research and innovation program through the Marie Skłodowska-Curie grant agreement no. 101007299 and by the Scientific Grant Agency VEGA, project no. 1/0445/23 (to T.H.).

**Data Availability Statement:** Not applicable.

**Acknowledgments:** M.D.S. gratefully acknowledges the Slovak Academic Information Agency (SAIA) and Department of Nuclear Physics and Biophysics, Faculty of Mathematics, Physics and Informatics, Comenius University, Bratislava, the Slovak Republic, for the sanction of scholarship under the framework of the National Scholarship Program (NSP) of the Slovak Republic. Moreover, M.D.S. also gratefully acknowledges Dr. Babasaheb Ambedkar Marathwada University, Aurangabad, MS., India, for the sanctioned study leave to visit Comenius University, Bratislava, the Slovak Republic.

**Conflicts of Interest:** The authors declare no conflict of interest.

## References

1. Sharma, S.K. *Heavy Metals in Water: Presence, Removal and Safety*; Royal Society of Chemistry: London, UK, 2014. [[CrossRef](#)]
2. Shadman, S.M.; Daneshi, M.; Shafiei, F.; Azimimehr, M.; Khorasgani, M.R.; Sadeghian, M.; Motaghi, H.; Mehrgardi, M.A. Aptamer-based electrochemical biosensors. In *Electrochemical Biosensors*; Ensafi, A.A., Ed.; Elsevier: Amsterdam, The Netherlands, 2019; pp. 213–251. [[CrossRef](#)]
3. Valko, M.; Morris, H.; Cronin, M. Metals, toxicity and oxidative stress. *Current Med. Chem.* **2005**, *12*, 1161–1208. [[CrossRef](#)]

4. Bagal-Kestwal, D.; Karve, M.S.; Kakade, B.; Pillai, V.K. Invertase inhibition based electrochemical sensor for the detection of heavy metal ions in aqueous system: Application of ultra-microelectrode to enhance sucrose biosensor's sensitivity. *Biosens. Bioelectron.* **2008**, *24*, 657–664. [[CrossRef](#)]
5. Zularisam, A.; Ismail, A.; Salim, R. Behaviours of natural organic matter in membrane filtration for surface water treatment—A review. *Desalination* **2006**, *194*, 211–231. [[CrossRef](#)]
6. Vetrimurugan, E.; Brindha, K.; Elango, L.; Ndwandwe, O.M. Human exposure risk to heavy metals through groundwater used for drinking in an intensively irrigated river delta. *Appl. Water Sci.* **2017**, *7*, 3267–3280. [[CrossRef](#)]
7. US EPA. *National Primary Drinking Water Regulations*; US EPA: Washington, DC, USA, 2015.
8. Ferrari, A.G.-M.; Carrington, P.; Rowley-Neale, S.J.; Banks, C.E. Recent advances in portable heavy metal electrochemical sensing platforms. *Environ. Sci. Water Res.* **2020**, *6*, 2676–2690. [[CrossRef](#)]
9. Srivastav, A.L. Chemical fertilizers and pesticides: Role in groundwater contamination. In *Agrochemicals Detection, Treatment and Remediation*; Elsevier: Amsterdam, The Netherlands, 2020; pp. 143–159. [[CrossRef](#)]
10. Liu, Y.; Deng, Y.; Dong, H.; Liu, K.; He, N. Progress on sensors based on nanomaterials for rapid detection of heavy metal ions. *Sci. China Chem.* **2017**, *60*, 329–337. [[CrossRef](#)]
11. Joshi, N.C.; Gururani, P. Advances of graphene oxide based nanocomposite materials in the treatment of wastewater containing heavy metal ions and dyes. *Curr. Res. Green Sustain. Chem.* **2022**, *5*, 100306. [[CrossRef](#)]
12. Huang, H.; Chen, T.; Liu, X.; Ma, H. Ultrasensitive and simultaneous detection of heavy metal ions based on three-dimensional graphene-carbon nanotubes hybrid electrode materials. *Anal. Chim. Acta* **2014**, *852*, 45–54. [[CrossRef](#)]
13. Pan, F.; Tong, C.; Wang, Z.; Han, H.; Liu, P.; Pan, D.; Zhu, R. Nanocomposite based on graphene and intercalated covalent organic frameworks with hydrosulphonyl groups for electrochemical determination of heavy metal ions. *Mikrochim. Acta* **2021**, *188*, 295. [[CrossRef](#)]
14. Devaraj, M.; Sasikumar, Y.; Rajendran, S.; Ponce, L.C. Metal organic framework based nanomaterials for electrochemical sensing of toxic heavy metal ions: Progress and their prospects. *J. Electrochem. Soc.* **2021**, *168*, 037513. [[CrossRef](#)]
15. Nguyen, M.B.; Nga, D.T.N.; Thu, V.T.; Piro, B.; Truong, T.N.P.; Yen, P.T.H.; Le, G.H.; Hung, L.Q.; Vu, T.A.; Ha, V.T.T. Novel nanoscale Yb-MOF used as highly efficient electrode for simultaneous detection of heavy metal ions. *J. Mater. Sci.* **2021**, *56*, 8172–8185. [[CrossRef](#)]
16. Wang, X.; Qi, Y.; Shen, Y.; Yuan, Y.; Zhang, L.; Zhang, C.; Sun, Y. A ratiometric electrochemical sensor for simultaneous detection of multiple heavy metal ions based on ferrocene-functionalized metal-organic framework. *Sens. Actuators B Chem.* **2020**, *310*, 127756. [[CrossRef](#)]
17. Lee, S.; Oh, J.; Kim, D.; Piao, Y. A sensitive electrochemical sensor using an iron oxide/graphene composite for the simultaneous detection of heavy metal ions. *Talanta* **2016**, *160*, 528–536. [[CrossRef](#)]
18. Akanji, S.P.; Ama, O.M.; Ray, S.S.; Osifo, P.O. Metal oxide nanomaterials for electrochemical detection of heavy metals in water. In *Nanostructured Metal-Oxide Electrode Materials for Water Purification: Fabrication, Electrochemistry and Applications*; Ama, O., Ray, S., Eds.; Springer: Cham, Germany, 2020; pp. 113–126. [[CrossRef](#)]
19. Bodkhe, G.A.; Hedau, B.S.; Deshmukh, M.A.; Patil, H.K.; Shirsat, S.M.; Phase, D.M.; Pandey, K.K.; Shirsat, M.D. Selective and sensitive detection of lead Pb (II) ions: Au/SWNT nanocomposite-embedded MOF-199. *J. Mater. Sci.* **2021**, *56*, 474–487. [[CrossRef](#)]
20. Sayyad, P.W.; Ingle, N.N.; Al-Gahouari, T.; Mahadik, M.M.; Bodkhe, G.A.; Shirsat, S.M.; Shirsat, M.D. Sensitive and selective detection of Cu<sup>2+</sup> and Pb<sup>2+</sup> ions using field effect transistor (FET) based on L-Cysteine anchored PEDOT: PSS/rGO composite. *Chem. Phys. Lett.* **2020**, *761*, 138056. [[CrossRef](#)]
21. Sayyad, P.W.; Ingle, N.N.; Al-Gahouari, T.; Mahadik, M.M.; Bodkhe, G.A.; Shirsat, S.M.; Shirsat, M.D. Selective Hg<sup>2+</sup> sensor: rGO-blended PEDOT:PSS conducting polymer OFET. *Appl. Phys. A* **2021**, *127*, 1–10. [[CrossRef](#)]
22. Bodkhe, G.A.; Hedau, B.S.; Deshmukh, M.A.; Patil, H.K.; Shirsat, S.M.; Phase, D.M.; Pandey, K.K.; Shirsat, M.D. Detection of Pb (II): Au nanoparticle incorporated CuBTC MOFs. *Front. Chem.* **2020**, *8*, 803. [[CrossRef](#)] [[PubMed](#)]
23. Sayyad, P.W.; Shaikh, Z.A.; Ingle, N.N.; Al-Gahouari, T.; Mahadik, M.M.; Bodkhe, G.A.; Shirsat, S.M.; Shirsat, M.D. Simultaneous reduction of graphene oxide (GO) and formation of rGO/Gly-Gly composite for sensitive detection of Cu<sup>2+</sup> ions. *J. Phys. Conf. Ser.* **2020**, *1644*, 012001. [[CrossRef](#)]
24. Mahadik, M.; Patil, H.; Bodkhe, G.; Ingle, N.; Sayyad, P.; Al-Gahaouri, T.; Shirsat, S.M.; Shirsat, M. EDTA modified PANI/GO composite based detection of Hg (II) ions. *Front. Mater.* **2020**, *7*, 81. [[CrossRef](#)]
25. AL-Gahouari, T.; Bodkhe, G.; Sayyad, P.; Ingle, N.; Mahadik, M.; Shirsat, S.M.; Deshmukh, M.; Musahwar, N.; Shirsat, M. Electrochemical sensor: L-cysteine induced selectivity enhancement of electrochemically reduced graphene oxide–multiwalled carbon nanotubes hybrid for detection of lead (Pb<sup>2+</sup>) ions. *Front. Mater.* **2020**, *7*, 68. [[CrossRef](#)]
26. Patil, H.K.; Deshmukh, M.A.; Bodkhe, G.A.; Shirsat, S.M.; Asokan, K.; Shirsat, M.D. Dimethylglyoxime modified swift heavy oxygen ions irradiated polyaniline/single walled carbon nanotubes composite electrode for detection of cobalt ions. *Mater. Res. Express* **2018**, *5*, 065048. [[CrossRef](#)]
27. Deshmukh, M.A.; Celiesiute, R.; Ramanaviciene, A.; Shirsat, M.D.; Ramanavicius, A. EDTA\_PANI/SWCNTs nanocomposite modified electrode for electrochemical determination of copper (II), lead (II) and mercury (II) ions. *Electrochim. Acta* **2018**, *259*, 930–938. [[CrossRef](#)]

28. Deshmukh, M.A.; Patil, H.K.; Bodkhe, G.A.; Yasuzawa, M.; Koinkar, P.; Ramanavicius, A.; Pandey, S.; Shirsat, M.D. EDA modified PANI/SWNTs nanocomposite for determination of Ni (II) metal ions. *Colloids Surf. A Physicochem. Eng. Asp.* **2018**, *537*, 303–309. [[CrossRef](#)]
29. Deore, K.B.; Patil, S.S.; Narwade, V.N.; Takte, M.A.; Khune, A.S.; Mohammed, H.Y.; Farea, M.A.; Sayyad, P.W.; Tsai, M.-L.; Shirsat, M.D. Chromium-benzenedicarboxylates metal organic framework for supersensitive and selective electrochemical sensor of toxic Cd<sup>2+</sup>, Pb<sup>2+</sup>, and Hg<sup>2+</sup> metal ions: Study of their interactive mechanism. *J. Electrochem. Soc.* **2023**, *170*, 046505. [[CrossRef](#)]
30. Kajal, N.; Singh, V.; Gupta, R.; Gautam, S. Metal organic frameworks for electrochemical sensor applications: A review. *Environ. Res.* **2022**, *204*, 112320. [[CrossRef](#)] [[PubMed](#)]
31. Munonde, T.S.; Nomngongo, P.N. Nanocomposites for electrochemical sensors and their applications on the detection of trace metals in environmental water samples. *Sensors* **2020**, *21*, 131. [[CrossRef](#)] [[PubMed](#)]
32. Buledi, J.A.; Amin, S.; Haider, S.I.; Bhangar, M.I.; Solangi, A.R. A review on detection of heavy metals from aqueous media using nanomaterial-based sensors. *Environ. Sci. Pollut. Res.* **2021**, *28*, 58994–59002. [[CrossRef](#)]
33. Sinha, A.; Kalambate, P.K.; Mugo, S.M.; Kamau, P.; Chen, J.; Jain, R. Polymer hydrogel interfaces in electrochemical sensing strategies: A review. *TrAC–Trends Anal. Chem.* **2019**, *118*, 488–501. [[CrossRef](#)]
34. Wang, H.; Xu, C.; Yuan, B. Polymer-based electrochemical sensing platform for heavy metal ions detection—A critical review. *Int. J. Electrochem. Sci.* **2019**, *14*, 8760–8771. [[CrossRef](#)]
35. Shoaie, N.; Daneshpour, M.; Azimzadeh, M.; Mahshid, S.; Khoshfetrat, S.M.; Jahanpeyma, F.; Gholaminejad, A.; Omidfar, K.; Foruzandeh, M. Electrochemical sensors and biosensors based on the use of polyaniline and its nanocomposites: A review on recent advances. *Mikrochim. Acta* **2019**, *186*, 465. [[CrossRef](#)]
36. Ahmad, R.; Tripathy, N.; Khosla, A.; Khan, M.; Mishra, P.; Ansari, W.A.; Syed, M.A.; Hahn, Y.-B. Recent advances in nanostructured graphitic carbon nitride as a sensing material for heavy metal ions. *J. Electrochem. Soc.* **2019**, *167*, 037519. [[CrossRef](#)]
37. Sawan, S.; Maalouf, R.; Errachid, A.; Jaffrezic-Renault, N. Metal and metal oxide nanoparticles in the voltammetric detection of heavy metals: A review. *TrAC–Trends Anal. Chem.* **2020**, *131*, 116014. [[CrossRef](#)]
38. Kumunda, C.; Adekunle, A.S.; Mamba, B.B.; Hlongwa, N.W.; Nkambule, T.T. Electrochemical detection of environmental pollutants based on graphene derivatives: A review. *Front. Mater.* **2021**, *7*, 616787. [[CrossRef](#)]
39. Tajik, S.; Beitollahi, H.; Nejad, F.G.; Dourandish, Z.; Khalilzadeh, M.A.; Jang, H.W.; Venditti, R.A.; Varma, R.S.; Shokouhimehr, M. Recent developments in polymer nanocomposite-based electrochemical sensors for detecting environmental pollutants. *Ind. Eng. Chem. Res.* **2021**, *60*, 1112–1136. [[CrossRef](#)] [[PubMed](#)]
40. Langari, M.M.; Antxustegi, M.M.; Labidi, J. Nanocellulose-based sensing platforms for heavy metal ions detection: A comprehensive review. *Chemosphere* **2022**, *302*, 134823. [[CrossRef](#)]
41. Raju, C.V.; Cho, C.H.; Rani, G.M.; Manju, V.; Umapathi, R.; Huh, Y.S.; Park, J.P. Emerging insights into the use of carbon-based nanomaterials for the electrochemical detection of heavy metal ions. *Coord. Chem. Rev.* **2023**, *476*, 214920. [[CrossRef](#)]
42. Meng, R.; Zhu, Q.; Long, T.; He, X.; Luo, Z.; Gu, R.; Wang, W.; Xiang, P. The innovative and accurate detection of heavy metals in foods: A critical review on electrochemical sensors. *Food Control* **2023**, *150*, 109743. [[CrossRef](#)]
43. Huang, R.; Lv, J.; Chen, J.; Zhu, Y.; Zhu, J.; Wågberg, T.; Hu, G. Three-dimensional porous high boron-nitrogen-doped carbon for the ultrasensitive electrochemical detection of trace heavy metals in food samples. *J. Hazard. Mater.* **2023**, *442*, 130020. [[CrossRef](#)]
44. Gao, Y.; Xu, M.; Sturgeon, R.E.; Mester, Z.; Shi, Z.; Galea, R.; Saull, P.; Yang, L. Metal ion-assisted photochemical vapor generation for the determination of lead in environmental samples by multicollector-ICPMS. *Anal. Chem.* **2015**, *87*, 4495–4502. [[CrossRef](#)]
45. Barbosa Jr, F.; Lima, É.C. On-line coupling of electrochemical preconcentration in tungsten coil electrothermal atomic absorption spectrometry for determination of lead in natural waters. *Spectrochim. Acta B* **1999**, *54*, 1155–1166. [[CrossRef](#)]
46. Rahmalan, A.; Abdullah, M.Z.; Sanagi, M.M.; Rashid, M. Determination of heavy metals in air particulate matter by ion chromatography. *J. Chromatogr. A* **1996**, *739*, 233–239. [[CrossRef](#)]
47. Nyholm, L. Electrochemical techniques for lab-on-a-chip applications. *Analyst* **2005**, *130*, 599–605. [[CrossRef](#)] [[PubMed](#)]
48. Piliarik, M.; Párová, L.; Homola, J. High-throughput SPR sensor for food safety. *Biosens. Bioelectron.* **2009**, *24*, 1399–1404. [[CrossRef](#)]
49. Li, Y.; Chen, M.; Han, Y.; Feng, Y.; Zhang, Z.; Zhang, B. Fabrication of a new corrole-based covalent organic framework as a highly efficient and selective chemosensor for heavy metal ions. *Chem. Mater.* **2020**, *32*, 2532–2540. [[CrossRef](#)]
50. Lv, M.; Zhou, W.; Tavakoli, H.; Bautista, C.; Xia, J.; Wang, Z.; Li, X. Aptamer-functionalized metal-organic frameworks (MOFs) for biosensing. *Biosens. Bioelectron.* **2021**, *176*, 112947. [[CrossRef](#)] [[PubMed](#)]
51. Vlasov, Y.; Legin, A.; Rudnitskaya, A. Cross-sensitivity evaluation of chemical sensors for electronic tongue: Determination of heavy metal ions. *Sens. Actuators B Chem.* **1997**, *44*, 532–537. [[CrossRef](#)]
52. Falina, S.; Syamsul, M.; Rhaffor, N.A.; Sal Hamid, S.; Mohamed Zain, K.A.; Abd Manaf, A.; Kawarada, H. Ten years progress of electrical detection of heavy metal ions (hmis) using various field-effect transistor (FET) nanosensors: A review. *Biosensors* **2021**, *11*, 478. [[CrossRef](#)]
53. Mohamad Nor, N.; Ramli, N.H.; Poobalan, H.; Qi Tan, K.; Abdul Razak, K. Recent advancement in disposable electrode modified with nanomaterials for electrochemical heavy metal sensors. *Crit. Rev. Anal. Chem.* **2023**, *53*, 253–288. [[CrossRef](#)]
54. Bansod, B.; Kumar, T.; Thakur, R.; Rana, S.; Singh, I. A review on various electrochemical techniques for heavy metal ions detection with different sensing platforms. *Biosens. Bioelectron.* **2017**, *94*, 443–455. [[CrossRef](#)]

55. Heidari, G.; Fallah, Z.; Zare, E.N. One-dimensional polymeric nanocomposites for heavy metal detection. In *One-Dimensional Polymeric Nanocomposites: Synthesis to Emerging Applications*, 1st ed.; Gupta, R.K., Nguyen, T.A., Eds.; CRC Press: London, UK, 2023; pp. 1–20. [\[CrossRef\]](#)
56. Jose, J.; Prakash, P.; Jeyaprabha, B.; Abraham, R.; Mathew, R.M.; Zacharia, E.S.; Thomas, V.; Thomas, J. Principle, design, strategies, and future perspectives of heavy metal ion detection using carbon nanomaterial-based electrochemical sensors: A review. *J. Iran. Chem. Soc.* **2023**, *20*, 775–791. [\[CrossRef\]](#)
57. Shen, Y.; Gao, X.; Lu, H.-J.; Nie, C.; Wang, J. Electrochemiluminescence-based innovative sensors for monitoring the residual levels of heavy metal ions in environment-related matrices. *Coord. Chem. Rev.* **2023**, *476*, 214927. [\[CrossRef\]](#)
58. Tatavarthi, S.S.; Wang, S.-L.; Wang, Y.-L.; Chen, J.-C. Rapid and highly sensitive extended gate FET-based sensors for arsenite detection using a handheld device. *ECS J. Solid State Sci. Technol.* **2020**, *9*, 115014. [\[CrossRef\]](#)
59. Krishnan, S.K.; Nataraj, N.; Meyyappan, M.; Pal, U. Graphene-based field-effect transistors in biosensing and neural interfacing applications: Recent advances and prospects. *Anal. Chem.* **2023**, *95*, 2590–2622. [\[CrossRef\]](#) [\[PubMed\]](#)
60. Farahmandpour, M.; Kordrostami, Z.; Rajabzadeh, M.; Khalifeh, R. Flexible bio-electronic hybrid metal-oxide channel FET as a glucose sensor. *IEEE Trans. Nanobiosci.* **2023**, *22*, 855–862. [\[CrossRef\]](#)
61. Zhang, X.; Pu, Z.; Su, X.; Li, C.; Zheng, H.; Li, D. Flexible organic field-effect transistors-based biosensors: Progress and perspectives. *Anal. Bioanal. Chem.* **2023**, *415*, 1607–1625. [\[CrossRef\]](#)
62. Jiang, D.; Sheng, K.; Gui, G.; Jiang, H.; Liu, X.; Wang, L. A novel smartphone-based electrochemical cell sensor for evaluating the toxicity of heavy metal ions Cd<sup>2+</sup>, Hg<sup>2+</sup>, and Pb<sup>2+</sup> in rice. *Anal. Bioanal. Chem.* **2021**, *413*, 4277–4287. [\[CrossRef\]](#)
63. Sivakumar, R.; Lee, N.Y. Recent progress in smartphone-based techniques for food safety and the detection of heavy metal ions in environmental water. *Chemosphere* **2021**, *275*, 130096. [\[CrossRef\]](#)
64. Xu, Z.; Liu, Z.; Xiao, M.; Jiang, L.; Yi, C. A smartphone-based quantitative point-of-care testing (POCT) system for simultaneous detection of multiple heavy metal ions. *Chem. Eng. J.* **2020**, *394*, 124966. [\[CrossRef\]](#)
65. Zhang, W.; Liu, C.; Liu, F.; Zou, X.; Xu, Y.; Xu, X. A smart-phone-based electrochemical platform with programmable solid-state-microwave flow digestion for determination of heavy metals in liquid food. *Food Chem.* **2020**, *303*, 125378. [\[CrossRef\]](#)
66. Liao, J.; Chang, F.; Han, X.; Ge, C.; Lin, S. Wireless water quality monitoring and spatial mapping with disposable whole-copper electrochemical sensors and a smartphone. *Sens. Actuators B Chem.* **2020**, *306*, 127557. [\[CrossRef\]](#)
67. Nemiroski, A.; Christodouleas, D.C.; Hennek, J.W.; Kumar, A.A.; Maxwell, E.J.; Fernández-Abedul, M.T.; Whitesides, G.M. Universal mobile electrochemical detector designed for use in resource-limited applications. *Proc. Natl. Acad. Sci. USA* **2014**, *111*, 11984–11989. [\[CrossRef\]](#) [\[PubMed\]](#)
68. Li, Y.; Chen, Y.; Yu, H.; Tian, L.; Wang, Z. Portable and smart devices for monitoring heavy metal ions integrated with nanomaterials. *TrAC-Trends Anal. Chem.* **2018**, *98*, 190–200. [\[CrossRef\]](#)
69. Li, Z.; Xu, D.; Zhang, D.; Yamaguchi, Y. A portable instrument for on-site detection of heavy metal ions in water. *Anal. Bioanal. Chem.* **2021**, *413*, 3471–3477. [\[CrossRef\]](#)
70. Xu, G.; Li, X.; Cheng, C.; Yang, J.; Liu, Z.; Shi, Z.; Zhu, L.; Lu, Y.; Low, S.S.; Liu, Q. Fully integrated battery-free and flexible electrochemical tag for on-demand wireless in situ monitoring of heavy metals. *Sens. Actuators B Chem.* **2020**, *310*, 127809. [\[CrossRef\]](#)
71. Muhammad-Aree, S.; Teepoo, S. On-site detection of heavy metals in wastewater using a single paper strip integrated with a smartphone. *Anal. Bioanal. Chem.* **2020**, *412*, 1395–1405. [\[CrossRef\]](#) [\[PubMed\]](#)
72. Hönicke, I.M.; Senkovska, I.; Bon, V.; Baburin, I.A.; Bönisch, N.; Raschke, S.; Evans, J.D.; Kaskel, S. Balancing mechanical stability and ultrahigh porosity in crystalline framework materials. *Angew. Chem. Int. Ed.* **2018**, *57*, 13780–13783. [\[CrossRef\]](#) [\[PubMed\]](#)
73. Morozan, A.; Jaouen, F. Metal organic frameworks for electrochemical applications. *Energy Environ. Sci.* **2012**, *5*, 9269–9290. [\[CrossRef\]](#)
74. Chuang, C.H.; Kung, C.W. Metal–organic frameworks toward electrochemical sensors: Challenges and opportunities. *Electroanalysis* **2020**, *32*, 1885–1895. [\[CrossRef\]](#)
75. Farha, O.K.; Hupp, J.T. Rational design, synthesis, purification, and activation of metal–organic framework materials. *Acc. Chem. Res.* **2010**, *43*, 1166–1175. [\[CrossRef\]](#)
76. Ma, D.; Li, Z.; Zhu, J.; Zhou, Y.; Chen, L.; Mai, X.; Liufu, M.; Wu, Y.; Li, Y. Inverse and highly selective separation of CO<sub>2</sub>/C<sub>2</sub>H<sub>2</sub> on a thulium–organic framework. *J. Mater. Chem. A* **2020**, *8*, 11933–11937. [\[CrossRef\]](#)
77. Luo, D.; Huang, J.; Jian, Y.; Singh, A.; Kumar, A.; Liu, J.; Pan, Y.; Ouyang, Q. Metal–organic frameworks (MOFs) as apt luminescent probes for the detection of biochemical analytes. *J. Mater. Chem. B* **2023**, *11*, 6802–6822. [\[CrossRef\]](#) [\[PubMed\]](#)
78. Tan, G.; Wang, S.; Yu, J.; Chen, J.; Liao, D.; Liu, M.; Nezamzadeh-Ejehieh, A.; Pan, Y.; Liu, J. Detection mechanism and the outlook of metal-organic frameworks for the detection of hazardous substances in milk. *Food Chem.* **2024**, *430*, 136934. [\[CrossRef\]](#) [\[PubMed\]](#)
79. Ke, F.; Pan, A.; Liu, J.; Liu, X.; Yuan, T.; Zhang, C.; Fu, G.; Peng, C.; Zhu, J.; Wan, X. Hierarchical camellia-like metal–organic frameworks via a bimetal competitive coordination combined with alkaline-assisted strategy for boosting selective fluoride removal from brick tea. *J. Colloid Interface Sci.* **2023**, *642*, 61–68. [\[CrossRef\]](#) [\[PubMed\]](#)
80. Liu, X.; Yang, H.; Diao, Y.; He, Q.; Lu, C.; Singh, A.; Kumar, A.; Liu, J.; Lan, Q. Recent advances in the electrochemical applications of Ni-based metal organic frameworks (Ni-MOFs) and their derivatives. *Chemosphere* **2022**, *307*, 135729. [\[CrossRef\]](#)

81. Li, D.; Shustova, N.B.; Martin, C.R.; Taylor-Pashow, K.; Seaman, J.C.; Kaplan, D.I.; Amoroso, J.W.; Chernikov, R. Anion-exchanged and quaternary ammonium functionalized MIL-101-Cr metal-organic framework (MOF) for  $\text{ReO}_4^-/\text{TcO}_4^-$  sequestration from groundwater. *J. Environ. Radioact.* **2020**, *222*, 106372. [[CrossRef](#)]
82. Faria, R.G.; Julião, D.; Balula, S.S.; Cunha-Silva, L. Hf-based UiO-66 as adsorptive compound and oxidative catalyst for denitrogenation processes. *Compounds* **2021**, *1*, 3–14. [[CrossRef](#)]
83. Railey, P.; Song, Y.; Liu, T.; Li, Y. Metal organic frameworks with immobilized nanoparticles: Synthesis and applications in photocatalytic hydrogen generation and energy storage. *Mat. Res. Bull.* **2017**, *96*, 385–394. [[CrossRef](#)]
84. Fang, X.; Chen, X.; Liu, Y.; Li, Q.; Zeng, Z.; Maiyalagan, T.; Mao, S. Nanocomposites of Zr(IV)-based metal-organic frameworks and reduced graphene oxide for electrochemically sensing ciprofloxacin in water. *ACS Appl. Nano Mater.* **2019**, *2*, 2367–2376. [[CrossRef](#)]
85. Dehdashtian, S.; Hashemi, B.; Aeenmehr, A. The application of perlite/cobalt oxide/reduced graphene oxide (PC-rGO)/metal organic framework (MOF) composite as electrode modifier for direct sensing of anticancer drug idarubicin. *IEEE Sens. J.* **2019**, *19*, 11739–11745. [[CrossRef](#)]
86. Altass, H.M.; Morad, M.; Khder, A.E.-R.S.; Mannaa, M.A.; Jassas, R.S.; Alsimaree, A.A.; Ahmed, S.A.; Salama, R.S. Enhanced catalytic activity for CO oxidation by highly active Pd nanoparticles supported on reduced graphene oxide/copper metal organic framework. *J. Taiwan Inst. Chem. Eng.* **2021**, *128*, 194–208. [[CrossRef](#)]
87. Baghayeri, M.; Ghanei-Motlagh, M.; Tayebee, R.; Fayazi, M.; Narenji, F. Application of graphene/zinc-based metal-organic framework nanocomposite for electrochemical sensing of As (III) in water resources. *Anal. Chim. Acta* **2020**, *1099*, 60–67. [[CrossRef](#)] [[PubMed](#)]
88. Huang, Y.; Niu, Q.; Jian, L.; Zhao, W.; Li, Y.; Dong, W.; Zhang, K.; Liang, W.; Yang, C. Synthesis of porphyrinic metal-organic framework/rGO nanocomposite for electrochemical recognition of copper ions in water. *J. Organomet. Chem.* **2023**, *985*, 122597. [[CrossRef](#)]
89. Li, D.; Yan, D.; Zhang, X.; Li, J.; Lu, T.; Pan, L. Porous CuO/reduced graphene oxide composites synthesized from metal-organic frameworks as anodes for high-performance sodium-ion batteries. *J. Colloid Interface Sci.* **2017**, *497*, 350–358. [[CrossRef](#)] [[PubMed](#)]
90. Cui, X.; Yang, B.; Zhao, S.; Li, X.; Qiao, M.; Mao, R.; Wang, Y.; Zhao, X. Electrochemical sensor based on ZIF-8@ dimethylglyoxime and  $\beta$ -cyclodextrin modified reduced graphene oxide for nickel (II) detection. *Sens. Actuators B Chem.* **2020**, *315*, 128091. [[CrossRef](#)]
91. Huo, D.; Zhang, Y.; Li, N.; Ma, W.; Liu, H.; Xu, G.; Li, Z.; Yang, M.; Hou, C. Three-dimensional graphene/amino-functionalized metal-organic framework for simultaneous electrochemical detection of Cd (II), Pb (II), Cu (II), and Hg (II). *Anal. Bioanal. Chem.* **2022**, *414*, 1575–1586. [[CrossRef](#)] [[PubMed](#)]
92. Guo, T.-T.; Cao, X.-Y.; An, Y.-Y.; Zhang, X.-L.; Yan, J.-Z. Sulfur-bridged Co (II)-thiacalix [4] arene metal-organic framework as an electrochemical sensor for the determination of toxic heavy metals. *Inorg. Chem.* **2023**, *62*, 4485–4494. [[CrossRef](#)] [[PubMed](#)]
93. Ding, Y.; Wei, F.; Dong, C.; Li, J.; Zhang, C.; Han, X. UiO-66 based electrochemical sensor for simultaneous detection of Cd (II) and Pb (II). *Inorg. Chem. Commun.* **2021**, *131*, 108785. [[CrossRef](#)]
94. Yang, S.; Yang, M.; Yao, X.; Fa, H.; Wang, Y.; Hou, C. A zeolitic imidazolate framework/carbon nanofiber nanocomposite based electrochemical sensor for simultaneous detection of co-existing dihydroxybenzene isomers. *Sens. Actuators B Chem.* **2020**, *320*, 128294. [[CrossRef](#)]
95. Yang, H.; Peng, C.; Han, J.; Song, Y.; Wang, L. Three-dimensional macroporous Carbon/Zr-2, 5-dimercaptoterephthalic acid metal-organic frameworks nanocomposites for removal and detection of Hg (II). *Sens. Actuators B Chem.* **2020**, *320*, 128447. [[CrossRef](#)]
96. Singh, S.; Numan, A.; Zhan, Y.; Singh, V.; Van Hung, T.; Nam, N.D. A novel highly efficient and ultrasensitive electrochemical detection of toxic mercury (II) ions in canned tuna fish and tap water based on a copper metal-organic framework. *J. Hazard. Mater.* **2020**, *399*, 123042. [[CrossRef](#)]
97. Ru, J.; Wang, X.; Cui, X.; Wang, F.; Ji, H.; Du, X.; Lu, X. GaOOH-modified metal-organic frameworks UiO-66-NH<sub>2</sub>: Selective and sensitive sensing four heavy-metal ions in real wastewater by electrochemical method. *Talanta* **2021**, *234*, 122679. [[CrossRef](#)]
98. Zhou, S.; Lu, L.; Liu, D.; Wang, J.; Sakiyama, H.; Muddassir, M.; Nezamzadeh-Ejhieh, A.; Liu, J. Series of highly stable Cd (II)-based MOFs as sensitive and selective sensors for detection of nitrofurantoin antibiotic. *Cryst. Eng. Comm.* **2021**, *23*, 8043–8052. [[CrossRef](#)]
99. Wang, N.; Zhao, W.; Shen, Z.; Sun, S.; Dai, H.; Ma, H.; Lin, M. Sensitive and selective detection of Pb (II) and Cu (II) using a metal-organic framework/polypyrrole nanocomposite functionalized electrode. *Sens. Actuators B Chem.* **2020**, *304*, 127286. [[CrossRef](#)]
100. Ru, J.; Wang, X.; Zhao, J.; Yang, J.; Zhou, Z.; Du, X.; Lu, X. Evaluation and development of GO/UiO-67@ PtNPs nanohybrid-based electrochemical sensor for invisible arsenic (III) in water samples. *Microchem. J.* **2022**, *181*, 107765. [[CrossRef](#)]
101. Zhao, J.; Long, Y.; He, C.; Yang, H.; Zhao, S.; Luo, X.; Huo, D.; Hou, C. Simultaneous electrochemical detection of Cd<sup>2+</sup> and Pb<sup>2+</sup> based on an MOF-derived carbon composite linked with multiwalled carbon nanotubes. *ACS Sustain. Chem. Eng.* **2023**, *11*, 2160–2171. [[CrossRef](#)]
102. Hanif, F.; Tahir, A.; Akhtar, M.; Waseem, M.; Haider, S.; Aboud, M.F.A.; Shakir, I.; Imran, M.; Warsi, M.F. Ultra-selective detection of Cd<sup>2+</sup> and Pb<sup>2+</sup> using glycine functionalized reduced graphene oxide/polyaniline nanocomposite electrode. *Synth. Met.* **2019**, *257*, 116185. [[CrossRef](#)]

103. Oularbi, L.; Turmine, M.; El Rhazi, M. Preparation of novel nanocomposite consisting of bismuth particles, polypyrrole and multi-walled carbon nanotubes for simultaneous voltammetric determination of cadmium (II) and lead (II). *Synth. Met.* **2019**, *253*, 1–8. [[CrossRef](#)]
104. Akhtar, M.; Tahir, A.; Zulfiqar, S.; Hanif, F.; Warsi, M.F.; Agboola, P.O.; Shakir, I. Ternary hybrid of polyaniline-alanine-reduced graphene oxide for electrochemical sensing of heavy metal ions. *Synth. Met.* **2020**, *265*, 116410. [[CrossRef](#)]
105. Mahmoudian, M.; Basirun, W.; Alias, Y.; MengWoi, P. Investigating the effectiveness of g-C<sub>3</sub>N<sub>4</sub> on Pt/g-C<sub>3</sub>N<sub>4</sub>/polythiophene nanocomposites performance as an electrochemical sensor for Hg<sup>2+</sup> detection. *J. Environ. Chem. Eng.* **2020**, *8*, 104204. [[CrossRef](#)]
106. Mahmoudian, M.; Alias, Y.; Woi, P.M.; Yousefi, R.; Basirun, W. An electrochemical sensor based on Pt/g-C<sub>3</sub>N<sub>4</sub>/polyaniline nanocomposite for detection of Hg<sup>2+</sup>. *Adv. Powder Technol.* **2020**, *31*, 3372–3380. [[CrossRef](#)]
107. Guo, X.; Cui, R.; Huang, H.; Li, Y.; Liu, B.; Wang, J.; Zhao, D.; Dong, J.; Sun, B. Insights into the role of pyrrole doped in three-dimensional graphene aerogels for electrochemical sensing Cd(II). *J. Electroanal. Chem.* **2020**, *871*, 114323. [[CrossRef](#)]
108. Katowah, D.F.; Alsulami, Q.A.; Alam, M.; Ismail, S.H.; Asiri, A.M.; Mohamed, G.G.; Rahman, M.M.; Hussein, M.A. The performance of various SWCNT loading into CuO-PMMA nanocomposites towards the detection of Mn<sup>2+</sup> ions. *J. Inorg. Organomet. Polym. Mater.* **2020**, *30*, 5024–5041. [[CrossRef](#)]
109. Deshmukh, M.A.; Shirsat, M.D.; Ramanaviciene, A.; Ramanavicius, A. Composites based on conducting polymers and carbon nanomaterials for heavy metal ion sensing. *Crit. Rev. Anal. Chem.* **2018**, *48*, 293–304. [[CrossRef](#)] [[PubMed](#)]
110. El Rhazi, M.; Majid, S.; Elbasri, M.; Salih, F.E.; Oularbi, L.; Lafdi, K. Recent progress in nanocomposites based on conducting polymer: Application as electrochemical sensors. *Int. Nano Lett.* **2018**, *8*, 79–99. [[CrossRef](#)]
111. Kaur, G.; Kaur, A.; Kaur, H. Review on nanomaterials/conducting polymer based nanocomposites for the development of biosensors and electrochemical sensors. *Polym. Plast. Technol. Mater.* **2021**, *60*, 504–521. [[CrossRef](#)]
112. Deshmukh, M.A.; Patil, H.K.; Bodkhe, G.A.; Yasuzawa, M.; Koinkar, P.; Ramanaviciene, A.; Shirsat, M.D.; Ramanavicius, A. EDTA-modified PANI/SWNTs nanocomposite for differential pulse voltammetry based determination of Cu(II) ions. *Sens. Actuators B Chem.* **2018**, *260*, 331–338. [[CrossRef](#)]
113. Bashir, S.; Ramesh, S.; Ramesh, K.; Numan, A.; Iqbal, J. *Conducting Polymer Composites in Electrochemical Sensors; Conducting Polymer Composites*, Central West Publishing: Orange, Australia, 2018; pp. 41–68.
114. Kumar, H.; Kumari, N.; Sharma, R. Nanocomposites (conducting polymer and nanoparticles) based electrochemical biosensor for the detection of environment pollutant: Its issues and challenges. *Environ. Impact Assess. Rev.* **2020**, *85*, 106438. [[CrossRef](#)]
115. Rashed, M.A.; Ahmed, J.; Faisal, M.; Alsareii, S.; Jalalah, M.; Harraz, F.A. Highly sensitive and selective thiourea electrochemical sensor based on novel silver nanoparticles/chitosan nanocomposite. *Colloids Surf. A Physicochem. Eng. Asp.* **2022**, *644*, 128879. [[CrossRef](#)]
116. Rahman, M.M.; Alamry, K.A.; Awual, M.R.; Mekky, A.E. Efficient Hg(II) ionic probe development based on one-step synthesized diethyl thieno [2, 3-b] thiophene-2, 5-dicarboxylate (DETTDC2) onto glassy carbon electrode. *Microchem. J.* **2020**, *152*, 104291. [[CrossRef](#)]
117. Feng, T.; Chen, K.; Zhong, J.; Cheng, Y.; Zhao, H.; Lan, M. In-situ polymerization of dendritic polyaniline nanofibers network embedded with Ag@SiO<sub>2</sub> core-shell nanoparticles for electrochemical determination of trace arsenic (III). *Sens. Actuators B Chem.* **2022**, *369*, 132265. [[CrossRef](#)]
118. Fall, B.; Diaw, A.K.; Fall, M.; Sall, M.L.; Lo, M.; Gningue-Sall, D.; Thotiyi, M.O.; Maria, H.J.; Kalarikkal, N.; Thomas, S. Synthesis of highly sensitive rGO@CNT@Fe<sub>2</sub>O<sub>3</sub>/polypyrrole nanocomposite for the electrochemical detection of Pb<sup>2+</sup>. *Mater. Today Commun.* **2021**, *26*, 102005. [[CrossRef](#)]
119. Deshmukh, M.A.; Bodkhe, G.A.; Shirsat, S.; Ramanavicius, A.; Shirsat, M.D. Nanocomposite platform based on EDTA modified Ppy/SWNTs for the sensing of Pb (II) ions by electrochemical method. *Front. Chem.* **2018**, *6*, 451. [[CrossRef](#)] [[PubMed](#)]
120. Wu, W.; Jia, M.; Zhang, Z.; Chen, X.; Zhang, Q.; Zhang, W.; Li, P.; Chen, L. Sensitive, selective and simultaneous electrochemical detection of multiple heavy metals in environment and food using a lowcost Fe<sub>3</sub>O<sub>4</sub> nanoparticles/fluorinated multi-walled carbon nanotubes sensor. *Ecotoxicol. Environ. Saf.* **2019**, *175*, 243–250. [[CrossRef](#)] [[PubMed](#)]
121. Xu, Z.; Fan, X.; Ma, Q.; Tang, B.; Lu, Z.; Zhang, J.; Mo, G.; Ye, J.; Ye, J. A sensitive electrochemical sensor for simultaneous voltammetric sensing of cadmium and lead based on Fe<sub>3</sub>O<sub>4</sub>/multiwalled carbon nanotube/laser scribed graphene composites functionalized with chitosan modified electrode. *Mater. Chem. Phys.* **2019**, *238*, 121877. [[CrossRef](#)]
122. Le Hai, T.; Hung, L.C.; Phuong, T.T.B.; Ha, B.T.T.; Nguyen, B.-S.; Hai, T.D.; Nguyen, V.-H. Multiwall carbon nanotube modified by antimony oxide (Sb<sub>2</sub>O<sub>3</sub>/MWCNTs) paste electrode for the simultaneous electrochemical detection of cadmium and lead ions. *Microchem. J.* **2020**, *153*, 104456. [[CrossRef](#)]
123. Mariyappan, V.; Manavalan, S.; Chen, S.-M.; Jaysiva, G.; Veerakumar, P.; Keerthi, M. Sr@FeNi-S nanoparticle/carbon nanotube nanocomposite with superior electrocatalytic activity for electrochemical detection of toxic mercury (II). *ACS Appl. Electron. Mater.* **2020**, *2*, 1943–1952. [[CrossRef](#)]
124. Katowah, D.F.; Hussein, M.A.; Alam, M.; Ismail, S.H.; Osman, O.; Sobahi, T.; Asiri, A.M.; Ahmed, J.; Rahman, M.M. Designed network of ternary core-shell PPCOT/NiFe<sub>2</sub>O<sub>4</sub>/C-SWCNTs nanocomposites. A Selective Fe<sup>3+</sup> ionic sensor. *J. Alloys Compd.* **2020**, *834*, 155020. [[CrossRef](#)]
125. Yıldız, C.; Bayraktepe, D.E.; Yazan, Z.; Önal, M. Bismuth nanoparticles decorated on Na-montmorillonite-multiwall carbon nanotube for simultaneous determination of heavy metal ions-electrochemical methods. *J. Electroanal. Chem.* **2022**, *910*, 116205. [[CrossRef](#)]

126. Yu, L.; Wan, J.-W.; Meng, X.-Z.; Gu, H.-W.; Chen, Y.; Yi, H.-C. A simple electrochemical method for Cd (II) determination in real samples based on carbon nanotubes and metal-organic frameworks. *Int. J. Environ. Anal. Chem.* **2022**, *102*, 4757–4767. [[CrossRef](#)]
127. Tan, R.; Jiang, P.; Pan, C.; Pan, J.; Gao, N.; Cai, Z.; Wu, F.; Chang, G.; Xie, A.; He, Y. Core-shell architected NH<sub>2</sub>-UiO-66@ZIF-8/multi-walled carbon nanotubes nanocomposite-based sensitive electrochemical sensor towards simultaneous determination of Pb<sup>2+</sup> and Cu<sup>2+</sup>. *Mikrochim. Acta* **2023**, *190*, 30. [[CrossRef](#)]
128. Fan, C.; Chen, L.; Jiang, R.; Ye, J.; Li, H.; Shi, Y.; Luo, Y.; Wang, G.; Hou, J.; Guo, X. ZnFe<sub>2</sub>O<sub>4</sub> nanoparticles for electrochemical determination of trace Hg(II), Pb(II), Cu(II), and glucose. *ACS Appl. Nano Mater.* **2021**, *4*, 4026–4036. [[CrossRef](#)]
129. Wang, Y.; Zhao, G.; Zhang, Q.; Wang, H.; Zhang, Y.; Cao, W.; Zhang, N.; Du, B.; Wei, Q. Electrochemical aptasensor based on gold modified graphene nanocomposite with different morphologies for ultrasensitive detection of Pb<sup>2+</sup>. *Sens. Actuat. B Chem.* **2019**, *288*, 325–331. [[CrossRef](#)]
130. Baghayeri, M.; Alinezhad, H.; Fayazi, M.; Tarahomi, M.; Ghanei-Motlagh, R.; Maleki, B. A novel electrochemical sensor based on a glassy carbon electrode modified with dendrimer functionalized magnetic graphene oxide for simultaneous determination of trace Pb(II) and Cd(II). *Electrochim. Acta* **2019**, *312*, 80–88. [[CrossRef](#)]
131. Priya, T.; Dhanalakshmi, N.; Karthikeyan, V.; Thinakaran, N. Highly selective simultaneous trace determination of Cd<sup>2+</sup> and Pb<sup>2+</sup> using porous graphene/carboxymethyl cellulose/fondaparinux nanocomposite modified electrode. *J. Electroanal. Chem.* **2019**, *833*, 543–551. [[CrossRef](#)]
132. Cheng, Y.; Li, H.; Fang, C.; Ai, L.; Chen, J.; Su, J.; Zhang, Q.; Fu, Q. Facile synthesis of reduced graphene oxide/silver nanoparticles composites and their application for detecting heavy metal ions. *J. Alloys Compd.* **2019**, *787*, 683–693. [[CrossRef](#)]
133. El-Shafai, N.M.; Abdelfatah, M.M.; El-Khouly, M.E.; El-Mehasseb, I.M.; El-Shaer, A.; Ramadan, M.S.; Masoud, M.S.; El-Kemary, M.A. Magnetite nano-spherical quantum dots decorated graphene oxide nano sheet (GO@Fe<sub>3</sub>O<sub>4</sub>): Electrochemical properties and applications for removal heavy metals, pesticide and solar cell. *Appl. Surf. Sci.* **2020**, *506*, 144896. [[CrossRef](#)]
134. Tan, Z.; Wu, W.; Feng, C.; Wu, H.; Zhang, Z. Simultaneous determination of heavy metals by an electrochemical method based on a nanocomposite consisting of fluorinated graphene and gold nanocage. *Mikrochim. Acta* **2020**, *187*, 1–9. [[CrossRef](#)]
135. Das, T.R.; Sharma, P.K. Hydrothermal-assisted green synthesis of Ni/Ag@rGO nanocomposite using Punica granatum juice and electrochemical detection of ascorbic acid. *Microchem. J.* **2020**, *156*, 104850. [[CrossRef](#)]
136. Hwa, K.-Y.; Sharma, T.S.K.; Ganguly, A. Design strategy of rGO-HNT-AgNPs based hybrid nanocomposite with enhanced performance for electrochemical detection of 4-nitrophenol. *Inorg. Chem. Front.* **2020**, *7*, 1981–1994. [[CrossRef](#)]
137. Bi, C.-C.; Ke, X.-X.; Chen, X.; Weerasooriya, R.; Hong, Z.-Y.; Wang, L.-C.; Wu, Y.-C. Assembling reduced graphene oxide with sulfur/nitrogen-“hooks” for electrochemical determination of Hg(II). *Anal. Chim. Acta* **2020**, *1100*, 31–39. [[CrossRef](#)]
138. Pang, J.; Fu, H.; Kong, W.; Jiang, R.; Ye, J.; Zhao, Z.; Hou, J.; Sun, K.; Zheng, Y.; Chen, L. Design of NiCo<sub>2</sub>O<sub>4</sub> nanoparticles decorated N, S co-doped reduced graphene oxide composites for electrochemical simultaneous detection of trace multiple heavy metal ions and hydrogen evolution reaction. *Chem. Eng. J.* **2022**, *433*, 133854. [[CrossRef](#)]
139. Erçarıkcı, E.; Alanyalıoğlu, M. Dual-functional graphene-based flexible material for membrane filtration and electrochemical sensing of heavy metal ions. *IEEE Sens. J.* **2020**, *21*, 2468–2475. [[CrossRef](#)]
140. Guo, C.; Wang, C.; Sun, H.; Dai, D.; Gao, H. A simple electrochemical sensor based on rGO/MoS<sub>2</sub>/CS modified GCE for highly sensitive detection of Pb(II) in tobacco leaves. *RSC Adv.* **2021**, *11*, 29590–29597. [[CrossRef](#)] [[PubMed](#)]
141. Bhardiya, S.R.; Asati, A.; Sheshma, H.; Rai, A.; Rai, V.K.; Singh, M. A novel bioconjugated reduced graphene oxide-based nanocomposite for sensitive electrochemical detection of cadmium in water. *Sens. Actuat. B Chem.* **2021**, *328*, 129019. [[CrossRef](#)]
142. Wang, L.; Peng, X.; Fu, H. An electrochemical aptasensor for the sensitive detection of Pb<sup>2+</sup> based on a chitosan/reduced graphene oxide/titanium dioxide. *Microchem. J.* **2022**, *174*, 106977. [[CrossRef](#)]
143. Kushwah, M.; Yadav, R.; Berlina, A.N.; Gaur, K.; Gaur, M. Development of an ultrasensitive rGO/AuNPs/ssDNA-based electrochemical aptasensor for detection of Pb<sup>2+</sup>. *J. Solid State Electrochem.* **2023**, *27*, 559–574. [[CrossRef](#)]
144. Zheng, H.; Ntuli, L.; Mbanjwa, M.; Palaniandy, N.; Smith, S.; Modibedi, M.; Land, K.; Mathe, M. The effect of gC<sub>3</sub>N<sub>4</sub> materials on Pb(II) and Cd(II) detection using disposable screen-printed sensors. *Electrocatalysis* **2019**, *10*, 149–155. [[CrossRef](#)]
145. Xiao, X.-Y.; Chen, S.-H.; Li, S.-S.; Wang, J.; Zhou, W.-Y.; Huang, X.-J. Synergistic catalysis of N vacancies and ~ 5 nm Au nanoparticles promoted the highly sensitive electrochemical determination of lead (II) using an Au/N-deficient-C<sub>3</sub>N<sub>4</sub> nanocomposite. *Environ. Sci. Nano* **2019**, *6*, 1895–1908. [[CrossRef](#)]
146. Ramalingam, M.; Ponnusamy, V.K.; Sangilimuthu, S.N. A nanocomposite consisting of porous graphitic carbon nitride nanosheets and oxidized multiwalled carbon nanotubes for simultaneous stripping voltammetric determination of cadmium (II), mercury (II), lead (II) and zinc (II). *Mikrochim. Acta* **2019**, *186*, 69. [[CrossRef](#)]
147. Karthika, A.; Nikhil, S.; Suganthi, A.; Rajarajan, M. A facile sonochemical approach based on graphene carbon nitride doped silver molybdate immobilized nafion for selective and sensitive electrochemical detection of chromium (VI) in real sample. *Adv. Powder Technol.* **2020**, *31*, 1879–1890. [[CrossRef](#)]
148. Hu, J.-Y.; Li, Z.; Zhai, C.-Y.; Wang, J.-F.; Zeng, L.-X.; Zhu, M.-S. Plasmonic photo-assisted electrochemical sensor for detection of trace lead ions based on Au anchored on two-dimensional gC<sub>3</sub>N<sub>4</sub>/graphene nanosheets. *Rare Met.* **2021**, *40*, 1727–1737. [[CrossRef](#)]
149. Hu, J.; Li, Z.; Zhai, C.; Zeng, L.; Zhu, M. Photo-assisted simultaneous electrochemical detection of multiple heavy metal ions with a metal-free carbon black anchored graphitic carbon nitride sensor. *Anal. Chim. Acta* **2021**, *1183*, 338951. [[CrossRef](#)]

150. Pu, Y.; Wu, Y.; Yu, Z.; Lu, L.; Wang, X. Simultaneous determination of Cd<sup>2+</sup> and Pb<sup>2+</sup> by an electrochemical sensor based on Fe<sub>3</sub>O<sub>4</sub>/Bi<sub>2</sub>O<sub>3</sub>/C<sub>3</sub>N<sub>4</sub> nanocomposites. *Talanta Open* **2021**, *3*, 100024. [[CrossRef](#)]
151. Eswaran, M.; Tsai, P.-C.; Wu, M.-T.; Ponnusamy, V.K. Novel nano-engineered environmental sensor based on polymelamine/graphitic-carbon nitride nanohybrid material for sensitive and simultaneous monitoring of toxic heavy metals. *J. Hazard. Mater.* **2021**, *418*, 126267. [[CrossRef](#)]
152. Wang, Y.; Nie, Z.; Li, X.; Zhao, Y.; Wang, H. Highly sensitive and selective electrochemical sensor based on porous graphitic carbon nitride/CoMn<sub>2</sub>O<sub>4</sub> nanocomposite toward heavy metal ions. *Sens. Actuat. B Chem.* **2021**, *346*, 130539. [[CrossRef](#)]
153. Hassanpoor, S.; Rouhi, N. Electrochemical sensor for determination of trace amounts of cadmium (II) in environmental water samples based on MnO<sub>2</sub>/RGO nanocomposite. *Int. J. Environ. Anal. Chem.* **2021**, *101*, 513–532. [[CrossRef](#)]
154. Sun, Y.-F.; Li, P.-H.; Yang, M.; Huang, X.-J. Highly sensitive electrochemical detection of Pb (II) based on excellent adsorption and surface Ni (II)/Ni (III) cycle of porous flower-like NiO/rGO nanocomposite. *Sens. Actuators B Chem.* **2019**, *292*, 136–147. [[CrossRef](#)]
155. Vajedi, F.; Dehghani, H. The characterization of TiO<sub>2</sub>-reduced graphene oxide nanocomposites and their performance in electrochemical determination for removing heavy metals ions of cadmium (II), lead (II) and copper (II). *Mater. Sci. Eng. B* **2019**, *243*, 189–198. [[CrossRef](#)]
156. Huang, W.; Zhang, Y.; Li, Y.; Zeng, T.; Wan, Q.; Yang, N. Morphology-controlled electrochemical sensing of environmental Cd<sup>2+</sup> and Pb<sup>2+</sup> ions on expanded graphite supported CeO<sub>2</sub> nanomaterials. *Anal. Chim. Acta* **2020**, *1126*, 63–71. [[CrossRef](#)]
157. Koshki, M.-S.; Baghayeri, M.; Fayazi, M. Application of sepiolite/FeS<sub>2</sub> nanocomposite for highly selective detection of mercury (II) based on stripping voltammetric analysis. *J. Food Meas. Charact.* **2021**, *15*, 5318–5325. [[CrossRef](#)]
158. Wei, J.; Zhao, J.; Li, C.-Y.; Xie, X.-Y.; Wei, Y.-Y.; Shen, W.; Wang, J.-P.; Yang, M. Highly sensitive and selective electrochemical detection of Pb(II) in serum via an α-Fe<sub>2</sub>O<sub>3</sub>/NiO heterostructure: Evidence from theoretical calculations and adsorption investigation. *Sens. Actuat. B Chem.* **2021**, *344*, 130295. [[CrossRef](#)]
159. Cheng, X.-L.; Xu, Q.-Q.; Li, S.-S.; Li, J.; Zhou, Y.; Zhang, Y.; Li, S. Oxygen vacancy enhanced Co<sub>3</sub>O<sub>4</sub>/ZnO nanocomposite with small sized and loose structure for sensitive electroanalysis of Hg (II) in subsidence area water. *Sens. Actuators B Chem.* **2021**, *326*, 128967. [[CrossRef](#)]
160. Buica, G.-O.; Stoian, A.B.; Manole, C.; Demetrescu, I.; Pirvu, C. Zr/ZrO<sub>2</sub> nanotube electrode for detection of heavy metal ions. *Electrochem. Commun.* **2020**, *110*, 106614. [[CrossRef](#)]
161. Jin, W.; Fu, Y.; Hu, M.; Wang, S.; Liu, Z. Highly efficient SnS-decorated Bi<sub>2</sub>O<sub>3</sub> nanosheets for simultaneous electrochemical detection and removal of Cd (II) and Pb (II). *J. Electroanal. Chem.* **2020**, *856*, 113744. [[CrossRef](#)]
162. Sun, Y.-F.; Li, J.-J.; Xie, F.; Wei, Y.; Yang, M. Ruthenium-loaded cerium dioxide nanocomposites with rich oxygen vacancies promoted the highly sensitive electrochemical detection of Hg(II). *Sens. Actuat. B Chem.* **2020**, *320*, 128355. [[CrossRef](#)]
163. Krishnan, S.; Chatterjee, S.; Solanki, A.; Guha, N.; Singh, M.K.; Gupta, A.K.; Rai, D.K. Aminotetrazole-functionalized SiO<sub>2</sub> coated MgO nanoparticle composites for removal of acid fuchsin dye and detection of heavy metal ions. *ACS Appl. Nano Mater.* **2020**, *3*, 11203–11216. [[CrossRef](#)]
164. Maleki, B.; Baghayeri, M.; Ghanei-Motlagh, M.; Zonoz, F.M.; Amiri, A.; Hajizadeh, F.; Hosseinfar, A.; Esmaeilnezhad, E. Polyamidoamine dendrimer functionalized iron oxide nanoparticles for simultaneous electrochemical detection of Pb<sup>2+</sup> and Cd<sup>2+</sup> ions in environmental waters. *Measurement* **2019**, *140*, 81–88. [[CrossRef](#)]
165. Karthika, A.; Raja, V.R.; Karuppasamy, P.; Suganthi, A.; Rajarajan, M. Electrochemical behaviour and voltammetric determination of mercury (II) ion in cupric oxide/poly vinyl alcohol nanocomposite modified glassy carbon electrode. *Microchem. J.* **2019**, *145*, 737–744. [[CrossRef](#)]
166. Singh, S.; Pankaj, A.; Mishra, S.; Tewari, K.; Singh, S.P. Cerium oxide-catalyzed chemical vapor deposition grown carbon nanofibers for electrochemical detection of Pb(II) and Cu(II). *J. Environ. Chem. Eng.* **2019**, *7*, 103250. [[CrossRef](#)]
167. Wang, L.; Lei, T.; Ren, Z.; Jiang, X.; Yang, X.; Bai, H.; Wang, S. Fe<sub>3</sub>O<sub>4</sub>@PDA@MnO<sub>2</sub> core-shell nanocomposites for sensitive electrochemical detection of trace Pb(II) in water. *J. Electroanal. Chem.* **2020**, *864*, 114065. [[CrossRef](#)]
168. Bakhsh, E.M.; Khan, S.B.; Asiri, A.M.; Shah, A. Zn/Fe nanocomposite based efficient electrochemical sensor for the simultaneous detection of metal ions. *Phys. E Low-Dimens. Syst. Nanostructures* **2021**, *130*, 114671. [[CrossRef](#)]
169. Li, G.; Qi, X.; Zhang, G.; Wang, S.; Li, K.; Wu, J.; Wan, X.; Liu, Y.; Li, Q. Low-cost voltammetric sensors for robust determination of toxic Cd(II) and Pb(II) in environment and food based on shuttle-like α-Fe<sub>2</sub>O<sub>3</sub> nanoparticles decorated β-Bi<sub>2</sub>O<sub>3</sub> microspheres. *Microchem. J.* **2022**, *179*, 107515. [[CrossRef](#)]
170. Hwang, J.-H.; Pathak, P.; Wang, X.; Rodriguez, K.L.; Cho, H.J.; Lee, W.H. A novel bismuth-chitosan nanocomposite sensor for simultaneous detection of Pb(II), Cd(II) and Zn(II) in wastewater. *Micromachines* **2019**, *10*, 511. [[CrossRef](#)] [[PubMed](#)]
171. Wei, P.; Zhu, Z.; Song, R.; Li, Z.; Chen, C. An ion-imprinted sensor based on chitosan-graphene oxide composite polymer modified glassy carbon electrode for environmental sensing application. *Electrochim. Acta* **2019**, *317*, 93–101. [[CrossRef](#)]
172. Wu, S.; Li, K.; Dai, X.; Zhang, Z.; Ding, F.; Li, S. An ultrasensitive electrochemical platform based on imprinted chitosan/gold nanoparticles/graphene nanocomposite for sensing cadmium (II) ions. *Microchem. J.* **2020**, *155*, 104710. [[CrossRef](#)]
173. Nguyen, L.D.; Doan, T.C.D.; Huynh, T.M.; Nguyen, V.N.P.; Dinh, H.H.; Dang, D.M.T.; Dang, C.M. An electrochemical sensor based on polyvinyl alcohol/chitosan-thermally reduced graphene composite modified glassy carbon electrode for sensitive voltammetric detection of lead. *Sens. Actuat. B Chem.* **2021**, *345*, 130443. [[CrossRef](#)]

174. He, Y.; Ma, L.; Zhou, L.; Liu, G.; Jiang, Y.; Gao, J. Preparation and application of bismuth/MXene nano-composite as electrochemical sensor for heavy metal ions detection. *Nanomaterials* **2020**, *10*, 866. [[CrossRef](#)]
175. Zhu, X.; Liu, B.; Li, L.; Wu, L.; Chen, S.; Huang, L.; Yang, J.; Liang, S.; Xiao, K.; Hu, J. A micromilled microgrid sensor with delaminated MXene-bismuth nanocomposite assembly for simultaneous electrochemical detection of lead (II), cadmium (II) and zinc (II). *Mikrochim. Acta* **2019**, *186*, 776. [[CrossRef](#)]
176. Hojjati-Najafabadi, A.; Mansoorianfar, M.; Liang, T.; Shahin, K.; Wen, Y.; Bahrami, A.; Karaman, C.; Zare, N.; Karimi-Maleh, H.; Vasseghian, Y. Magnetic-MXene-based nanocomposites for water and wastewater treatment: A review. *J. Water Process Eng.* **2022**, *47*, 102696. [[CrossRef](#)]
177. Rhouati, A.; Berkani, M.; Vasseghian, Y.; Golzadeh, N. MXene-based electrochemical sensors for detection of environmental pollutants: A comprehensive review. *Chemosphere* **2022**, *291*, 132921. [[CrossRef](#)]
178. Dhillon, A.; Singh, N.; Nair, M.; Kumar, D. Analytical methods to determine and sense heavy metal pollutants using MXene and MXene-based composites: Mechanistic prophecy into sensing properties. *Chemosphere* **2022**, *303*, 135166. [[CrossRef](#)] [[PubMed](#)]
179. Zhang, X.; An, D.; Bi, Z.; Shan, W.; Zhu, B.; Zhou, L.; Yu, L.; Zhang, H.; Xia, S.; Qiu, M.  $\text{Ti}_3\text{C}_2$ -MXene@ N-doped carbon heterostructure-based electrochemical sensor for simultaneous detection of heavy metals. *J. Electroanal. Chem.* **2022**, *911*, 116239. [[CrossRef](#)]
180. Chen, Y.; Zhao, P.; Liang, Y.; Ma, Y.; Liu, Y.; Zhao, J.; Hou, J.; Hou, C.; Huo, D. A sensitive electrochemical sensor based on 3D porous melamine-doped rGO/MXene composite aerogel for the detection of heavy metal ions in the environment. *Talanta* **2023**, *256*, 124294. [[CrossRef](#)] [[PubMed](#)]
181. Ganesh, P.-S.; Kim, S.-Y. Electrochemical sensing interfaces based on novel 2D-MXenes for monitoring environmental hazardous toxic compounds: A concise review. *J. Ind. Eng. Chem.* **2022**, *109*, 52–67. [[CrossRef](#)]
182. Zhu, X.; Liu, B.; Hou, H.; Huang, Z.; Zeinu, K.M.; Huang, L.; Yuan, X.; Guo, D.; Hu, J.; Yang, J. Alkaline intercalation of  $\text{Ti}_3\text{C}_2$  MXene for simultaneous electrochemical detection of Cd(II), Pb(II), Cu(II) and Hg(II). *Electrochim. Acta* **2017**, *248*, 46–57. [[CrossRef](#)]
183. Feng, X.; Yu, Z.; Long, R.; Li, X.; Shao, L.; Zeng, H.; Zeng, G.; Zuo, Y. Self-assembling 2D/2D (MXene/LDH) materials achieve ultra-high adsorption of heavy metals  $\text{Ni}^{2+}$  through terminal group modification. *Sep. Purif. Technol.* **2020**, *253*, 117525. [[CrossRef](#)]
184. Rasheed, P.A.; Pandey, R.P.; Jabbar, K.A.; Ponraj, J.; Mahmoud, K.A. Sensitive electrochemical detection of l-cysteine based on a highly stable Pd@ $\text{Ti}_3\text{C}_2\text{T}_x$  (MXene) nanocomposite modified glassy carbon electrode. *Anal. Methods* **2019**, *11*, 3851–3856. [[CrossRef](#)]
185. Desai, M.L.; Basu, H.; Singhal, R.K.; Saha, S.; Kailasa, S.K. Ultra-small two dimensional MXene nanosheets for selective and sensitive fluorescence detection of  $\text{Ag}^+$  and  $\text{Mn}^{2+}$  ions. *Colloids Surf. A Physicochem. Eng. Asp.* **2019**, *565*, 70–77. [[CrossRef](#)]
186. Naseri, M.; Mohammadniaei, M.; Ghosh, K.; Sarkar, S.; Sankar, R.; Mukherjee, S.; Pal, S.; Ansari Dezfouli, E.; Halder, A.; Qiao, J. A robust electrochemical sensor based on butterfly-shaped silver nanostructure for concurrent quantification of heavy metals in water samples. *Electroanalysis* **2023**, *35*, e202200114. [[CrossRef](#)]
187. Theerthagiri, J.; Lee, S.J.; Karuppasamy, K.; Park, J.; Yu, Y.; Kumari, M.A.; Chandrasekaran, S.; Kim, H.-S.; Choi, M.Y. Fabrication strategies and surface tuning of hierarchical gold nanostructures for electrochemical detection and removal of toxic pollutants. *J. Hazard. Mater.* **2021**, *420*, 126648. [[CrossRef](#)]
188. Malakootian, M.; Hamzeh, S.; Mahmoudi-Moghaddam, H. A new electrochemical sensor for simultaneous determination of Cd(II) and Pb(II) using  $\text{FeNi}_3/\text{CuS}/\text{BiOCl}$ : RSM optimization. *Microchem. J.* **2020**, *158*, 105194. [[CrossRef](#)]
189. Pathak, P.; Hwang, J.-H.; Li, R.H.; Rodriguez, K.L.; Rex, M.M.; Lee, W.H.; Cho, H.J. Flexible copper-biopolymer nanocomposite sensors for trace level lead detection in water. *Sens. Actuat. B Chem.* **2021**, *344*, 130263. [[CrossRef](#)]
190. He, Y.; Wang, Z.; Ma, L.; Zhou, L.; Jiang, Y.; Gao, J. Synthesis of bismuth nanoparticle-loaded cobalt ferrite for electrochemical detection of heavy metal ions. *RSC Adv.* **2020**, *10*, 27697–27705. [[CrossRef](#)]
191. Lei, P.; Zhou, Y.; Zhao, S.; Dong, C.; Shuang, S. Carbon-supported X-manganate (XNi, Zn, and Cu) nanocomposites for sensitive electrochemical detection of trace heavy metal ions. *J. Hazard. Mater.* **2022**, *435*, 129036. [[CrossRef](#)] [[PubMed](#)]
192. Qureashi, A.; Pandith, A.H.; Bashir, A.; Manzoor, T.; Malik, L.A.; Sheikh, F.A. Citrate coated magnetite: A complete magneto dielectric, electrochemical and DFT study for detection and removal of heavy metal ions. *Surf. Interfaces* **2021**, *23*, 101004. [[CrossRef](#)]
193. Teodoro, K.B.; Shimizu, F.M.; Scagion, V.P.; Correa, D.S. Ternary nanocomposites based on cellulose nanowhiskers, silver nanoparticles and electrospun nanofibers: Use in an electronic tongue for heavy metal detection. *Sens. Actuat. B Chem.* **2019**, *290*, t387–395. [[CrossRef](#)]
194. Zhou, J.; Sun, G.; Pan, J.; Pan, Y.; Wang, S.; Zhai, H. A nanocomposite consisting of ionic liquid-functionalized layered Mg (II)/Al (III) double hydroxides for simultaneous electrochemical determination of cadmium (II), copper (II), mercury (II) and lead (II). *Mikrochim. Acta* **2010**, *172*, 269–276. [[CrossRef](#)] [[PubMed](#)]
195. Padmalaya, G.; Sreeja, B.; Dinesh Kumar, P.; Radha, S.; Poornima, V.; Arivanandan, M.; Shrestha, S.; Uma, T. A facile synthesis of cellulose acetate functionalized zinc oxide nanocomposite for electrochemical sensing of cadmium ions. *J. Inorg. Organomet. Polym. Mater.* **2019**, *29*, 989–999. [[CrossRef](#)]
196. Mourya, A.; Sinha, S.K.; Mazumdar, B. Glassy carbon electrode modified with blast furnace slag for electrochemical investigation of  $\text{Cu}^{2+}$  and  $\text{Pb}^{2+}$  metal ions. *Microchem. J.* **2019**, *147*, 707–716. [[CrossRef](#)]

197. Shang, J.; Zhao, M.; Qu, H.; Li, H.; Gao, R.; Chen, S. New application of pn junction in electrochemical detection: The detection of heavy metal ions. *J. Electroanal. Chem.* **2019**, *855*, 113624. [[CrossRef](#)]
198. Wang, W.; Xu, Y.; Cheng, N.; Xie, Y.; Huang, K.; Xu, W. Dual-recognition aptazyme-driven DNA nanomachine for two-in-one electrochemical detection of pesticides and heavy metal ions. *Sens. Actuat. B Chem.* **2020**, *321*, 128598. [[CrossRef](#)]
199. Xin, X.; Hu, N.; Ma, Y.; Wang, Y.; Hou, L.; Zhang, H.; Han, Z. Polyoxometalate-based crystalline materials as a highly sensitive electrochemical sensor for detecting trace Cr(VI). *Dalton Trans.* **2020**, *49*, 4570–4577. [[CrossRef](#)] [[PubMed](#)]
200. Cao, L.; Kang, Z.-W.; Ding, Q.; Zhang, X.; Lin, H.; Lin, M.; Yang, D.-P. Rapid pyrolysis of Cu<sup>2+</sup>-polluted eggshell membrane into a functional Cu<sup>2+</sup>-Cu<sup>+</sup>/biochar for ultrasensitive electrochemical detection of nitrite in water. *Sci. Total Environ.* **2020**, *723*, 138008. [[CrossRef](#)] [[PubMed](#)]
201. Li, Y.; Shi, Z.; Zhang, C.; Wu, X.; Liu, L.; Guo, C.; Li, C.M. Highly stable branched cationic polymer-functionalized black phosphorus electrochemical sensor for fast and direct ultratrace detection of copper ion. *J. Colloid Interface Sci.* **2021**, *603*, 131–140. [[CrossRef](#)]
202. Xiong, W.; Zhang, P.; Liu, S.; Lv, Y.; Zhang, D. Catalyst-free synthesis of phenolic-resin-based carbon nanospheres for simultaneous electrochemical detection of Cu(II) and Hg(II). *Diam. Relat. Mater.* **2021**, *111*, 108170. [[CrossRef](#)]
203. Yadav, R.; Kushwah, V.; Gaur, M.; Bhadauria, S.; Berlina, A.N.; Zherdev, A.V.; Dzantiev, B. Electrochemical aptamer biosensor for As<sup>3+</sup> based on apta deep trapped Ag-Au alloy nanoparticles-impregnated glassy carbon electrode. *Int. J. Environ. Anal. Chem.* **2020**, *100*, 623–634. [[CrossRef](#)]
204. Yadav, R.; Berlina, A.N.; Zherdev, A.V.; Gaur, M.; Dzantiev, B. Rapid and selective electrochemical detection of Pb<sup>2+</sup> ions using aptamer-conjugated alloy nanoparticles. *SN Appl. Sci.* **2020**, *2*, 1–11. [[CrossRef](#)]
205. Oularbi, L.; Turmine, M.; El Rhazi, M. Electrochemical determination of traces lead ions using a new nanocomposite of polypyrrole/carbon nanofibers. *J. Solid State Electrochem.* **2017**, *21*, 3289–3300. [[CrossRef](#)]
206. Seenivasan, R.; Chang, W.-J.; Gunasekaran, S. Highly sensitive detection and removal of lead ions in water using cysteine-functionalized graphene oxide/polypyrrole nanocomposite film electrode. *ACS Appl. Mater.* **2015**, *7*, 15935–15943. [[CrossRef](#)]
207. Lo, M.; Seydou, M.; Bensghaier, A.; Pires, R.; Gningue-Sall, D.; Aaron, J.-J.; Mekhalif, Z.; Delhalle, J.; Chehimi, M.M. Polypyrrole-wrapped carbon nanotube composite films coated on diazonium-modified flexible ITO sheets for the electroanalysis of heavy metal ions. *Sensors* **2020**, *20*, 580. [[CrossRef](#)]
208. Dahaghin, Z.; Kilmartin, P.A.; Mousavi, H.Z. Simultaneous determination of lead (II) and cadmium (II) at a glassy carbon electrode modified with GO@Fe<sub>3</sub>O<sub>4</sub>@ benzothiazole-2-carboxaldehyde using square wave anodic stripping voltammetry. *J. Mol. Liq.* **2018**, *249*, 1125–1132. [[CrossRef](#)]
209. Lo, M.; Diaw, A.K.; Gningue-Sall, D.; Aaron, J.-J.; Oturan, M.A.; Chehimi, M.M. Tracking metal ions with polypyrrole thin films adhesively bonded to diazonium-modified flexible ITO electrodes. *Environ. Sci. Pollut. Res.* **2018**, *25*, 20012–20022. [[CrossRef](#)] [[PubMed](#)]
210. Sayyad, P.W.; Sontakke, K.S.; Farooqui, A.A.; Shirsat, S.M.; Tsai, M.-L.; Shirsat, M.D. A novel three-dimensional electrochemical Cd (II) biosensor based on l-glutathione capped poly (3,4-ethylenedioxythiophene): Polystyrene sulfonate/carboxylated multiwall CNT network. *J. Sci. Adv. Mater. Devices* **2022**, *7*, 100504. [[CrossRef](#)]
211. Pillai, A.S.; Chandran, A.; Peethambharan, S.K. MWCNT Ink with PEDOT: PSS as a multifunctional additive for energy efficient flexible heating applications. *Appl. Mater. Today* **2021**, *23*, 100987. [[CrossRef](#)]
212. Gao, Z.; Wang, Y.; Wang, H.; Li, X.; Xu, Y.; Qiu, J. Recent aptamer-based biosensors for Cd<sup>2+</sup> detection. *Biosensors* **2023**, *13*, 612. [[CrossRef](#)]

**Disclaimer/Publisher’s Note:** The statements, opinions and data contained in all publications are solely those of the individual author(s) and contributor(s) and not of MDPI and/or the editor(s). MDPI and/or the editor(s) disclaim responsibility for any injury to people or property resulting from any ideas, methods, instructions or products referred to in the content.